



Review

# Application of Modeling and Control Approaches of Piezoelectric Actuators: A Review

Mithun Kanchan <sup>1</sup>, Mohith Santhya <sup>2</sup>, Ritesh Bhat <sup>1</sup> and Nithesh Naik <sup>1,\*</sup>

<sup>1</sup> Department of Mechanical and Industrial Engineering, Manipal Institute of Technology, Manipal Academy of Higher Education, Manipal 576104, India; mithun.kanchan@manipal.edu (M.K.); ritesh.bhat@manipal.edu (R.B.)

<sup>2</sup> Department of Mechanical Engineering, National Institute of Technology Karnataka, Surathkal, P.O. Srinivasnagar, Mangalore 575025, India; mohith.sdattanagar@yahoo.com

\* Correspondence: nithesh.naik@manipal.edu

**Abstract:** Piezoelectric actuators find extensive application in delivering precision motion in the micrometer to nanometer range. The advantages of a broader range of motion, rapid response, higher stiffness, and large actuation force from piezoelectric actuators make them suitable for precision positioning applications. However, the inherent nonlinearity in the piezoelectric actuators under dynamic working conditions severely affects the accuracy of the generated motion. The nonlinearity in the piezoelectric actuators arises from hysteresis, creep, and vibration, which affect the performance of the piezoelectric actuator. Thus, there is a need for appropriate modeling and control approaches for piezoelectric actuators, which can model the nonlinearity phenomenon and provide adequate compensation to achieve higher motion accuracy. The present review covers different methods adopted for overcoming the nonlinearity issues in piezoelectric actuators. This review highlights the charge-based and voltage-based control methods that drive the piezoelectric actuators. The survey also includes different modeling approaches for the creep and hysteresis phenomenon of the piezoelectric actuators. In addition, the present review also highlights different control strategies and their applications in various types of piezoelectric actuators. An attempt is also made to compare the piezoelectric actuator's different modeling and control approaches and highlight prospects.



**Citation:** Kanchan, M.; Santhya, M.; Bhat, R.; Naik, N. Application of Modeling and Control Approaches of Piezoelectric Actuators: A Review. *Technologies* **2023**, *11*, 155. <https://doi.org/10.3390/technologies11060155>

Academic Editors: Ronald A. Coutu, Jr. and Valeri Mladenov

Received: 13 July 2023

Revised: 12 September 2023

Accepted: 27 September 2023

Published: 1 November 2023



**Copyright:** © 2023 by the authors. Licensee MDPI, Basel, Switzerland. This article is an open access article distributed under the terms and conditions of the Creative Commons Attribution (CC BY) license (<https://creativecommons.org/licenses/by/4.0/>).

**Keywords:** capacitor insertion; digital charge control; Bouc–Wen model; Prandtl–Ishlinskii model; PID controller; sliding mode control;  $H_\infty$  control

## 1. Introduction

The general requirement of precision motion in manufacturing and other commercial devices has led to extensive research and development in precision engineering. Having emerged as an integrated domain, precision engineering focuses on movement, measurement, and maintaining precision motion with higher accuracy and repeatability [1–3]. Piezoelectric actuators have been extensively used over the past few years as a source of precision positioning in a wide range of commercial applications. Piezoelectric actuators offer the advantage of precision motion in a few nanometers range to the tens of micrometer range. Furthermore, the faster response, low voltage actuation, high stiffness/load capacity/force generation smooth, backlash-free motion, non-magnetic actuation, wear resilience, cleanroom compatibility, vacuum, and cryogenic condition, low energy consumption adds to the advantages of the piezoelectric actuators [4–6]. Typical application domains of the piezoelectric actuators include precision manufacturing, fluidic applications, medical technology, micro-optics, aviation, defense, automation, robotics, aerospace, and consumer electronics.

Piezoelectric actuators are effectively employed in different applications such as micropumps/microreactors/micromixers [7,8], micromanipulators [9,10], microvalves [11], micro jet dispensers [12,13], atomic force microscopes [14,15], tool feed mechanisms [16,17],

vibration isolation systems [18], etc. Piezoelectric actuators suffer from system nonlinearity when operated under dynamic conditions despite many advantages. The inherent hysteresis and creep limit the performance of the piezoelectric actuators under dynamic conditions, leading to nonlinearity in the system. Moreover, a badly damped system leads to undesirable vibrations, which add to the nonlinearity [4,19,20]. The present review aims to bring out different modeling and control approaches employed in recent years to overcome the nonlinearities in piezoelectric actuators. The organization of the review is as follows. Section 2 briefly highlights the different piezoelectric actuators used in commercial applications. Section 3 sheds light on the piezoelectric actuators' modeling, control, and comprehensive modeling approach. Section 4 illustrates different methods of driving the piezoelectric actuators. Section 5 highlights the various methods, comparisons, and applications of charge-based control of the piezoelectric actuators. Sections 6–8 highlight various aspects of voltage-based control, emphasizing different hysteresis models, creep models, control methods, and applications. The review ends with a conclusion and scope for future work in Section 9. Figure 1 shows the organization of the current review.

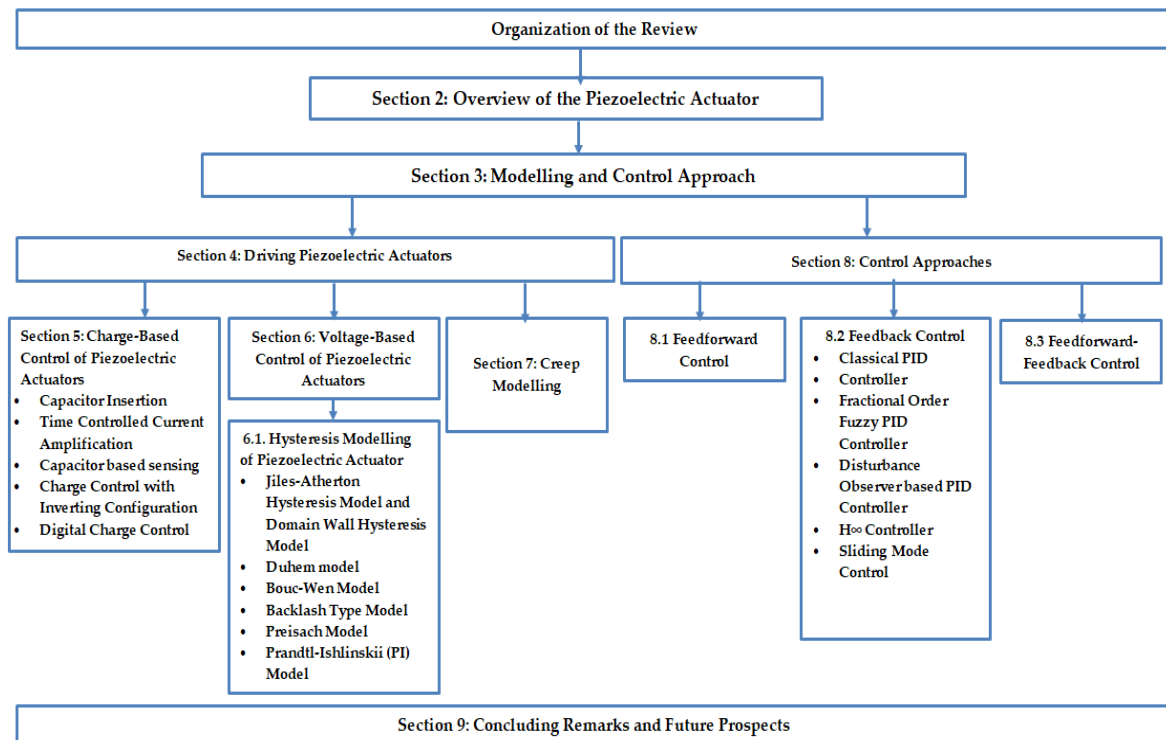
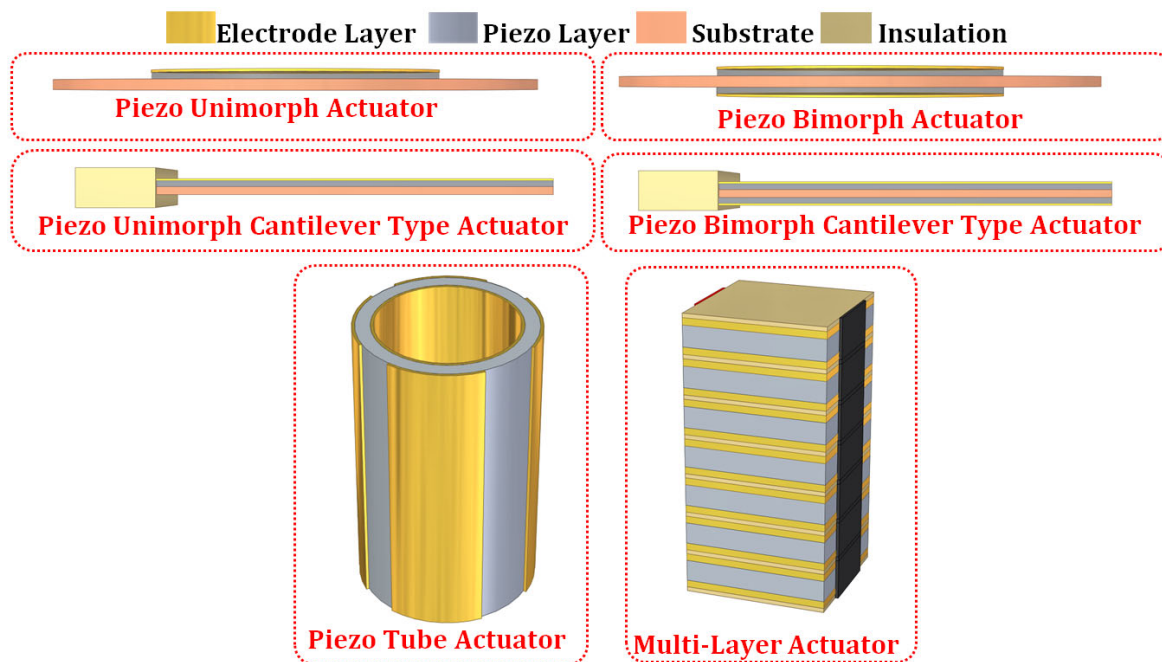


Figure 1. Organization of the review.

## 2. Overview of the Piezoelectric Actuation System

Piezoelectric actuators are a class of electromechanical devices that convert electrical signals to precise, controllable displacement. Typically, piezoelectric actuators are made of a group of smart materials that possess the property of piezoelectricity due to electromechanical coupling, which produces electric charge or mechanical strain based on the input stimulus [21]. When subjected to an external force, the piezoelectric materials produce electric charges corresponding to the direct piezoelectric effect. The application of piezoelectric materials as precision actuators adopts the inverse piezoelectric effect, which develops mechanical strain based on the applied electric potential, which in turn produces precision motion [21–23]. The early stage of discovering piezoelectric materials constituted quartz, Rochelle salt, and tourmaline, producing a comparable piezoelectric effect. However, the commercial need for large-range precision motion led to the discovery of synthetic piezoelectric materials such as Lead Zirconium Titanate (PZT) [24], Barium Titanate (BaTiO<sub>3</sub>) [25], PVDF [26], ZnO [27], etc.

Figure 2 represents the basic configuration of the piezoelectric actuators used in different applications. The basic configuration of piezoelectric actuators is unimorph and bimorph, wherein the single-layer or two-layer piezo materials are bonded onto the metal substrate [28,29]. The unimorph and bimorph actuators are also available in a cantilever configuration, which is more flexible and produces a significant range of motion. However, the cantilever configuration lacks generated force [30,31]. The piezoelectric tube actuators can generate linear or lateral motion and are effectively adopted in many precision motion applications [32,33]. The multi-layered stacked configuration of the piezoelectric actuators can operate in linear or shear mode to produce linear or lateral precision motion. The range of motion developed by the stacked configuration is limited; however, the blocked force generated has an advantage over other types of actuators [5,21,34,35]. The amplified piezo actuators are developed with a flexural-compliant structural member to enhance the deflection of the stacked piezo actuators. Flexural-based amplification enhances the deflection range of the stacked actuators with moderate force [36,37]. Typically, the amplified piezo actuators in elliptical type, rhombus type, bridge type, symmetric five bar type, honeycomb type, Scott–Russell type, and lever type are extensively used in precision positioning applications [21,38–41].



**Figure 2.** Basic configurations of the piezoelectric actuators.

Further advancement in piezoelectric actuator technology led to the development of stepping-piezoelectric actuators intended to generate a broader range of bi-directional linear and rotary motion. The stepping configuration of the piezoelectric actuators is also known as the piezo motor, which typically involves traditional piezoelectric actuators such as the unimorph/bimorph/multi-layered stacked actuators and the amplified piezo actuators as the primary source of actuation [21,42,43]. Inchworm piezoelectric motors [21,44,45], inertial piezoelectric motors [21,46,47], and ultrasonic piezoelectric motors [21,48,49] have been extensively reported in recent years which are effective in fulfilling the need of large range stepping motion. These piezoelectric motors can produce either linear/rotational motion or both, depending on the design and arrangement of the primary piezoelectric actuation mechanism. Researchers have also developed a series/parallel arrangement of multiple piezoelectric stepping stages to achieve multi-degree freedom linear/rotational motion along different coordinates [50,51]. A detailed review of different configurations of traditional, stepping, and multi-degree freedom piezoelectric actuators are presented in the

works of Mohith et al. [21], Jianping Li et al. (2019) [52], Liang Wang et al. (2019) [53], and Shupeng Wang et al. (2019) [54].

The traditional piezoelectric actuators such as unimorph, bimorph, tube, and multi-layered actuators are a primary source of precision actuation in many commercial actuation systems. The constitutive Equations (1) and (2) represent the piezoelectric phenomena occurring in piezoelectric actuators is represented as follows [55] (IEEE Ultrasonics, Ferroelectrics, and Frequency Control Society)

$$\varepsilon_i = e_{ij}^E \sigma_j + d_{ki} E_k \quad (1)$$

$$D_m = d_{mj} \sigma_j + \epsilon_{mk}^T E_k \quad (2)$$

where  $\sigma$  and  $\varepsilon$  correspond to the stress tensor and strain tensor,  $D$  and  $E$  correspond to the vector representing the electric displacement and the electric field,  $d$  represents the piezoelectric material constant,  $e^E$  the elastic compliance matrix,  $\epsilon^T$  represents the dielectric constant,  $i, j = 1, 2, 3, 4, 5, 6$  and  $m, k = 1, 2, 3$  refers to the different directions in the Cartesian coordinates. As observed in Equations (1) and (2), the mechanical strain developed in the piezoelectric materials follows a linear relationship with the applied electric field. However, when the piezoelectric actuators are put into operation under dynamic conditions, there exist system nonlinearities that affect the performance of the piezoelectric actuators. Therefore, there is a need for better modeling and control approaches that can model the inherent system nonlinearities of the piezoelectric actuation systems and minimize the error occurring due to nonlinearity through appropriate compensation models and control strategies.

### 3. Comprehensive Dynamic System Model and Modeling/Control Issues of the Piezoelectric Actuator

The promising potential of piezoelectric actuators has led to their application across wide ranges of precision manipulation to the extent of the nanometer scale. However, the dynamics of the piezoelectric actuator in specific applications lead to inherent nonlinearity that causes positioning errors. Thus, the development of modeling and control strategies for minimizing the nonlinearity errors in piezoelectric actuators have been given considerable attention. The constitutive relationship of piezoelectric materials (Equations (1) and (2)) does not account for any dynamic nonlinearity in the piezoelectric actuators. The nonlinearity emanates from hysteresis and creep, which significantly degrades the performance of the piezoelectric actuators in dynamic applications. Moreover, a badly damped system with piezoelectric actuation leads to dynamic vibrations, adding to the system's nonlinearity [55,56].

Figure 3 represents the schematic of nonlinearity occurring in the piezoelectric actuators due to hysteresis, creep, and vibration. Hysteresis in the piezoelectric actuators occurs due to specific extrinsic contributions that induce nonlinearity between the actuation voltage and precision output displacement. The extent of hysteresis error depends on the present value of the input voltage and the previous history, thus developing a memory-based phenomenon. The amplitude and the frequency of the actuation signals majorly affect the extent of hysteresis error occurring under the dynamic operation of the piezoelectric actuators. Thus, the hysteresis in piezoelectric actuators shows either amplitude-dependent or rate-dependent behavior. The model approximating the hysteresis is either rate-dependent or rate-independent [56–62]. The piezoelectric actuators under dynamic operation experience hysteresis error of about 15%, but with the increase in the driving frequency of the actuation signal, the error can shoot up to almost 35%, thus leading to the error in precision motion [55].

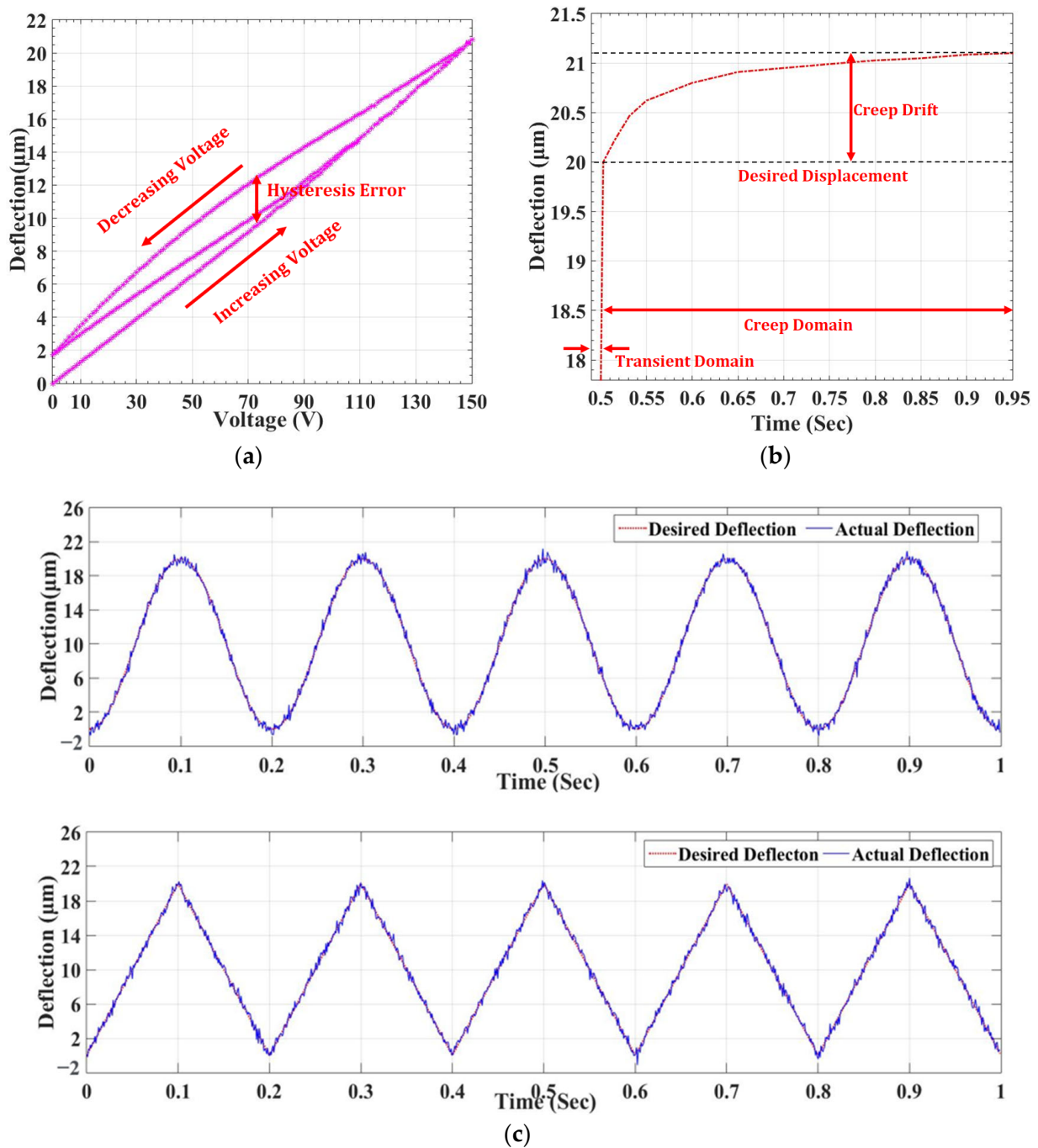


**Figure 3.** Schematic representation of the nonlinearity in the piezoelectric actuators due to (a) hysteresis, (b) creep, and (c) Vibration.

The creep in the piezoelectric actuators occurs due to the effect of applied electric potential on the remnant polarization of the electric dipole. The root cause for creep drift is the realignment of the crystal structure on the application of the electric field. The effect of creep drift significantly occurs at a low speed of operation and leads to a broad range of nonlinearity with the increase in time [55,56]. The combined effect of hysteresis and creep hinders the performance of the piezoelectric actuators in precision positioning applications where higher accuracy and precision are the significant criteria [57–62]. Implementing an appropriate modeling approach can model the piezoelectric actuator system behavior under hysteresis and creep, which can provide suitable compensation by adopting proper control approaches to overcome the nonlinearity errors.

The piezoelectric actuators are modeled as a combination of electrical and mechanical systems based on the electromechanical interaction at different stages [63–65]. Figure 4 represents the schematic of the electromechanical model of the piezoelectric actuator. Goldfarb et al. [63] developed and implemented the following electromechanical model of the piezoelectric actuator with hysteresis nonlinearity. Adriaens et al. [64] also adopted a similar approach in defining the electromechanical model of the piezoelectric actuator with hysteresis. Gao et al. [63] proposed a linear modeling approach with the electromechanical interaction, which excluded the effect of nonlinearity occurring due to hysteresis.

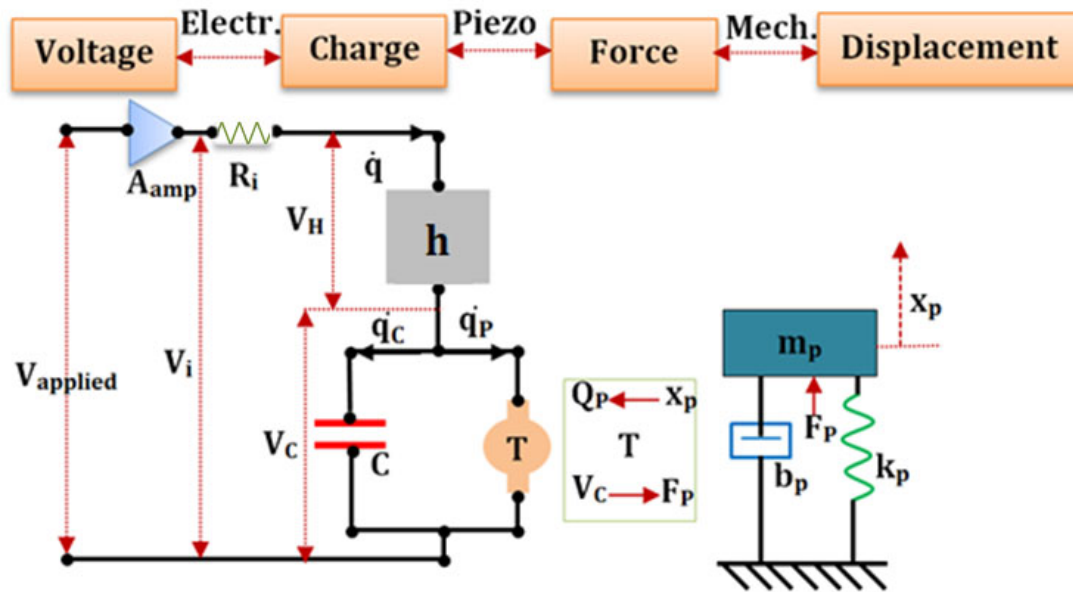


Figure 4. Schematic representation of the electromechanical model of the piezoelectric actuator.

Mathematically the comprehensive dynamic model of the piezoelectric actuator can be written as shown in Equations (3)–(9)

$$A_{amp}V_i(t) = V_h(t) + V_C(t) + R_iq(t) \quad (3)$$

$$V_H(t) = h(q) \quad (4)$$

$$q(t) = q_c(t) + q_p(t) \quad (5)$$

$$V_C(t) = q_c(t)/C \quad (6)$$

$$q_p(t) = Tx_p(t) \quad (7)$$

$$F_p = TV_C(t) \quad (8)$$

$$m_p\ddot{x}_p(t) + b_p\dot{x}_p(t) + k_px_p(t) = F_p \quad (9)$$

where  $V_{applied}$  is the control voltage fed through a linear amplifier of gain  $A_{amp}$ ,  $R_i$  is the overall resistance of the driving circuit.  $V_i$  is the amplified voltage that drives the piezo actuator,  $q$  and  $\dot{q}$  are the total charge and current through the circuit,  $H$  and  $T$  represent the hysteresis and electromechanical piezo coefficient with corresponding voltage drop  $V_H$ ,  $V_T$ , and  $C$  corresponds to the total capacitance of the piezoelectric circuit which stores charge  $q_c$ . The piezoelectric effect induces a charge of  $q_p$  across the transformer element  $T$ . The conversion of the applied voltage across the piezoelectric element induces force  $F_p$  with the piezoelectric element of mass  $m_p$ , stiffness  $k_p$ , and damping coefficient of  $b_p$ , resulting in the displacement of  $x_p$ .

#### 4. Driving and Control Methods of Piezoelectric Actuators

Piezoelectric actuators are subject to inherent nonlinearities due to hysteresis, creep, and vibration. The extent of nonlinearity in the system could be controlled by driving the piezoelectric actuator. Figure 5 represents the control and driving approaches for piezoelectric actuators. Generally, actuators are either voltage-driven or charge-driven [58,60,66]. Both the charge-based and voltage-based control approaches of piezoelectric actuators effectively minimize the nonlinearity occurring in the piezoelectric actuators. However, both methods possess their disadvantages, which limit their applications. The basic principle of charge-based control considers effective control of charge applied to the piezoelectric actuator, thus controlling the internal electric field and resulting displacement. The voltage-based control adopts control of the piezoelectric actuator through appropriate modeling and control algorithms to eliminate the system's nonlinearities. The following section presents the different methods of charge-based and voltage-based control of the piezoelectric actuators.

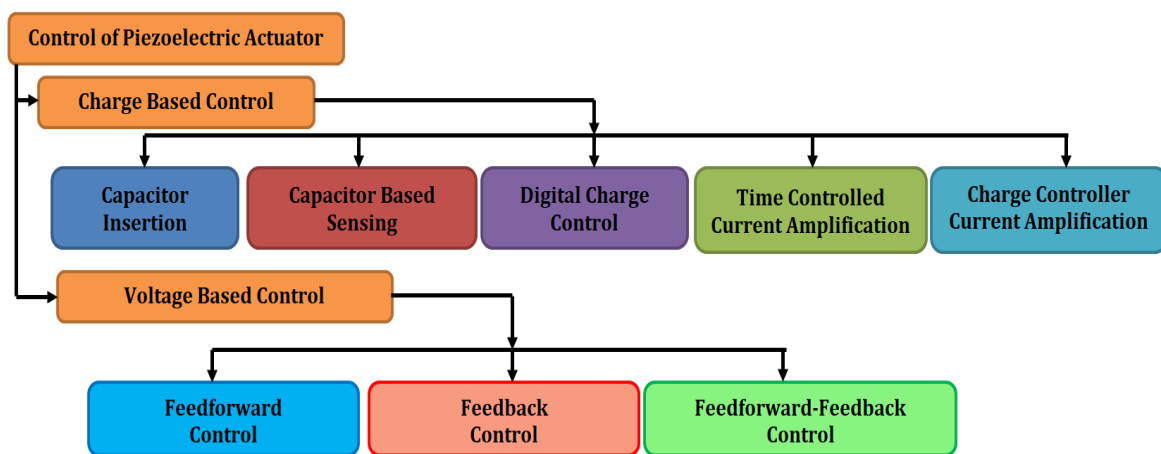


Figure 5. Driving and control approaches for the piezoelectric actuators.

#### 5. Charge-Based Control of Piezoelectric Actuators

The charge-driven mode effectively minimizes the dynamic nonlinearities occurring in the piezoelectric actuators due to hysteresis and creep effect. When supplied with an external electric field, the piezoelectric actuator behaves like a capacitor due to its dielectric property. Under dynamic operating conditions, the piezoelectric actuator behaves like a nonlinear capacitor. Thus, the charge across the piezoelectric actuator varies due to the nonlinear variation in capacitance of the piezoelectric actuator, which induces nonlinearity due to hysteresis and creep. The regulation of charge through control of current significantly reduces the nonlinearity due to hysteresis and creep [66].

From Equation (9), the input voltage  $V_i$  into the piezo actuator can be represented mathematically in terms of charge  $q(t)$  as shown in Equation (10)

$$m_p \ddot{x}_p(t) + b_p \dot{x}_p(t) + \bar{k}_s x_p(t) = Tq_C(t)/C \quad (10)$$

where  $\bar{k}_s = k_s + (T^2/c)$ . From Equation (10), it is evident that the charge control of the piezoelectric actuator is independent of the hysteresis effect. Therefore, regulating the actuator capacitance by controlling the input current; therefore, the charge across the actuator results in substantial hysteresis and creep minimization. Thus, the charge input into the piezoelectric actuator gives almost a linear displacement with the minimum error [55,66,67]. The following section highlights the different approaches to charge-based control of the piezo actuators.

### 5.1. Capacitor Insertion

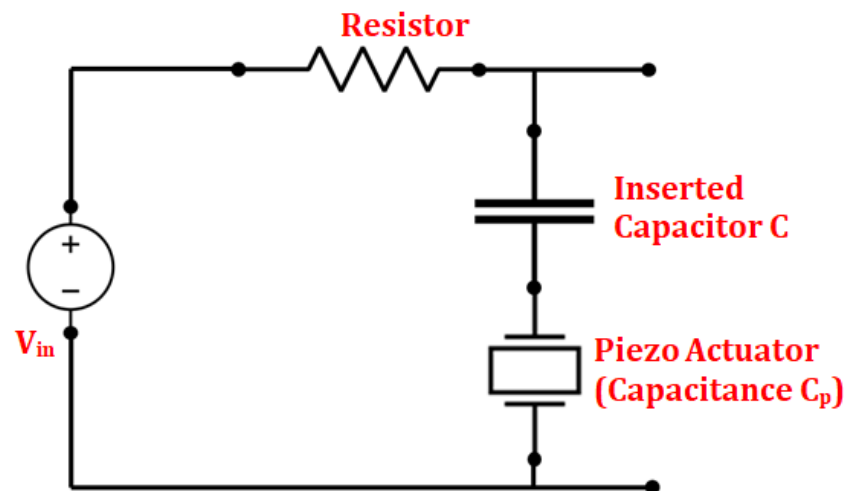
Under dynamic conditions, the application of time-varying voltage results in capacitance variation across the actuator due to the inherent dielectric properties of the piezoelectric material. This variation in the capacitance leads to variation in charge across the actuator, which induces hysteresis. Inserting a capacitor in series makes the piezoelectric actuator insensitivity to change in charge, limiting the hysteretic nonlinearity.

Figure 6 represents the schematic of the capacitor insertion method for charge-based control of piezoelectric actuators. From Figure 6,

$$V_{in} = q_p \left( \frac{1}{C_p} + \frac{1}{C} \right) \Rightarrow q_p = V_{in} \left( \frac{C \times C_p}{C + C_p} \right) \Rightarrow \frac{dq_p}{dC_p} = V_{in} \left( \frac{C}{C + C_p} \right)^2 \quad (11)$$

$$V_p = V_{in} \left( \frac{C}{C + C_p} \right) \Rightarrow V = V_p \left( \frac{C + C_p}{C} \right) \Rightarrow \frac{dq_p}{dC_p} = \left( \frac{C}{C + C_p} \right) V_p \quad (12)$$

where  $C$ ,  $C_p$  corresponds to the capacitance of the inserted capacitor and the piezoelectric actuator with charge  $q$  and  $q_p$ . From Equations (11) and (12), it is evident that the sensitivity decreases by a factor  $C/(C + C_p)$ , which reduces the hysteresis loop due to the charge regulation across the piezo actuator by inserted capacitor  $C$ . Since the applied voltage from the source is divided between the inserted capacitor and the piezo actuator, the actual voltage available for actuation reduces, leading to a reduced range of motion. Thus, the capacitor insertion method requires a higher voltage source for achieving the same range of motion [66,68,69].



**Figure 6.** Schematic of the charge-driven piezoelectric actuator with the capacitor insertion.

### 5.2. Time Controlled Current Amplification

The charge-based approach with current amplification is typically considered for high-dynamic applications. Figure 7 represents the schematic representation of the current amplification charge-based approach of the piezoelectric actuators. Since the integral of the charge on piezoelectric actuators represents the electric current, a current amplification can effectively be used as a source of charge control. In a real sense, the current amplification adopts a high gain voltage amplifier, which amplifies the input voltage, thus the input current [66]. As observed from Figure 7, the load current  $I_L$  passes through the piezo actuator and the sensing resistor  $R_s$  to the ground.

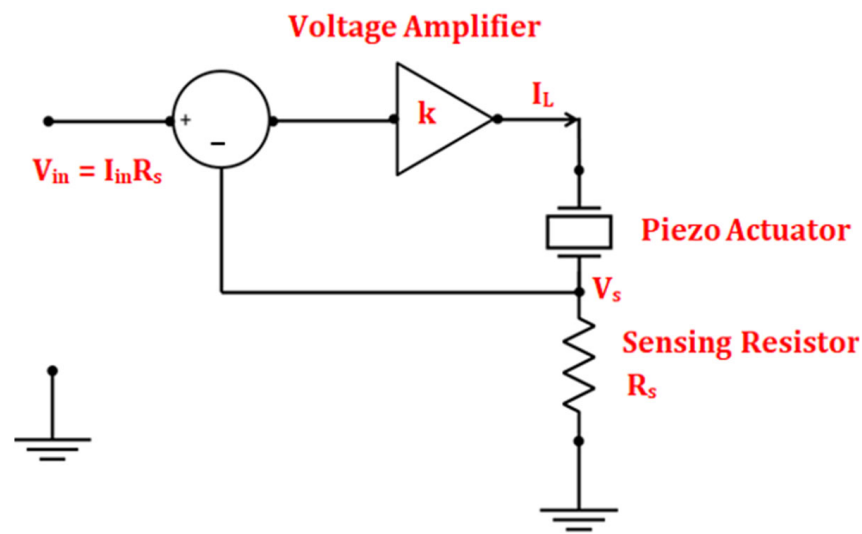


**Figure 7.** Charge-driven piezoelectric actuator with time-controlled current amplification.

Therefore, as shown in Equation (13),

$$I_L = \frac{V_s}{R_s} \quad (13)$$

The control circuit of the current amplification approach involves a voltage amplifier with gain factor 'k' with the input voltage  $V_{in}$ , which in turn controls the input current  $I_{in}$ . The implementation of a voltage amplifier with a close loop leads to  $V_{in} = V_L$ , as shown in Equation (14)

$$I_L = \frac{V_{in}}{R_s} \quad (14)$$

Thus, with the implementation of a time-controlled current approach, the charge on the piezoelectric actuator can be amplified. A smaller value of the sensing resistor is adopted in the faster response of the actuator, whereas a higher value of the sensing resistor is used for precise positioning [66]. In addition, switching circuits can be implemented with the charge amplifier to control the direction of motion, rate of actuation, and precision motion achieved with the actuator [70,71].

### 5.3. Capacitor Based Sensing

Most of the charge amplifier used for the piezoelectric actuator adopts a secondary capacitor for sensing. Figure 8 represents the schematic of the charge-driven approach of the piezoelectric actuator with capacitor-based sensing with the sensing capacitor  $C_s$  with a high gain ( $k$ ) feedback loop [72,73].

The grounding of the sensing capacitor  $C_s$  leads to the current flow from the source through  $C_s$ , as evident from Figure 8a. Therefore, the total charge ( $q_L$ ) across the piezoelectric actuator is represented in Equation (15)

$$q_L(s) = C_s V_s(s) \quad (15)$$

The presence of a high gain feedback loop renders the voltage  $V_s$  across the sensing capacitor  $C_s$  equal to the input voltage  $V_{in}$ . Therefore, the charge across the load within the frequency bandwidth of the control loop is shown in Equation (16)

$$q_L(s) = C_s V_{in}(s) \quad (16)$$

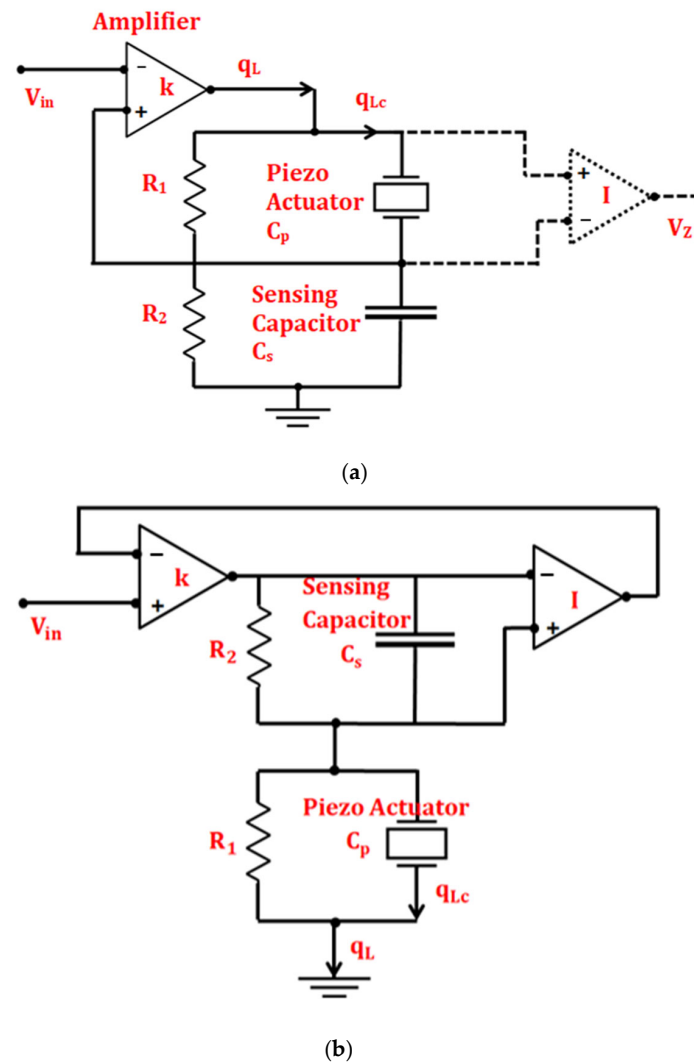


**Figure 8.** Schematic of the charge-driven piezoelectric actuator with the capacitor-based sensing (a) Generic charge amplifier (b) Grounded load DC accurate charge amplifier.

Thus, the charge across the piezoelectric actuator varies as a function of the input voltage if the control loop has ideal characteristics. Equation (16) does not consider the effect of the resistors  $R_1$  and  $R_2$ . However, in actual physical amplifiers, these resistors model the leakage current at input terminals of the voltage amplifier, sensing capacitor, and piezoelectric actuator and the resistance required for managing the voltage drift of the op-amp due to the input bias current. Considering the effect of  $R_1$  and  $R_2$ , the transfer function between the input voltage and the charge across the piezoelectric actuators is represented as shown in Equation (17)

$$\frac{q_{Lc}(s)}{V_{in}(s)} = C_s \frac{S}{1 + \frac{s}{R_1 C_p}} \quad (17)$$

Thus, from Equation (17), it is evident that the capacitor-based sensing circuit, as shown in Figure 8a, contains a low pass filter with a cut-off frequency ( $\omega_c$ ) equal to  $1/R_1 C_p$ . When the system operates below the cut-off frequency, the impedance offered by  $R_1$  and  $R_2$  is much lower than the impedance of  $C_s$  and  $C_p$ . Therefore, it is represented as in Equation (18)

$$V_p(s) = \frac{R_1}{R_2} V_{in}(s) \quad (18)$$

Thus, at low frequencies, the circuit acts like a voltage amplifier, which does not produce charge-based control of the piezoelectric actuator. Adding additional voltage feedback with a grounded load DC charge amplifier eliminates the low-frequency effect and generates a constant charge-based control [73]. Figure 8b represents the grounded load accurate charge amplifier, which typically consists of a voltage feedback loop. The amplifier sets the voltage drop across the sensing capacitor equal to the input voltage  $V_{in}$ . The transfer function of the amplifier between the charge across the actuator of capacitance  $C_p$  and the input voltage is given by Equation (19)

$$\frac{q_L(s)}{V_{in}(s)} = C_s \frac{s + \frac{1}{R_2 C_s}}{s} \quad (19)$$

From Equations (17) and (19)

$$\frac{q_{Lc}(s)}{V_{in}(s)} = \frac{q_L(s)}{V_{in}(s)} \frac{q_{Lc}(s)}{q_L(s)} = C_s \frac{s + \frac{1}{R_2 C_s}}{s} \frac{s}{s + \frac{1}{R_1 C_p}} \quad (20)$$

The low-frequency characteristics of the amplifier will be eliminated if  $R_2 C_s = R_1 C_p$ , thus achieving a constant gain factor of  $C_s$ . The frequency corresponding to  $V_z = V_p$  renders the amplifier in charge-dominant mode, whereas  $V_z = 0$  in the voltage-dominant mode. The transfer function of  $V_p$  to  $V_z$  suggests the voltage and charge dominance of the amplifier when  $V_{ref} = 0$ ,  $q_L = 0$ . When  $V_{in} = 0$ , the transfer function is represented as in Equation (21)

$$\frac{V_z(s)}{V_p(s)} = \frac{s}{s + \frac{1}{R_1 C_p}} \quad (21)$$

Therefore, the amplifier is charge dominant above the frequency value of  $1/R_1 C_p$ , which could be achieved by the selection of the larger value of  $R_1$  considering the effects of current noise attenuation of the op-amp, bias current based offset voltages, and the differential and common mode leakages of the op-amp [73–75]

#### 5.4. Charge Control with Inverting Configuration

The charge controller approach also effectively reduces the hysteresis and creep non-linearity and is effectively used in open-loop sensorless controlled piezoelectric stages. Two types of approaches, such as the linear charge controller (LCC) and the nonlinear charge controller (NCC), have been reported in the charge controller approach of the piezoelectric actuators [76–79]. Figure 9 represents the schematic of the charge controller approach of piezoelectric actuators.

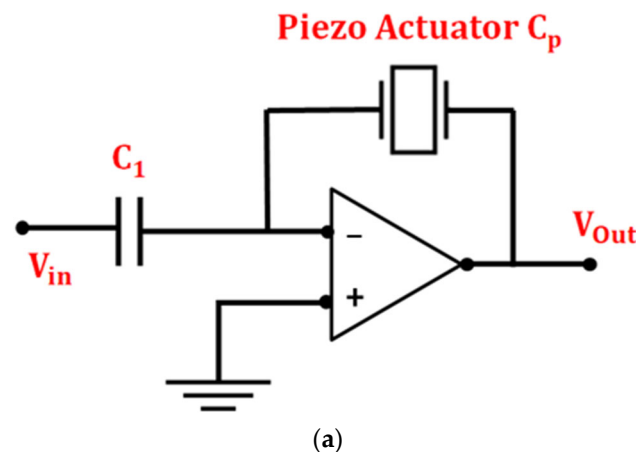
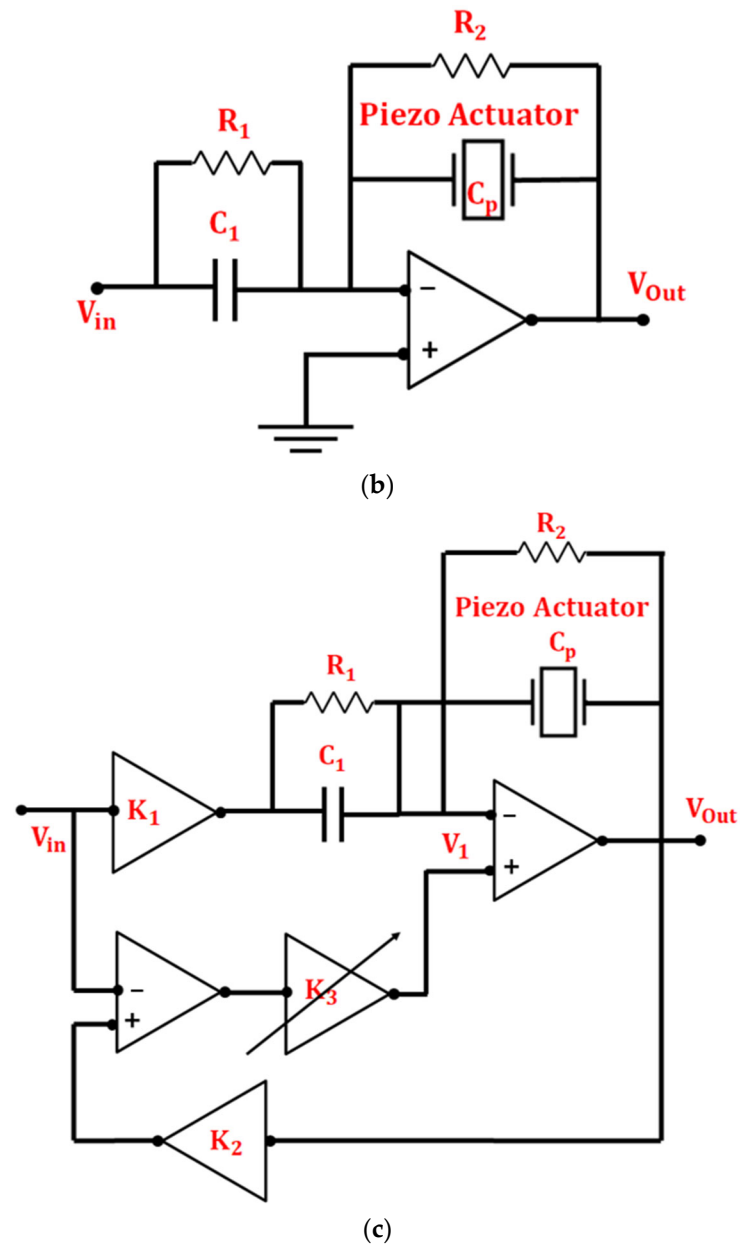


Figure 9. Cont.



**Figure 9.** Schematic of (a) linear charge controller without DC feedback, (b) linear charge controller with DC feedback, and (c) nonlinear charge controller.

The basic form of a linear charge controller without DC feedback consists of inverting op-amp with a capacitor  $C_1$  and a piezoelectric actuator of capacitance  $C_P$  connected across it, as shown in Figure 9a [76,77,79]. With the ideal characteristics of the op-amp and the capacitance of the piezoelectric actuator, the actual charge across the piezoelectric actuator  $Q_{actual}$  when supplied with input voltage  $V_{in}$  is represented by the following Equation (22)

$$Q_{actual} = V_{in}C_1 = -V_{out}C_P \quad (22)$$

Due to the linear relationship of displacement of the piezoelectric actuator with  $Q_{actual}$ , the displacement of the piezoelectric actuator remains linear as long as the input voltage remains linear. A resistive DC feedback path enhances the frequency response of the charge controller and reduces the low-frequency drift. Figure 9b represents the linear charge controller with DC feedback, which consists of resistors  $R_1$  and  $R_2$  connected across  $C_1$  and

$C_p$ . The following Equation (23) represents the transfer function of the circuit shown in Figure 9b,

$$H(s) = \frac{V_{actual}(s)}{V_{in}(s)} = -\frac{R_2}{R_1} \cdot \frac{R_1 C_1 s + 1}{R_2 C_p s + 1} \quad (23)$$

As evident from Equation (23), there is a zero point and pole point at  $-1/R_1 C_1$  and  $-1/R_2 C_p$ . The effect of zero and pole point is minimized by setting the gain factor such that  $R_1 C_1 = R_2 C_p$ . In actual practice, the frequency of the actuation signal is kept far away from the zero and pole points. Therefore, the relationship between the input voltage  $V_{in}$  and the output voltage  $V_{out}$  is represented as follows in Equation (24),

$$V_{out} = -\frac{C_1}{C_p} V_{in} \quad (24)$$

The effectiveness of the reduction in nonlinearity with a charge controller can be enhanced by the implementation of a nonlinear charge controller (NCC) represented in Figure 9c [79]. The amplifier with gain  $K_1$  is an inverting amplifier with gain  $-1$ . The capacitor  $C_1$  plays the role of the sensing capacitor, the charge across which equals the charge across the actuator. Therefore, from Figure 9c,

$$Q_{actual} = (V_{in} + V_1)C_1 = (V_0 - V_1)(C_p + \Delta C_p) \quad (25)$$

$$\text{Since } V_0 \gg V_1, V_0 = (V_{in} + V_1) \frac{C_1}{(C_p + \Delta C_p)} \quad (26)$$

$$V_1 = K_3(V_{in} - K_2 V_0) \quad (27)$$

The value of  $K_2 = C_p/C_1$ , which is the reciprocal of the voltage gain of the amplifier. From Equations (25)–(27),

$$V_1 = \frac{K_3 \Delta C_p}{(K_3 + 1)C_p + \Delta C_p} V_{in} \quad (28)$$

$$V_0 = \frac{C_1}{C_p + \frac{\Delta C_p}{K_3 + 1}} V_{in} \quad (29)$$

From Equations (28) and (29), it is evident that the  $K_3$  plays a vital role in controlling the nonlinearity of  $V_0$ . Tuning the value of  $K_3$  can compensate for  $V_0$  to minimize the nonlinearity. Accordingly, three regions can be identified for the value of  $K_3$ , i.e.,  $K_3 > 0$  where the nonlinear deviation of  $V_0$  is reduced,  $K_3 = 0$  where the charge controller adopts linear behavior,  $-1 > K_3 > 0$  where the nonlinear deviation of  $V_0$  is strengthened.

### 5.5. Digital Charge Control

Figure 10 represents the schematic of the digital charge amplifier adopted for charge-based control of the piezoelectric actuators. The voltage amplifier, analog-to-digital converter (ADC), digital-to-analog converter (DAC), and digital signal processor (DSP) constitute the integral parts of the digital charge amplifier [80,81]. The charge across the piezoelectric actuator  $q_p(t)$  is the integral of current flowing through given by the Equation (30)

$$q_p(t) = \int I_s(t) dt = \int \frac{V_s(t)}{R_T} dt = \int \frac{V_s(t)}{R_s \parallel R_{inputADC}} dt \quad (30)$$

where  $R_T$  is the total resistance that consists of sensing resistor  $R_s$  in parallel with the input resistance  $R_{inputADC}$  of the ADC. Thus, the charge across the piezoelectric actuator varies as a function of the voltage across the sensing resistor. The presence of a high-gain feedback loop equates to the actual and the desired charge for driving the actuator.

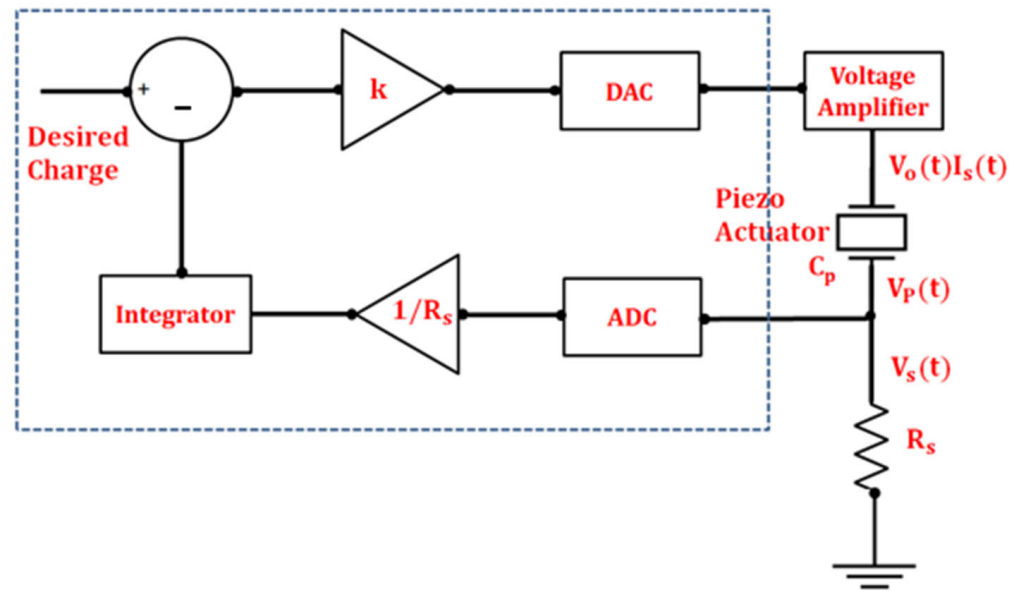


**Figure 10.** Schematic of the charge-driven piezoelectric actuator with the digital charge control.

The transfer function between the output voltage of the amplifier and the voltage across the sensing resistor is represented as follows in Equation (31)

$$H(s) = \frac{V_s(s)}{V_0(s)} = \frac{R_T C_p}{R_T C_p + 1} \quad (31)$$

where  $C_p$  is the capacitance of the piezoelectric actuator. The discrete transfer function of Equation (31) is as follows as shown in Equation (32)

$$H(z) = \frac{V_s(z)}{V_0(z)} = \frac{z - 1}{z - e^{-\frac{T}{R_T C_p}}} \quad (32)$$

where  $T_s$  is the sampling time,  $V_0(z) = k \left( q_{desired}(z) - \frac{T_s}{(z-1)R_T} V_s(z) \right)$ ,  $V_s(z) = \frac{q_{actual}(z)R_T(z-1)}{T_s}$   
Therefore, Equation (33)

$$\frac{q_{actual}(z)}{q_{desired}(z)} = \frac{\frac{T_s k}{R_T}}{z - e^{-\left(\frac{T_s}{R_T C_p}\right)} + \frac{T_s k}{R_T}} \quad (33)$$

The digital charge amplifier results in displacement drift because of the non-ideal characteristics of the ADC. Thus, a current leakage leads to bias voltage  $V_{bias}$  at the input, leading to charge drift. The expression for the measured charge is given by Equation (34)

$$q_{measured} = \frac{1}{R_T} \int (V_s(t) + V_{bias}) dt \quad (34)$$

Due to the charge drift, the output voltage  $V_0(t) = k(q_{desired} - q_{bias})$  also drifts leading until it extends to the power supply rails [76,77].

### 5.6. Comparison and Applications of the Charge-Based Control of the Piezoelectric Actuators

The charged-based driving methods have effectively reduced the inherent nonlinearity of piezoelectric actuators. Several researchers have implemented the charge-based approach in different applications comprising different piezoelectric actuators. Table 1 represents the charge-based driving of piezoelectric actuators implemented by different researchers and their application to reduce nonlinearity.

**Table 1.** Application of charge-based control of the piezoelectric actuators reported in recent years.

Author	Year	Ref. No.	Type of Actuator	Method of Charge Control	Voltage (V)	Frequency (Hz)	Range of Motion ( $\mu\text{m}$ )	Approximate % Reduction in Hysteresis	Approximate % Reduction in Creep
J. Minase	2010	[68]	Piezo Stack	Capacitor Insertion	100	10	2.25	99.59	99.87
Y. T. Ma	2011	[69]	Piezo Stack	Capacitor Insertion	5	5	5	94.36	77.00
A. J. Fleming	2005	[73]	Piezo Tube	Capacitor based sensing	$\pm 6$	10	$\pm 3.00$	89.00	----
A. J. Fleming	2010	[74]	Piezo Stack	Capacitor based sensing	150	100	7.8	95.35	----
Shannon A.	2015	[75]	Bimorph	Capacitor based sensing	−50 to +200	15	$\pm 1250$	92.00	----
C. Yang	2017	[77]	Piezo Stack	Nonlinear Charge Controller	100	2	6.50–7.00	88.00	----
T. Jin	2019	[79]	Piezo Stack	Linear Charge Controller	4.5	2	2.50–3.00	71.33	----
T. Jin	2019	[79]	Piezo Stack	Nonlinear Charge Controller	4.5	2	2.50–3.00	91.29	----
M. Bazghaleh	2014	[81]	Piezo Stack	Digital Charge Amplification	40	10	11.54	91.00	----
J. Zhong	2021	[82]	Piezo Stack	Digital Charge Control	120	1–1000	$\pm 2.00$	99	
Chen Yang	2022	[83]	Piezo Stack	Nonlinear Charge Controller	50	10–400	3.3	97	

## 6. Voltage-Based Control of Piezoelectric Actuators

The limitations of the charge-based driving approach led to the extensive use of voltage-based driving methods for piezoelectric actuators. The voltage-based driving methods proved more comfortable and convenient for the piezoelectric actuators. The voltage-driven mode does not require any calibration or specially designed amplifier and does not affect the range and bandwidth of the piezoelectric actuator. Mathematically, the electromechanical model for voltage-driven piezoelectric actuators can be written from Equations (3)–(9) as follows, represented in Equations (35) and (36),

$$CR_i \dot{q}(t) + q(t) - Tx_p(t) = CA_{amp}(V_i(t) - h(q)/A_{amp}) \quad (35)$$

$$m_p \ddot{x}_p(t) + b_p \dot{x}_p(t) + \bar{k}_s x_p(t) = T[(CA_{amp}(V_i(t) - h(q)/A_{amp}) - CR_i \dot{q}(t))] \quad (36)$$

where,  $\bar{k}_s = k_s + T^2((1/c) - 1)$ .

As observed in Equation (33), the inherent nonlinearity due to hysteresis is evident with voltage-driven piezoelectric actuators. Appropriate hysteresis modeling and control approaches can help reduce the nonlinearity of voltage-driven piezoelectric actuators [55,84]. The following sections highlight some hysteresis modeling approaches adopted for piezoelectric actuators.

### 6.1. Hysteresis Modeling of Piezoelectric Actuator

Over the past few years, many mathematical models have been developed and adopted to describe piezoelectric actuators' hysteresis behavior. There are diverse classifications of hysteresis models for piezoelectric actuators, as represented in Figure 11. The hysteresis model for piezoelectric actuators can be classified at three different levels. One such level of classification contains phenomenological hysteresis models and physics-based hysteresis models. Physics-based models for hysteresis of the piezoelectric actuators are developed based on the first principles of the physics effect [55]. The phenomenological models are developed based on the empirical relationship of the phenomena of hysteresis occurrence in the piezoelectric actuators, consistent with the theoretical base [85–87].

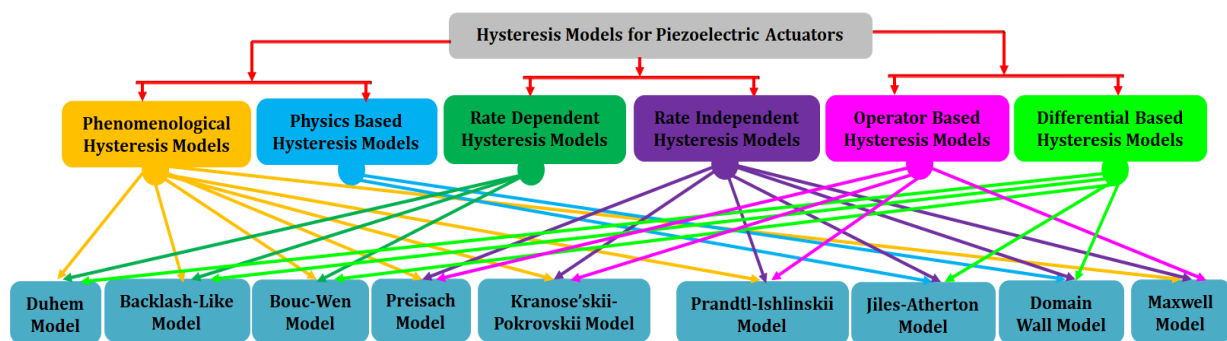


Figure 11. Classification of hysteresis model of the piezoelectric actuators.

Further, the hysteresis models are either rate-dependent or rate-independent, which describes the dependence of hysteresis behavior on the rate of change in input signal [80,81]. The third classification level is based on the mathematical formulations of the hysteresis models, which involve operator and differential equation-based models. The differential equation-based models are typically represented in differential equation form, whereas the operator-based models contain weighted hysteresis operators [55,88,89].

#### 6.1.1. Jiles–Atherton Hysteresis Model and Domain Wall Hysteresis Model

The Jiles–Atherton model is one of the popularly known physical-based models for hysteresis modeling. The Jiles–Atherton model was proposed for modeling the hysteresis behavior of ferromagnetic material, which was adopted later than the piezoelectric materi-

als [90–92]. Another physical-based modeling approach is domain wall modeling, which is derived based on the Jiles–Atherton model by Smith and Ounaies [92]. The hysteresis operator can be represented according to Jiles–Atherton shown in Equation (37) [90,91]

$$h[E](t) = ch_{an}(t) + (1 - c)h_{irr}(t) \quad (37)$$

The model consists of a superposition of the anhysteretic part  $h_{an}$  and the hysteric part, which is irreversible  $h_{irr}$ . The internal variables  $h_{an}(t)$ ,  $h_{irr}(t)$ , and input variable  $E(t)$  are functions of time. The model follows the assumption of isotropic material with polarization in any direction. The anhysteretic part is defined in terms of electric field  $E(t)$  and saturation part  $h_s$  as follows, represented by Equation (38)

$$h_{an}(t) = h_s \left[ \left( \coth \left( \frac{(E(t) + \alpha h_{irr}(t))}{c} \right) \right) - \left( \frac{a}{(E(t) + \alpha h_{irr}(t))} \right) \right] \quad (38)$$

The hysteresis model through domain wall dynamics with irreversible  $h_{irr}$  is presented in Equation (39)

$$\frac{dh_{irr}}{dt}(t) = \frac{dE}{dt}(t) \frac{\tilde{\delta}(h_{an}(t) - h_{irr}(t))}{k\delta - \alpha(h_{an}(t) - h_{irr}(t))} \quad (39)$$

where  $\delta = \text{sign}(dE/dt)$  signifies the change in the direction of the electric field. Another operator  $\tilde{\delta}$  prevents an increase in hysteresis operator  $h$  when the electric field changes its direction. The operator  $\tilde{\delta}$  is defined as Equation (40),

$$\tilde{\delta} = \begin{cases} 1, & \text{for } (dE < 0, h < h_{an}) \text{ or } (dE < 0, h > h_{an}) \\ 0, & \text{else} \end{cases} \quad (40)$$

The Jiles–Atherton and the Domain wall model involves parameters such as  $c$ ,  $a$ ,  $\alpha$ , and  $k$ , which must be identified through appropriate parameter identification techniques for the particular material. Solving the above set of algebraic and differential equations over a specific time interval can represent the hysteresis of the piezoelectric actuator with respect to the applied electric field. Even though the identification of only five model parameters ( $c$ ,  $a$ ,  $\alpha$ ,  $k$ , and  $H_s$ ) adds to the advantage of the simplicity of the model, the disability to follow the minor loops in the hysteresis results in the major drawback of the Jiles–Atherton and Domain Wall Hysteresis Models [92,93].

### 6.1.2. Duhem Model

The Duhem model is one of the differential equation-based models implemented for describing the hysteresis behavior of the ferromagnetic materials which was subjected to the magnetic field of  $H(t)$  and the magnetic flux of  $B(t)$  defined as in Equation (41) [94]

$$\dot{B}(t) = \alpha |B(t)| \cdot [\beta(H(t)) - B(t)] + \gamma H(t) \quad (41)$$

Equation (41) consists of parameters  $\alpha$ ,  $\beta$ ,  $\gamma$ , which control the shape of the hysteresis loop. Further, for a system with single input (voltage)  $v(t)$  and single-output (displacement)  $x(t)$ , the generalized Duhem model is expressed as in Equation (42)

$$\begin{aligned} \dot{x}(t) &= f(y(t), v(t), \dot{v}(t)), \quad y(0) = y_0, \quad t \geq 0, \\ x(t) &= h(y(t), v(t)) \end{aligned} \quad (42)$$

Based on the above equation, the generalized Duhem model for a piezoelectric actuator with the linear component of  $X(t)$ , input voltage of  $v(t)$ , and hysteresis component of  $h(t)$  be expressed as follows in Equation (43) [95,96]

$$X(t) = Y(t) - h(t)$$

$$X(t) = k \cdot v(t) \quad (43)$$

$$\dot{h}(t) = \alpha \dot{v}(t) - \beta |\dot{v}(t)| h(t) + \gamma |\dot{v}(t)| v(t)$$

The model contains parameters  $k$ ,  $\alpha$ ,  $\beta$ , and  $\gamma$ , which have to be identified through appropriate parameter identification methods. Duhem model of hysteresis is rate-dependent, which helps in modeling the rate-dependent hysteresis characteristics of the piezoelectric actuator at a high frequency of actuation.

### 6.1.3. Bouc–Wen Model

The Bouc–Wen model hysteresis model was derived based on the Duhem model, largely used for modeling the nonlinear hysteresis behavior of the piezoelectric actuators. R. Bouc and Yi-Kwei Wen developed the Bouc–Wen model, which involves the superposition of linear component  $Y(t)$  and hysteresis component  $h(t)$ . The conventional Bouc–Wen model is represented as follows in Equations (44) and (45) [97,98]

$$x(t) = Y(t) + h(t) = k \cdot v(t) + h(t) \quad (44)$$

$$\dot{h}(t) = \alpha \dot{v}(t) - \beta \dot{v}(t) |h(t)|^n - \gamma |\dot{v}(t)| |h(t)|^{n-1} h(t) \quad (45)$$

For a piezoelectric actuator, usually the value of  $n$  is taken as one. Thus, it is represented by Equation (46).

$$\dot{h}(t) = \alpha \dot{v}(t) - \beta \dot{v}(t) |h(t)| - \gamma |\dot{v}(t)| h(t) \quad (46)$$

The shape of the hysteresis loop depends on the estimated values of the model parameters  $\alpha$ ,  $\beta$ , and  $\gamma$ . The Bouc–Wen model has the advantage of more straightforward implementation to represent a large class of hysteresis. Furthermore, the differential and inverse form of the Bouc–Wen model is more comfortable to implement in the control system for nonlinearity compensation [98,99].

### 6.1.4. Backlash Type Model

The mathematical representation (Equation (47)) of the backlash model is as follows [100,101]

$$\frac{dx}{dt} = \alpha \left| \frac{dv}{dt} \right| [cv - x] + B_1 \frac{dv}{dt} \quad (47)$$

where  $\alpha$ ,  $c$ , and  $B_1$  are the constants such that  $c > B_1$ . The solution for Equation (47) is presented as

$$x(t) = cv(t) + d(v(t)) \quad (48)$$

$$d(v(t)) = [x_0 - cv_0] e^{-\alpha(v-v_0)\text{sgn}(\dot{v})} + e^{-\alpha v \text{sgn}(\dot{v})} \int_{v_0}^v [B_1 - c] e^{\alpha \zeta \text{sgn}(\dot{v})} d\zeta \quad (49)$$

The backlash model represents the nonlinear hysteresis as a linear function of the input signal with some disturbances (Equations (48) and (49)). With the implementation of the backlash-type model, the conventional control approach can be adopted for compensating the hysteresis error without the inverse model [55].

### 6.1.5. Preisach Model

The Preisach model for hysteresis of piezoelectric materials is an extension of the model developed to interpret ferromagnetic materials. The Preisach model adopts an operator-based approach for defining the hysteresis behavior between the input and the output through the relay operator, as represented in Figure 12. The representation of the

classical Preisach model with weighting operator  $\mu(\alpha, \beta)$  with two parameters  $\alpha, \beta$  and hysteresis operator of  $\hat{\gamma}_{\alpha\beta}[v(t)]$  is as follows in Equation (50) [102,103]

$$H(t) = \iint_{\alpha \geq \beta} \mu(\alpha, \beta) \hat{\gamma}_{\alpha\beta}[v(t)] d\alpha d\beta \quad (50)$$

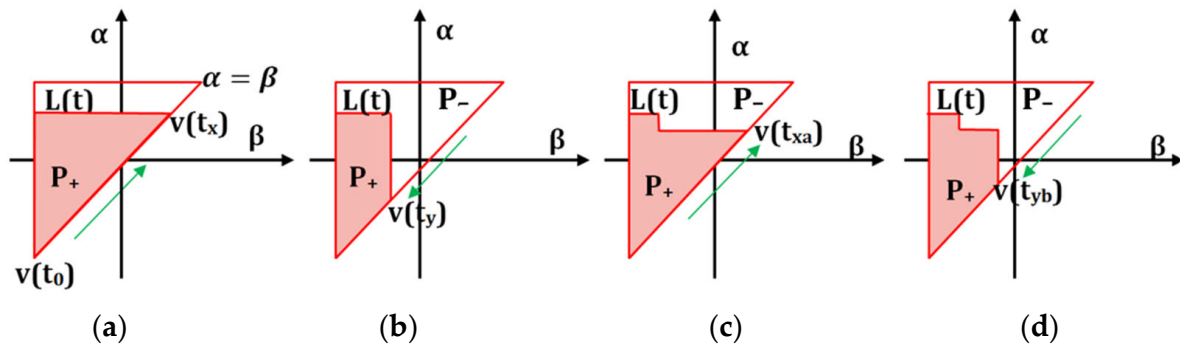


Figure 12. Mapping of Hysteresis in the  $\alpha$ - $\beta$  plane for the Preisach model.

The hysteresis effect through the Preisach model can be considered as integrating the hysteresis operator, which is represented in plane Figure 12. When the input voltage to the piezoelectric actuator increases from  $v(t_0)$  to  $v(t_x)$ , the line  $L(t)$  moves horizontally from  $\alpha_{\min}$  to  $\alpha v(t_x)$ . The value of the hysteresis operator  $\hat{\gamma}_{\alpha\beta}[v(t)]$  varies between 1 and 0 for the integral region below to the above of  $L(t)$ , leading to  $H(t) = \iint_{P_+} \mu(\alpha, \beta) d\alpha d\beta$ . Further, the line  $L(t)$  drops vertically down when the input to the piezo actuator decreases from  $v(t_x)$  to  $v(t_y)$ , leading to the variation of the value of  $\hat{\gamma}_{\alpha\beta}[v(t)]$  between 1 (left of  $L(t)$ ) and 0 (right of  $L(t)$ ). Thus, a memory-based effect is produced when  $H(t)$  equals the integral of the weighing function in the  $P_+$  region [55,104,105]. Due to the general structure of the Preisach model, a wide range of hysteresis could be modeled for different actuators. The major limitation exists due to the lack of understanding of the physical significance of the model. Moreover, obtaining the inverse of the model is quite difficult; thus, it requires numerical methods for obtaining the inverse of the model [104,105].

#### 6.1.6. Prandtl–Ishlinskii (PI) Model

The Prandtl–Ishlinskii is an operator-based model derived from the Preisach model, effectively used to characterize the hysteresis behavior of the piezoelectric actuators through play or stop operator with a density function. The geometric representation of the continuous rate-independent hysteresis operator has been presented in Figure 13 [106,107].

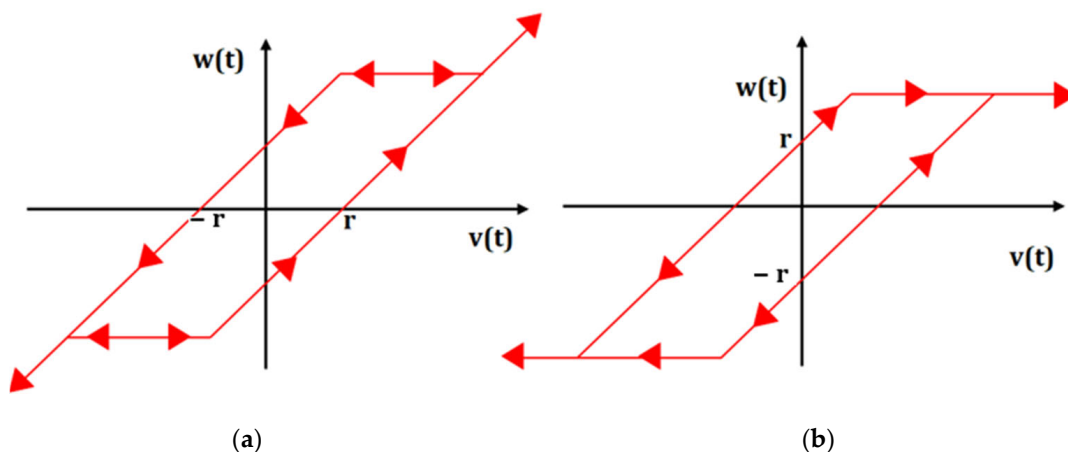


Figure 13. Geometric representation of (a) Play Operator (b) Stop Operator.

The play or stop operators are characterized by threshold parameter  $r$  and the input to the piezoelectric actuator  $v$ . The play hysteresis operator  $t_0 = 0, t_0 < t_1 < \dots < t_N = t_E$  with an input  $v(t) \in C_m[t_0, t_E]$  with  $C_m$  being a space piecewise monotone continuous function and  $v(t)$  which is monotonous in interval  $[t_i, t_{i+1}]$  can be represented as Equation (51) [106–109].

$$\begin{aligned} F_r[v](0) &= f_r(v(0), 0) = w(0) \\ F_r[v](t) &= f_r(v(t), F_r[v](t_i)) \\ \text{For } t_i \leq t \leq t_{i+1} \text{ and } 0 \leq i \leq N - 1 \\ f_r(v, w) &= \max(v - r, \min(v + r, w)) \end{aligned} \quad (51)$$

Based on the above play operator the  $F_r[v(t)]$ , the relationship between the input  $v$  and output  $x$  of the actuator is represented by the PI model as follows Equation (52)

$$x(t) = qv(t) + \int_0^R p(r)F_r[v](t)dr \quad (52)$$

where  $q$  is a positive constant,  $p(r)$  is a density function with  $p(r) \geq 0$  identified through the experimental data. The control and characterization of the rate-independent hysteresis could be effectively achieved through the PI model with few play operators.

#### 6.1.7. Krasnoselskii–Pokrovskii Model

Krasnoselskii–Pokrovskii (K–P) model is hypothesized and improvised from the Preisach model [110]. The K–P model incorporates an improved play operator called the K–P kernel represented as  $k_P[v, \zeta(\rho)](t)$  (Figure 14), which replaces the traditional play operator of the Preisach model [106,107].

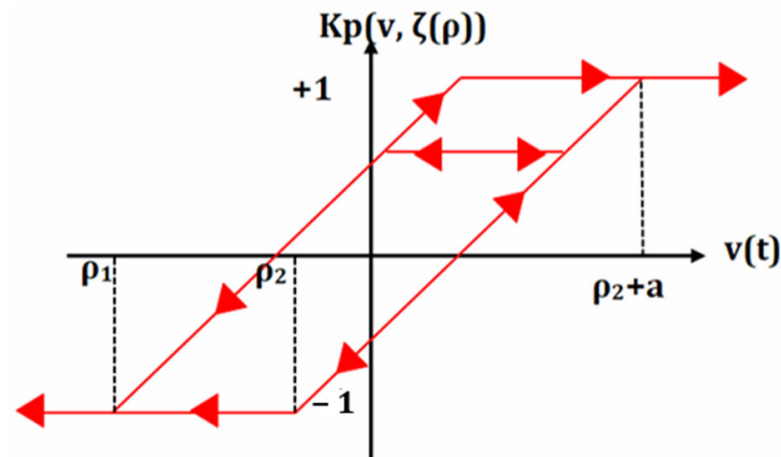


**Figure 14.** Schematic of the Krasnoselskii–Pokrovskii kernel.

The K–P model is represented mathematically as follows in Equation (53),

$$x(t) = \int_{T_0} k_P[v, \zeta(\rho)](t)\mu(\rho)d\rho \quad (53)$$

where  $v(t)$  and  $x(t)$  represent the input and output of the K–P model,  $\mu(\rho)$  is the weight factor of the Krasnoselskii–Pokrovskii operator with the Preisach plane points of  $\rho = (\rho_1, \rho_2) \in T_0$  such that  $T_0 = \{(\rho_1, \rho_2) \in R^2 | T_{min} \leq \rho_1 \leq \rho_2 \leq T_{max}\}$   $T_{max}$ ,  $T_{min}$  are the maximum and minimum values on the Preisach plane, respectively. Since the K–P model is an improvised form of the Preisach model, the Preisach plane can be extended for determining the output of the K–P model with an operator K–P kernel defined as follows in Equation (54)

$$k_P[v, \zeta(\rho)] = \begin{cases} \max_{\rho \in T_0} \{\zeta(\rho), r(v - \rho_2)\}, & \dot{v} < 0 \\ \min_{\rho \in T_0} \{\zeta(\rho), r(v - \rho_1)\}, & \dot{v} > 0 \end{cases} \quad (54)$$

where  $r(v)$  represents the ridge function defined as shown in Equation (55)

$$r(v) = \begin{cases} -1, & v \leq 0 \\ -1 + \frac{2v}{a}, & 0 < v < a, \\ +1, & a \leq v \end{cases} \quad (55)$$

The slope of the ridge function depends on the value of  $a$ . The K–P kernel incorporates two ridge functions with parameters  $\rho_1$  and  $\rho_2$ , such that  $\rho_1 \leq \rho_2$ . When the input  $v(t)$  is applied, the response of the K–P kernel follows either a horizontal line between  $r(v - \rho_2)$  and  $r(v - \rho_1)$  or follows one of the curves of the ridge function as shown in Figure 14 [111]. The complications associated with the Preisach model are very much evident in the K–P model due to the similarity with the Preisach model.

#### 6.1.8. Maxwell–Slip Model

The Maxwell–Slip model is a quasi-static model intended to relate the nonlinearity between the force and displacement of the spring system. Later on, the same approach was extended to model the nonlinearity hysteresis of the piezoelectric actuators [112,113]. The Maxwell–Slip model considers the analogy of the massless friction element and the massless spring, as represented in Figure 15.

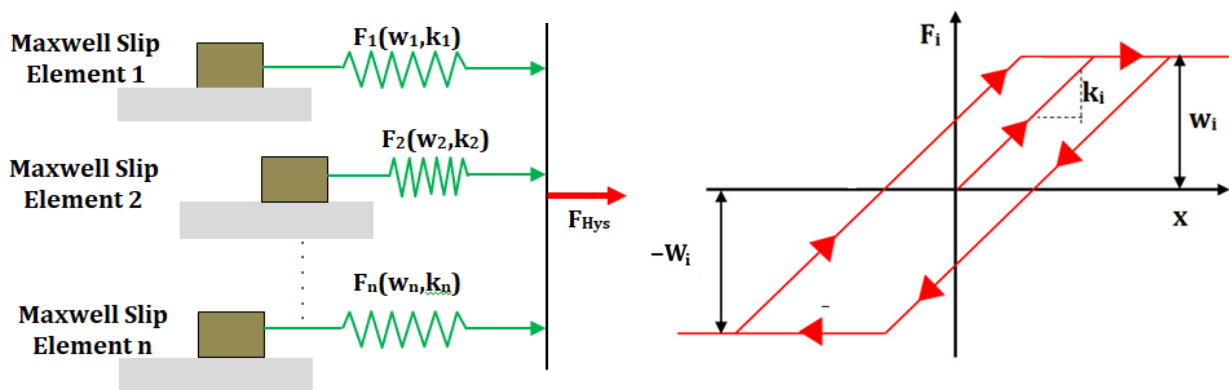


Figure 15. Schematic representation of the Maxwell–Slip Hysteresis model.

Mathematically, the Maxwell–Slip model with the input displacement of  $x$ , output force of  $F$ , and spring constant of  $K$  as follows as shown in Equation (56) [106,107],

$$F_i = \begin{cases} k_i(x - x_{bi}) & |k(x - x_{bi})| < f_i \\ f_i \operatorname{sgn}(\dot{x}) & x_{bi} = x - \frac{f_i}{k_i} \operatorname{sgn}(\dot{x}) \end{cases} \quad (56)$$

where  $\mu$  represents the coefficient of friction between the sliding element such that the frictional force  $f = \mu N$ . For an accurate representation of the hysteresis behavior, numbers of friction elements are taken in parallel, with  $x_i$  being the initial position of the  $i$ th slider [112–115]. Though the Maxwell model of hysteresis is simple to understand and implement, the rate-independent nature of the model cannot represent hysteresis behavior at high frequency.

## 6.2. Applications and Comparison of the Hysteresis Model

A large number of hysteresis models are proposed to minimize nonlinearity errors in piezoelectric actuators for precision applications. Several researchers have contributed significantly to developing and optimizing the hysteresis model for piezoelectric actuators through an appropriate mathematical approach. Tables 2 and 3 represents the applications of different hysteresis models for modeling the hysteresis behavior of the piezoelectric actuators upto the year 2020 and onwards respectively.

**Table 2.** Application of the hysteresis models in the piezo actuation technology reported upto the year 2020.

Author	Year	Ref. No.	Type of Actuator	Hysteresis Model	Observation
T. Hegewald	2008	[116]	Piezo Stack	Jiles–Atherton	<ul style="list-style-type: none"> <li>The rate-independent hysteresis model is considered</li> <li>Parameters estimated through the least squares algorithm</li> <li>No consideration of the rate-dependent hysteresis behavior</li> </ul>
L. Deng	2008	[117]	Piezo Positioning Stage	Backlash	<ul style="list-style-type: none"> <li>Modified model to include rate-dependent hysteresis with diagonal recurrent neural network (DRNN)</li> <li>Model parameters and weights are estimated through the Levenberg–Marquardt (L–M) algorithm</li> </ul>
M. Zhou	2013	[118]	Piezo Stack	Duhem	<ul style="list-style-type: none"> <li>The rate-independent hysteresis phenomenon is considered</li> <li>Model parameters and weights are estimated through a gradient correction algorithm</li> <li>Model accuracy of 0.11%</li> </ul>
Y. Liu	2013	[119]	Piezo Positioning Stage	Maxwell–Slip	<ul style="list-style-type: none"> <li>The rate-independent hysteresis behavior is considered</li> <li>Model parameters are identified through the piecewise linear fit of the experimental hysteresis curve, normalized root-mean-square</li> <li>An error of the model is about 0.43% to 2.28%</li> </ul>
T.-G. Zsurzsan	2015	[120]	Piezo Motor	Preisach	<ul style="list-style-type: none"> <li>The rate-independent hysteresis behavior is considered</li> <li>Amplitude-dependent behavior was considered with the 50 reversal cycles</li> <li>Model accuracy of 95.8% was achieved</li> </ul>
J. Gan	2016	[121]	Preloaded Piezo Stack	Prandtl–Ishlinskii	<ul style="list-style-type: none"> <li>The rate-dependent for frequencies 1 Hz to 100 Hz and the rate-independent behavior are considered</li> <li>Model parameters are estimated through the self-adaptive particle swarm optimization</li> </ul>
G. Wang	2017	[122]	Amplified Piezo Stack	Duhem	<ul style="list-style-type: none"> <li>The rate-dependent hysteresis model is considered</li> <li>Model implementation and parameters identified through the Neural Network approach</li> </ul>

Table 2. Cont.

Author	Year	Ref. No.	Type of Actuator	Hysteresis Model	Observation
Y. Qin	2017	[123]	Compliant Piezo Stage	Prandtl–Ishlinskii	<ul style="list-style-type: none"> <li>The rate-dependent hysteresis model is considered</li> <li>Model parameters are estimated through the curve fitting with respect to experimental data</li> <li>The maximum error observed is about 8.25% of the measured displacement</li> </ul>
J. Gan	2018	[124]	Compliant Piezo Stage	Bouc–Wen	<ul style="list-style-type: none"> <li>Considered enhanced model to include the rate-dependent behavior in the range of 1 Hz–150 Hz</li> <li>Parameters identification through the particle swarm optimization</li> <li>Reduction in modeling error by 75%</li> </ul>
Y. Luo	2018	[125]	Piezo Stack	Preisach	<ul style="list-style-type: none"> <li>The hysteresis model considered the rate-independent and amplitude-dependent behavior</li> <li>Maximum error of 5.24% is obtained with respect to experimental data</li> </ul>
Z. Li	2018	[126]	Piezo Positioning Stage	Krasnoselskii–Pokrovskii	<ul style="list-style-type: none"> <li>The rate-independent, amplitude-dependent hysteresis behavior is considered</li> <li>The maximum model error achieved is about 1.30% to 2.11%</li> </ul>
D. Gan	2019	[127]	Compliant Piezo Stage	Duhem	<ul style="list-style-type: none"> <li>The modified model is considered to include the rate-dependent behavior of the actuator</li> <li>Parameter estimation is through the nonlinear least squares method</li> <li>Rate Dependent behavior is considered in the range of 30 Hz to 50 Hz with an optimization ratio of 12.05% and 14.04%</li> </ul>
J. Gan	2019	[128]	Compliant Piezo Stage	Bouc–Wen	<ul style="list-style-type: none"> <li>The rate-dependent hysteresis is considered in the frequency range of 5 Hz to 110 Hz</li> <li>Parameters are estimated through the least squares algorithm</li> <li>Reduction in modeling error by about 19.07%, 7.34% at 5 Hz, 110 Hz respectively</li> </ul>
Y. Chen	2019	[129]	Piezo Stack	Preisach	<ul style="list-style-type: none"> <li>Implementation of hysteresis model with neural network approach</li> <li>Model parameter identification through the standard neural network training algorithm</li> </ul>
Y. Li	2019	[130]	Piezo Stack	Prandtl–Ishlinskii	<ul style="list-style-type: none"> <li>The rate-dependent hysteresis behavior in the frequency range of 1 Hz to 80 Hz is considered</li> <li>Model parameters are estimated through the Particle Swarm Optimization algorithm</li> <li>Maximum relative error varied between 5.07% to 12.13%</li> </ul>

Table 2. Cont.

Author	Year	Ref. No.	Type of Actuator	Hysteresis Model	Observation
W. Pan	2019	[131]	Piezo Positioning Stage	Krasnoselskii–Pokrovskii	<ul style="list-style-type: none"> <li>The rate-dependent hysteresis behavior is considered in the frequency range of 1 Hz to 100 Hz</li> <li>Parameter estimation through the interior point algorithm and bat search optimization algorithm</li> <li>The range of maximum error rate achieved is 0.92% to 2.51% for 1 Hz to 100 Hz</li> </ul>
D. Liu	2020	[132]	Piezo Bimorph	Bouc–Wen	<ul style="list-style-type: none"> <li>The rate-dependent hysteresis is considered in the frequency range of 5 Hz to 25 Hz</li> <li>Model parameter estimation through the region based mixed-species swarm optimization</li> </ul>
L. Liu	2020	[133]	Amplified Piezo Stack	Bouc–Wen	<ul style="list-style-type: none"> <li>The rate-dependent hysteresis behavior is considered</li> <li>Model parameter estimation through the least square algorithm</li> </ul>

The rate-independent models are best suited for modeling the hysteresis behavior of the piezoelectric actuators operating at a low-frequency range. With the increase in the actuation frequency to a higher level, the implementation of rate-dependent models can describe the hysteretic behavior effectively. The differential-based models are easy to implement due to a more straightforward approach to solving the differential equations and methods to identify the model parameters. Implementing operator-based models is challenging due to the complexity associated with finding the solution and model parameters. There have been continuous efforts in improvisation of the existing hysteresis model, such as the modified P-I model [134,135] and the modified Preisach model [136,137] for better compensation of dynamic nonlinearity. Furthermore, the neural network-based models [138,139], fuzzy logic models [140,141], and support vector machine-based models [142,143] have also proved to help model the hysteretic characteristics of the piezoelectric actuators.

Table 3. Application of the hysteresis models in the piezo actuation technology reported after 2020.

Author	Year	Ref. No.	Type of Actuator	Hysteresis Model	Observation
C. Zhou	2021	[144]	Piezo Stack	Modified Prandtl–Ishlinskii	<ul style="list-style-type: none"> <li>Modified Prandtl–Ishlinskii with the dead-zone operators (MPI) hysteresis model to describe the asymmetric hysteresis</li> <li>RMSE for modeling the piezoelectric actuator hysteresis is around 0.76%.</li> </ul>
X. Shan	2021	[145]	Pizeo Stack	Prandtl–Ishlinskii	<ul style="list-style-type: none"> <li>Dynamic hysteresis nonlinear model and its inverse model based quasi-static model and linear transfer function</li> <li>Frequency increased from 0.5 Hz to 50 Hz, the average fitting error of the static hysteresis model from 0.027 to 0.187, and for the dynamic hysteresis model from 0.044 to 0.052.</li> </ul>

Table 3. Cont.

Author	Year	Ref. No.	Type of Actuator	Hysteresis Model	Observation
K. Ahmed	2021	[146]	Piezoelectric nano-stage	Duhem	<ul style="list-style-type: none"> <li>Modeling and parameter identification of the Duhem model and parameter optimization modified particle swarm optimization (MPSO) technique</li> <li>The maximum displacement error between the model and experimental data is 0.063 <math>\mu\text{m}</math></li> </ul>
C. Zhou	2022	[147]	Piezo Stack	Prandtl–Ishlinskii	<ul style="list-style-type: none"> <li>Asymmetric Hysteresis modeling through Classical, Modified, and dual-operators-based model</li> <li>Maximum error 38.56 <math>\mu\text{m}</math>, 9.73 <math>\mu\text{m}</math> and 4.15 <math>\mu\text{m}</math> with Classical, Modified and Dual-operators-based model</li> </ul>
W. Wang	2022	[148]	Piezoelectric Positioning Stage	Prandtl–Ishlinskii	<ul style="list-style-type: none"> <li>Multi-slope Prandtl–Ishlinskii (MPI) based hysteresis modeling and compensation for two-dimensional piezoelectric positioning stage</li> <li>More than 99.6% of the fitting coefficient under the driving voltage of 20 V~120 V, and the average absolute error is 0.1192.</li> <li>The average absolute displacement error of the piezoelectric actuator is 0.1192 <math>\mu\text{m}</math>, as well as the mean square error is 0.2949 <math>\mu\text{m}</math>.</li> </ul>
A. G. Baziyad	2023	[149]	Piezoelectric-driven nanopositioning Stage	Preisach	<ul style="list-style-type: none"> <li>Improved Preisach model using least-squares support vector machines (LSSVMs) to deal with the rate-dependent properties</li> <li>The achieved results with the suggested control strategy show that both hysteresis modeling accuracy and tracking performance are significantly improved with average root-mean-square error (RMSE) values of 0.0107 <math>\mu\text{m}</math> and 0.0212 <math>\mu\text{m}</math></li> </ul>
J. Lu	2023	[150]	Fast piezo-driven scanner	Bouc–Wen	<ul style="list-style-type: none"> <li>Weighted polynomial modified Bouc–Wen (WPMBW) model with a linear dynamic model to describe counter-clockwise, asymmetric, and rate-dependent hysteresis loops</li> <li>Maximum percentage modeling error is about 2.17%, 5.03%, 9.56%, 15.01%, and root-mean-square error 0.0113, 0.0295, 0.0592, 0.0983 at 5 Hz, 10 Hz, 15 Hz, and 20 Hz, respectively</li> </ul>

Based on the understanding of the above-described modeling approaches, implementing a particular model majorly depends on rate-dependent or rate-independent behavior. Besides factors such as ease of obtaining the inverse model of the hysteresis model, ease of identification of the model parameters, compatibility and ease of the hysteresis model, and suitable controller occupy significant importance. Table 4 describes, in brief, the comparison of the different hysteresis modeling models.

**Table 4.** Comparison of Hysteresis Models.

Hysteresis Model Parameter	Jiles– Atherton	Domain Wall	Duhem	Bouc–Wen	Backlash Type	Preisach	Prandtl– Ishlinskii	Krasnoselskii– Pokrovskii	Maxwell– Slip
Inverse Model	Easy	Easy	Difficult	Easy	Easy	Difficult	Easy	Difficult	Difficult
Rate-Independent	Yes	Yes	No	No	No	Yes	Yes	Yes	Yes
Rate-Dependent	No	No	Yes	Yes	Yes	No	No	No	No
Parameter Identification	Easy	Easy	Difficult	Easy	Easy	Difficult	Easy	Easy	Easy

## 7. Modeling of Creep Behavior of the Piezoelectric Actuators

The application of a piezoelectric actuator for precision motion requires positioning accuracy and retaining the specific position without any fluctuation. Under the dynamic application of piezoelectric actuators, there is difficulty in maintaining a particular position due to the inherent effect of the creep phenomenon. Creep in the piezoelectric actuator is a time-dependent phenomenon resulting in the slow drift of the output displacement when there is a sudden change in the input voltage [151,152]. The root cause for the creep in the piezoelectric actuators occurs due to the interaction between the applied electric field and the retained polarization. The application of voltage across the piezoelectric materials results in specific orientations of the crystal structure. When there is a change in the applied voltage, the interaction of polarization retained in the materials continues, resulting in a drift termed a creep. Thus, the extent of creep in piezoelectric materials varies as a function of time and the applied voltage. Further, the rate of creep nonlinearity decreases logarithmically with respect to time [153–155].

The mathematical modeling approaches for the creep phenomenon in the piezoelectric actuators are either linear or nonlinear [156]. The linear modeling approach adopts a linear time-invariant dynamic viscoelastic model consisting of springs and dampers connected in series, as shown in Figure 16 [157]. The mathematical formulation of the low-frequency response of the viscoelastic creep model represented in Figure 16 is expressed as follows in Equation (57)

$$\frac{x(s)}{V(s)} = G_x = \frac{1}{k_0} + \sum_{i=1}^{N_{cx}} \frac{1}{C_i s + k_i} \quad (57)$$

where  $V(s)$  represents the input voltage,  $x(s)$  represents the output displacement,  $k_0$  represents stiffness corresponding to elastic deflection,  $N_{cx}$  represents the order of the model, i.e., the number of spring ( $K_i$ ) and damper ( $C_i$ ) elements. The standard deviation and the maximum error corresponding to the model with the measure output  $x_i$ , predicted output of the model  $\bar{x}_i$  is described by Equation (57) is represented as shown in Equation (58) [158]

$$\sigma_c = \sqrt{\frac{1}{N-1} \sum_{i=1}^N (x_i - \bar{x}_i)^2} \quad (58)$$

$$E_{max} = \max_i |x_i - \bar{x}_i| \quad (59)$$

Reasonable accuracy in modeling the creep behavior of the piezoelectric actuators is possible to achieve with the linear model of the third-order model, i.e.,  $N = 3$ . Moreover, the linear creep model has the flexibility of up-gradation to include the high-frequency system dynamics through which the controller can be designed for compensation of non-linearity [158,159].

The second approach to modeling the creep phenomenon in piezoelectric actuators is a logarithmic approach, which follows the logarithmic response of the piezoelectric actuators over time [155]. Mathematically, the nonlinear model can be represented as in Equation (60)

$$x(t) = x_0 \left( 1 + \gamma \log_{10} \left( \frac{t}{t_0} \right) \right) \quad (60)$$

where  $x(t)$  defines the displacement of the piezoelectric actuator upon application of electric potential at time  $t$ ,  $x_0$  corresponds to the displacement of the piezoelectric actuator after the application of electric potential at time  $t_0$ ,  $\gamma$  corresponds to a factor that determines the rate of logarithmic creep response [160,161]. Though the logarithmic-based models effectively describe the creep behavior of the piezoelectric actuators, the dependence of  $x_0$  and  $\gamma$  on the selection of time factor  $t_0$  adds to the complexity of the model. Moreover, the logarithmic model is valid for a specific domain of  $0 > t > \infty$ , the output displacement  $x(t)$  becomes unbounded as the value of  $t$  becomes too large or too small, i.e., as  $t \rightarrow 0$  or  $t \rightarrow \infty$  [55,159–162].

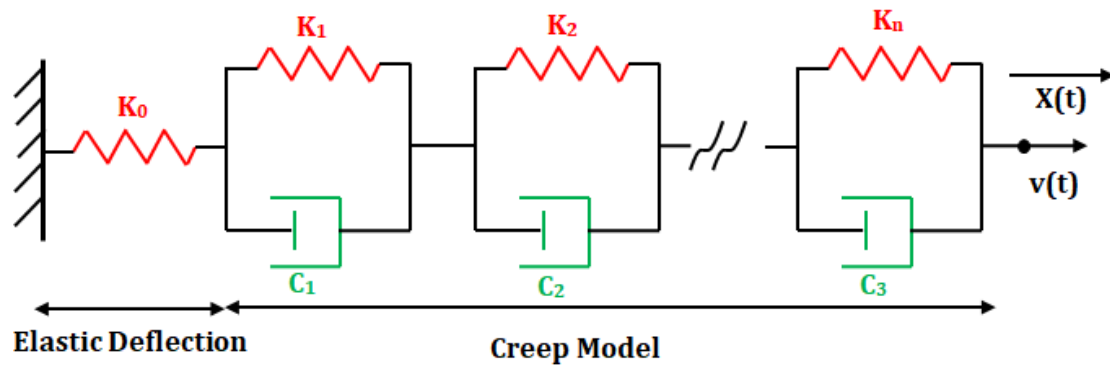


**Figure 16.** Viscoelastic creep model of the piezoelectric actuators.

The linear and the nonlinear creep models for piezoelectric actuators are just the phenomenological descriptions of the creep phenomenon. Therefore, these models provide a brief insight into the creep phenomenon and do not holistically describe the creep phenomenon of the piezoelectric actuator. Other than the lumped model parameter, the piezoelectric actuators can also be modeled as distributed parameter elements with a memory effect. Considering this fact, a fractional-order approach can be adapted to model the creep phenomenon of the distributed parameter model of the piezoelectric actuators. The fractional-order model of order 0 to 1 can adequately define the drift, which can model the creep phenomenon of piezoelectric actuators [133,159].

When the piezoelectric actuators are excited through step input voltage, the early part of the response from the actuators exists for a few milliseconds with resonance, followed by creep, which can be represented as follows in Equation (61) [159].

$$\lim_{s \rightarrow 0} G(s) = \frac{b}{s^\alpha} \quad (61)$$

Since the effect of resonance response of the actuator occurs for a very short duration, i.e., in the order of milliseconds of time  $t_c$ , its effect can be ignored for most applications. Therefore, as shown in Equation (62),

$$\lim_{s \rightarrow 0} G(s) = \frac{b}{s^\alpha} \quad t \geq t_c \quad (62)$$

The response of the piezo actuator after time  $t_c$  with a step input of  $V(s) = 1/s$  can be represented by Equation (63),

$$(t)|_{t \geq t_c} = L^{-1}[G(s)V(s)] = \frac{bt^\alpha}{\alpha\Gamma(\alpha)} \quad (63)$$

where  $\Gamma(\alpha)$  corresponds to the gamma function. Therefore, the mathematical representation of the response of the piezoelectric actuator after the time  $t_c$  based on power law is as follows as shown in Equation (64),

$$\log x(t)|_{t \geq t_c} = \alpha \log t + \log \frac{b}{\alpha \Gamma(\alpha)} \quad (64)$$

Equation (64) represents a creep model of the piezoelectric actuators through the fractional-order approach, also termed the double logarithm creep model. This particular model is useful in predicting the creep behavior of the piezoelectric actuators, which matches well with the experimental data. However, the complexity of the double logarithmic model, when compared with the nonlinear logarithmic model, limits its applications. Moreover, the model applies to time-domain  $t \geq t_c$  and does not consider the effect of time-domain  $t \leq t_c$  [55,159].

## 8. Control Approaches for Piezoelectric Actuator

Precision manipulation through the piezoelectric actuators significantly requires higher accuracy and resolution from the range of micrometers to the nanometers range with a stable response. Such a high level of accuracy and stability is possible if the piezoelectric actuation systems are immune to nonlinear errors occurring under dynamic conditions. The undesirable effects of hysteresis in piezoelectric actuators raise significant concern due to its contribution to possible positioning errors and system inaccuracies. Thus, there is a need to design and develop appropriate control approaches to address and compensate for the undesirable effects of inherent system nonlinearity and to control the actuators to have precise positioning with minimum errors. As mentioned earlier, charge-based control of the piezoelectric actuators can significantly reduce hysteresis errors, but specialized hardware and software requirement limits such an approach. Therefore, voltage-driven mode with Feedforward control, Feedback control, and Feedforward–feedback control approaches are predominantly used to control the piezoelectric actuators [68,163].

### 8.1. Feedforward Control of Piezoelectric Actuators

The feedforward control is the most straightforward and most commonly reported control approach for the precision positioning application of the piezoelectric actuators. The feedforward control is an open-loop approach with an integrated controller that compensates and eliminates the hysteresis nonlinearity error. The critical factor that governs the performance of such a control approach involves the identification of the appropriate hysteresis model and the development of the controller based on the selected hysteresis model [55,163,164].

Figure 17 represents the schematic block diagram of the feedforward control approach of the piezoelectric actuators. One of the approaches towards controller development of feedforward control is associated with obtaining the inverse of the hysteresis model selected. The desired displacement range is input to the feedforward controller embedded with the inverse hysteresis model. The controller output delivers a voltage that drives the piezoelectric actuator to compensate for the hysteresis. Such an approach is effective with operator-based models such as the Preisach model and the Prandtl–Ishlinskii models, whose inverse models are obtained through appropriate numerical methods and are implemented with the feedforward controller to compensate the nonlinearity errors [165–167]. The second approach involves implementing the adopted hysteresis model in the feedforward compensator without any inverse approach. Such an approach predominantly incorporates differential equation-based models such as the Bouc–Wen, Duhem, and Backlash Type models in the feedforward compensator [168,169].

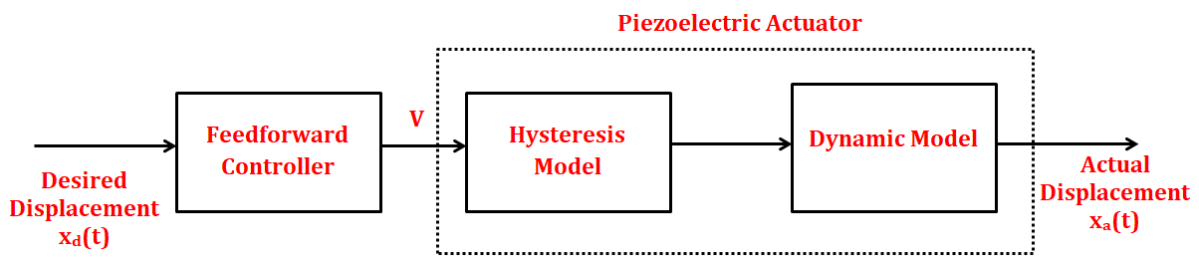


Figure 17. Block diagram of the Feedforward control of the piezoelectric actuator.

The third approach exploits the direct hysteresis inverse compensation technique since the inversion of hysteresis nonlinearity by nature represents the hysteresis loop. The direction of orientation of the hysteresis loop of the piezoelectric actuators depicts the difference between inverse hysteresis and real hysteresis. The readily available inverse hysteresis model can be effectively utilized to characterize the inverse hysteresis effect instead of modeling the real hysteresis nonlinearity, thus eliminating the complex mathematical approach for obtaining the inverse of the identified hysteresis model [170,171]. Such an approach of using the direct inverse model with the inverse Prandtl–Ishlinskii model has been reported in [172,173].

### 8.2. Feedback Control of Piezoelectric Actuators

Feedback control of the piezoelectric actuators is a closed-loop control approach that monitors the real-time information of the output displacement and eliminates the non-linearity error to have linear output. Figure 18 represents the schematic block diagram of the feedback control of the piezoelectric actuator. The feedback controller designs for piezoelectric actuators are categorized based on the utilization of the hysteresis model. One of the design approaches for feedback control does not consider any predefined hysteresis models and considers the hysteresis error as a nonlinear disturbance, which is eliminated according to the error generated between the desired and the actual displacement fed into the controller [174]. The second approach involves selecting and integrating an appropriate hysteresis model in the controller design, which can accurately depict the hysteresis behavior of the piezoelectric actuator [175].

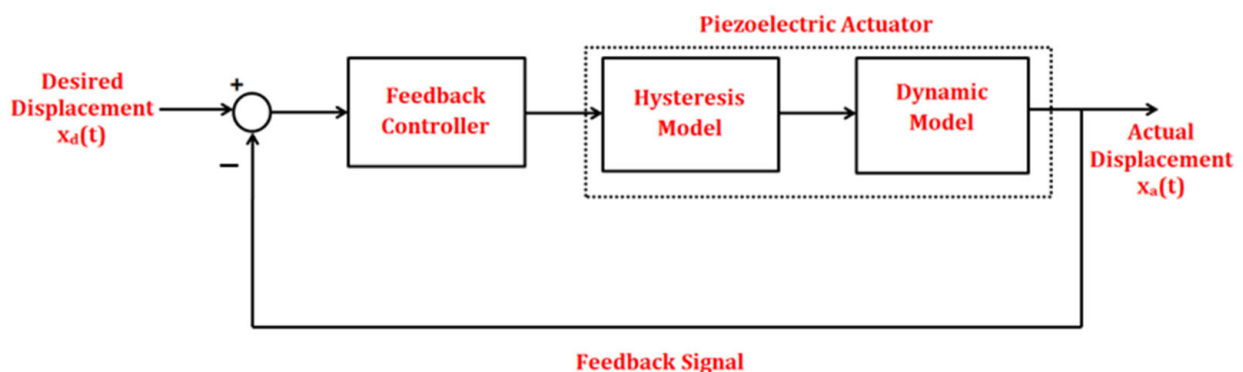


Figure 18. Block diagram of the feedback control of the piezoelectric actuator.

As a feedback controller, the PID controller (proportional integral derivative controller) is suitable for piezoelectric actuators and is utilized extensively in commercial control applications in the form of integral controllers, proportional–integral controllers, and proportional integral derivative controllers [176,177]. Since the feedback control without hysteresis model considers hysteresis nonlinearity as disturbances, modified PID controllers such as adaptive PID controllers [178], Self-tuning PID controllers [179], disturbance observer-based PID controllers [180] and nonlinear PID controllers with extended state observer [181] have been proposed for performance enhancement. Moreover, modern

feedback control approaches such as Neural Network control [182],  $H_\infty$  control [183], and sliding mode control [184] have also been proposed and effectively adopted in feedback control of the piezoelectric actuators. The following sections highlight some feedback control approaches adopted in piezoelectric actuators.

### 8.2.1. Classical PID Controller

The proportional integral derivative (PID) controller is one of the easiest and most convenient control approaches adapted to precision positioning through piezoelectric actuators. The PID controllers effectively suppress the nonlinearity errors occurring in the piezoelectric actuator due to inherent hysteresis and creep by providing high-gain feedback at low frequencies [185]. Figure 19 represents the schematic representation of the generalized PID controller for a piezoelectric actuator.

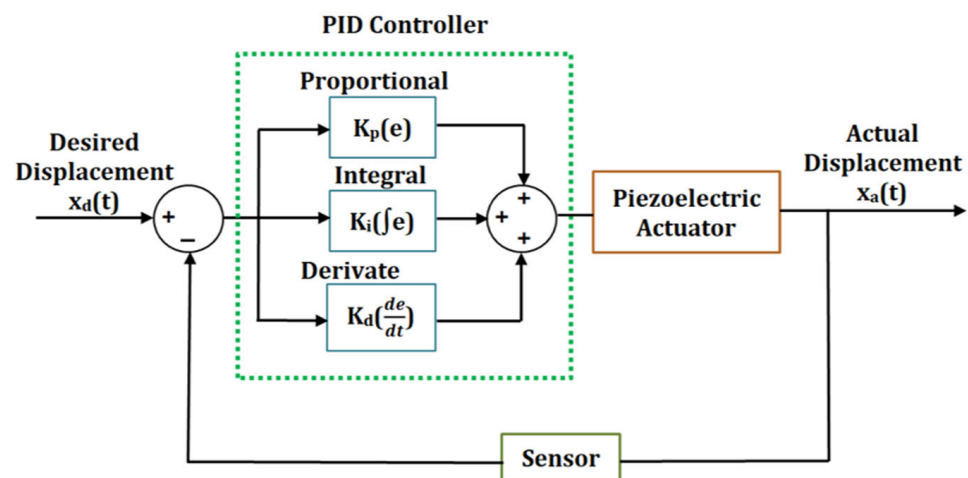


**Figure 19.** General representation of the proportional integral derivative (PID) controller.

The mathematical representation of the PID controller can be expressed as represented in Equation (65)

$$v(t) = K_p e(t) + K_i \int_0^t e(t) dt + K_d \frac{de(t)}{dt} \quad (65)$$

where  $v(t)$  represents the input signal to the piezoelectric actuator with an error  $e(t) = x_d(t) - x_a(t)$ ,  $x_d(t)$  and  $x_a(t)$  corresponds to the desired displacement, and the actual displacement from the piezoelectric actuator,  $K_p$ ,  $K_i$ ,  $K_d$  corresponds to gain factors of proportional, integral and derivative controllers [186–188]. The main factors of the controller have to be tuned to achieve effective control of the actuator. Ziegler–Nichols (Z–N) method, Haalman and  $\lambda$  Tuning method, Pole placement method, Graphic tuning methods, M-constrained integral gain optimization (MIGO) tuning methods, Approximate-constrained integral gain, optimization (AMIGO) and Kappa–Tau tuning method, Internal model principle (IMC) etc. are some of the strategies adopted in tuning the gain factors of the PID controller [185–188].

### 8.2.2. Self-Tuning Fuzzy PID Controller

A self-tuning fuzzy PID controller is another helpful approach to overcoming the nonlinearity in piezoelectric actuators due to continuous variation in the system parameters. The main factors of the PID controller are self-tuned according to the change in the parameters to achieve a stable response [179,189]. Figure 20 represents the schematic block diaphragm of the self-tuning fuzzy PID controller.

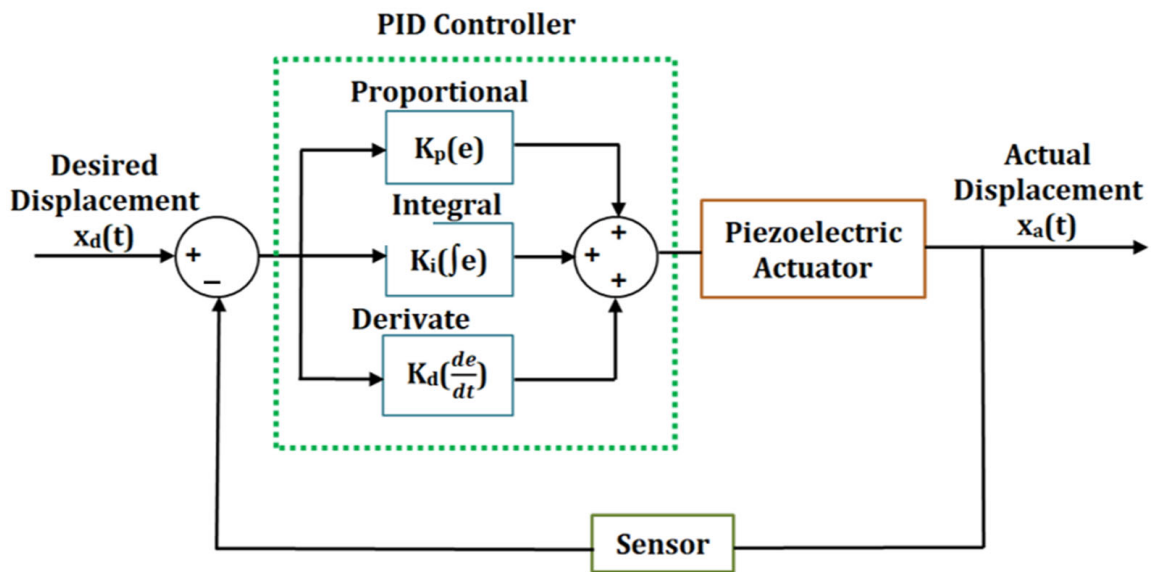


Figure 20. Schematic of the self-tuning fuzzy PID controller.

The control algorithm for the self-tuning fuzzy PID control in a discrete manner is represented as shown in Equation (66)

$$V(t) = K_P e(t) \left[ e(t) + \frac{1}{T_i} \sum_0^t T e(i) + T_d \frac{e(t) - e(t-1)}{T} \right] \quad (66)$$

where,  $K_p$  is the gain factor of the proportional control, and  $T$ ,  $T_d$ , and  $T_i$  are sampling time, derivative time, and integral time intervals. During the control action, the PID controller evaluated the error  $e$  and change in error  $e_c$ . The region of error and error change are  $[-x_e, +x_e]$  and  $[-x_{de}, +x_{de}]$ , and the corresponding control change is  $[-y_v, +y_v]$ . The fuzzy subset of  $e$ ,  $e_c$ ,  $K_p$ ,  $K_i$ , and  $K_d$  are designated with {NB, NM, NS, O, PS, PM, PB}. The effectiveness of self-tuning fuzzy PID controllers depends on the set control rules, with each rule having two causes and three consequences. For example, if  $e$  and  $e_c$  correspond to NB, then  $K_p$ ,  $K_i$ ,  $K_d$  correspond to PB, NB, and NS, respectively [179,189–192]. Thus, there exist 49 sets of control rules according to which the gain factors will be tuned with modification factors  $q_p$ ,  $q_i$ , and  $q_d$ , as follows represented by Equation (67);

$$\begin{aligned} K_P &= K'_P + \{e, e_c\} * q_p \\ K_i &= K'_i + \{e, e_c\} * q_i \\ K_d &= K'_d + \{e, e_c\} * q_d \end{aligned} \quad (67)$$

The control rules of the self-tuning PID controller are tabulated, processed, and tuned automatically through an online approach [192].

### 8.2.3. Fractional Order Fuzzy PID Controller

Typically, the FOFPID controller is a generalization of the PID controller, and the non-integer nature of the order of derivative  $\mu$  and integral  $\lambda$  leads to the better dynamic performance of the system [193]. The transfer function  $G(s)$  and the output  $v(t)$  of the FOFPID controller are represented as shown in Equations (68) and (69),

$$G(s) = K_p + K_i s^{-\lambda} + K_d s^\mu \quad (68)$$

$$v(t) = K_p e(t) + K_i D^{-\lambda} e(t) + K_d D^\mu e(t) \quad (69)$$

where  $K_p$ ,  $K_i$ ,  $K_d$  are the gains of the proportional, integral, and derivative gains and  $\lambda$ ,  $\mu > 0$ . Figure 21 represents the schematic of a fractional-order Fuzzy PID (FOFPID) controller. The parameters of the controller, such as  $K_{de}$ ,  $K_e$ ,  $\alpha$ ,  $\beta$ , and  $\mu$ , are determined through the dynamic parameter estimation algorithms. A set of fuzzy rules are defined for the controller with the fuzz values NL (Negative Large), NM (Negative Medium), NS (Negative Small), ZO (Zero), PS (Positive Small), PM (Positive Medium), PL (Positive Large), respectively. For optimal performance, the controller parameters  $K_{de}$ ,  $K_e$ ,  $\alpha$ ,  $\beta$ ,  $\lambda$ , and  $\mu$  are to be determined and optimized according to the fuzzy control rules defined [193–196].

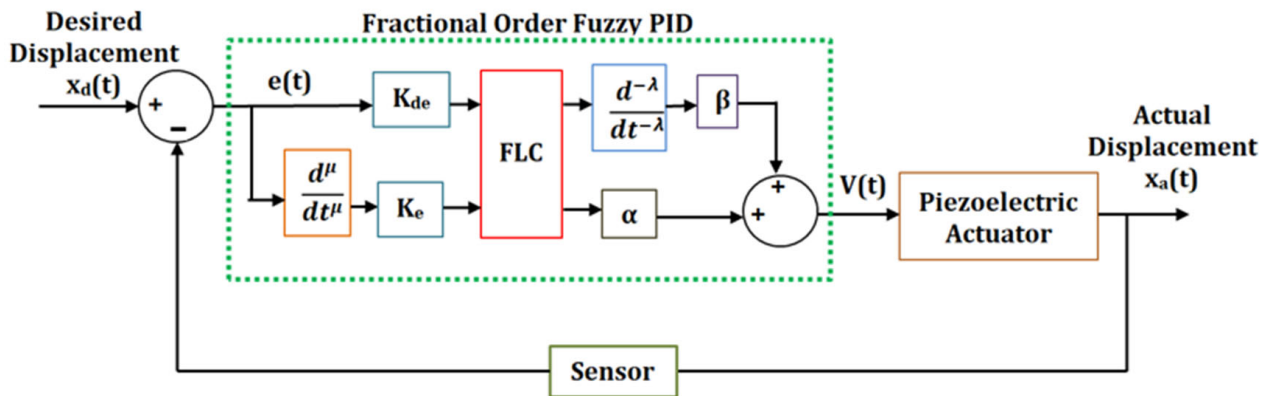


Figure 21. Schematic of the fractional order fuzzy PID controller.

#### 8.2.4. Disturbance Observer-Based PID Controller

The schematic representation of the disturbance observer-based PID controller for the piezoelectric actuator is represented in Figure 22. The disturbance observer-based controls find extensive application in motion control applications. The disturbance observer determines the error in the displacement of the piezoelectric device based on the reference input and the output displacement [180,197–200].

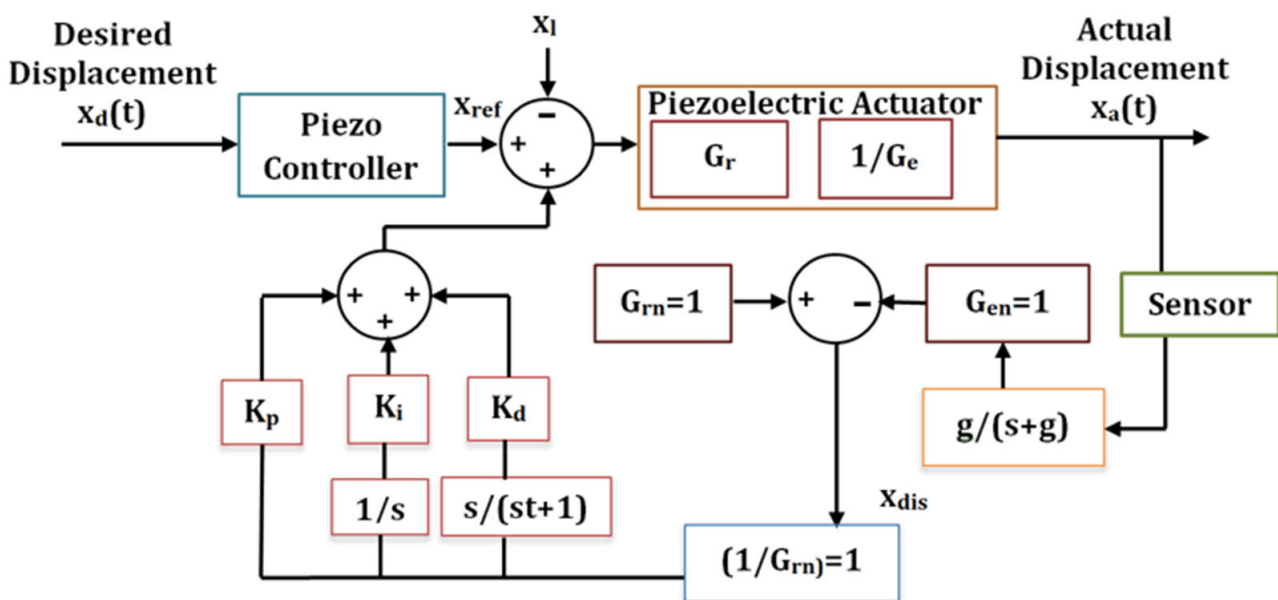


Figure 22. Schematic of the disturbance observer-based PID Controller.

The control value of the disturbance observer is the position value of the piezoelectric actuator. The concept of disturbance observer is based on the following formulations in Equations (70) and (71),

$$\begin{aligned} G_e &= G_{en} + \Delta G_e \\ G_r &= G_{rm} + \Delta G_r \end{aligned} \quad (70)$$

$$\begin{aligned} x_{dis} &= x_l + \Delta G_e x - \Delta G_r x_{ref} \\ x_{dis} &= G_{rm} x_{ref} - G_{en} x \end{aligned} \quad (71)$$

where  $G_r, G_e$  corresponds to the coefficient transfer ratio between the desired displacement, the actual displacement, and the coefficient of transfer ratio between the actual displacement and the measured displacement from the sensor, respectively.  $G_{rm}$  and  $G_{en}$  represent the optimal value of the disturbance observer parameter with corresponding errors  $\Delta G_r$  and  $\Delta G_e$ , respectively;  $x_l$  represents error displacements of the piezoelectric actuator with disturbance. Thus, according to the disturbance fed, the gain factors of the PID controller are tuned as expressed in Equation (65), where  $K_p, K_i, K_d$  are the gains of the proportional, integral, and derivative gains, and  $x_p, x_i, x_d$  are the corresponding control values [198].

$$x_p = K_p x_{dis} \quad x_i = \frac{K_i x_{dis}}{s} \quad x_d = \frac{K_d x_{dis}}{st + 1} \quad (72)$$

$$x_{dis} = x_p + x_i + x_d \quad (73)$$

### 8.2.5. H $\infty$ Controller

The H $\infty$  control approach is adopted in the piezoelectric actuators to ensure stabilized motion under dynamic operating conditions [183,200–203]. The control of the piezoelectric actuator with H $\infty$  can be represented in generalized form as shown in Figure 23a, with  $X_a$  representing the measured output of the piezoelectric actuator  $P(s)$ , which produces an error signal  $e$ , controlled through a controller  $K(s)$  with a control signal  $u$  and input signal  $x$  consisting of command signal with noise and interference signal from the sensor [204]. The H $\infty$  approach aims at determining the controller parameters such that the ratio between the error and the external signal  $w$  is minimized [205,206]. Based on the H $\infty$  rule, the expression for the transfer function matrix between  $x$  and  $e$  is represented in (74) [207],

$$\begin{pmatrix} E(s) \\ Y(s) \end{pmatrix} = P(s) \begin{pmatrix} X(s) \\ U(s) \end{pmatrix} = \begin{pmatrix} P_{ex}(s) & P_{eu}(s) \\ P_{xa}(s) & P_{xa}(s) \end{pmatrix} \begin{pmatrix} X(s) \\ U(s) \end{pmatrix} \quad (74)$$

The linear fraction transformation of the transfer function between  $x$  and  $e$  is as follows in (75)

$$E(s) = F_l(P(s), K(s))W(s) \quad (75)$$

$$F_l(P(s), K(s)) = P_{ew}(s) + P_{eu}(s)K(s)(I - P_{yu}(s)K(s))^{-1}P_{yw}(s)$$

Figure 23b represents the schematic of control of the piezoelectric actuator under the closed-loop H $\infty$  control method with weighting filters. The effectiveness of the H $\infty$  controller in the stabilization of the response of the piezoelectric actuator is based on Equation (76), where the factor  $\gamma$  is updated iteratively to maintain the condition.

$$\|F_l(P(s), K(s))\|_{\infty} < \gamma \quad (76)$$

Therefore, based on the configuration of the H $\infty$  controller, the transfer matrix and the condition to be satisfied by the controller  $K(s)$  be represented as follows

$$\begin{pmatrix} \varepsilon \\ u \end{pmatrix} = \begin{pmatrix} K & SG \\ KS & KSG \end{pmatrix} \begin{pmatrix} r \\ b \end{pmatrix}; S = \frac{1}{(1 + KG)} \Rightarrow \left\| \begin{pmatrix} K & SG \\ KS & KSG \end{pmatrix} \right\| < \gamma \quad (77)$$

where  $S$  corresponds to the factor of sensitivity, which equals the transfer function between the desired displacement  $X_d$  and the error  $e$ . To satisfy the above condition, the  $H_\infty$  is assigned weighting filters ( $W_i$ ), as represented in Figure 23b, based on the frequency domain of the plant [206]. Thus, the transfer matrix of the  $H_\infty$  controller with the weighting filters can be represented as

$$\begin{pmatrix} e_1 \\ e_2 \end{pmatrix} = \begin{pmatrix} W_1 S & W_1 S G W_3 \\ W_2 K S & W_2 K S G W_3 \end{pmatrix} \begin{pmatrix} r \\ d \end{pmatrix} \quad (78)$$

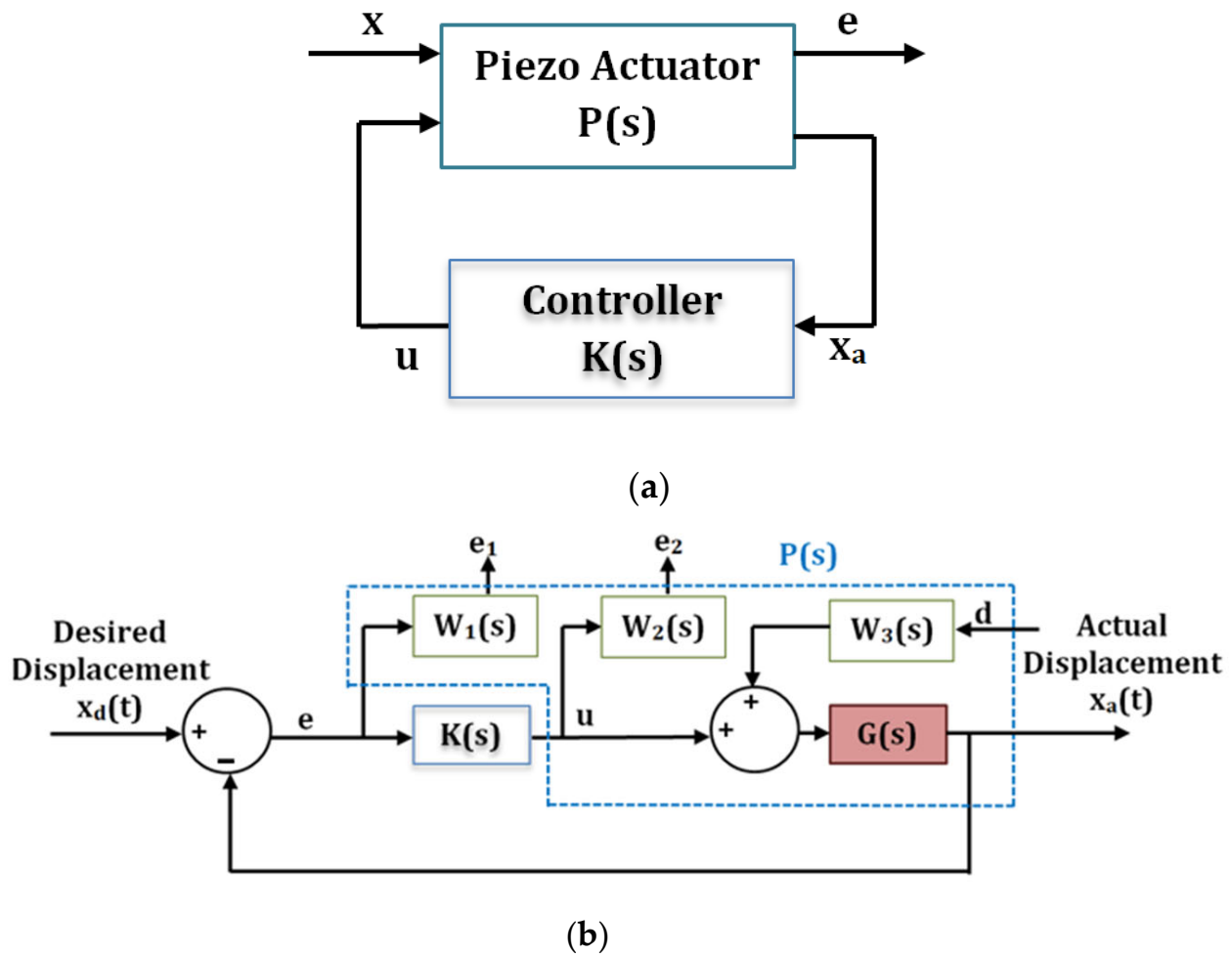


**Figure 23.** (a) Schematic of the piezoelectric actuator as a generalized plant (b) Schematic of control of the piezoelectric actuator under closed loop  $H_\infty$  control method with weighting filters.

Based on the frequency domain of the system, the expression for the weighting filter parameters with a close loop bandwidth of  $\omega_0$  is expressed as in Equation (79)

$$W_i = \frac{\frac{s}{M} + \omega_0}{s + A\omega_0} \quad (79)$$

where,  $A$ ,  $M$  correspond to minimum steady-state error and high-frequency amplification gain, respectively. The performance of the  $H_\infty$  greatly depends on the selection of weighting filter parameters [206]. The selection of weighing filter parameters depends on factors such as frequency bandwidth, stability margin, and the extent of steady-state error acceptable under the dynamic operation of the piezoelectric actuator [204–207].

### 8.2.6. Sliding Mode Control

Sliding mode control is a nonlinear control approach characterized by a discontinuous feedback control structure that triggers a change in the positioning trajectory of the system and ensures the system can reach and maintain a specific position/surface through a state space called the sliding surface. The feedback approach adopted in the sliding mode control is not continuous; instead, it adopts a switching function, which switches from one continuous structure to another based on the current position of the actuator [208–211]. Figure 24 represents the block diagram of the sliding mode control approach for the piezoelectric actuator.

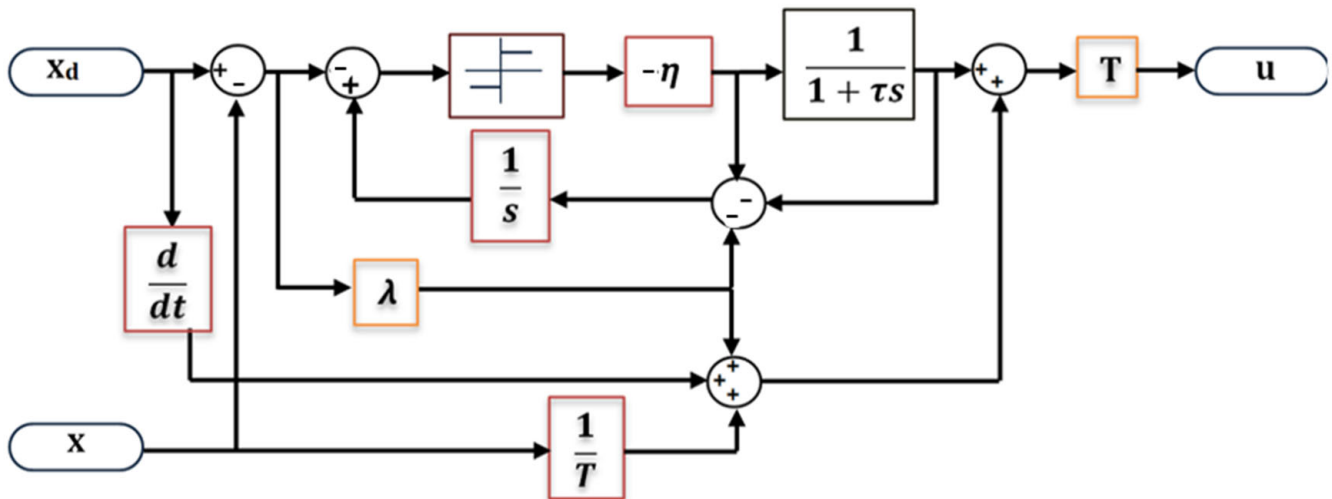


Figure 24. Schematic representation of the sliding mode controller of the piezoelectric actuator.

Mathematically, the control law under sliding mode control can be expressed as in Equation (80) [208]

$$u = y + T(\lambda e + \dot{x}_d) + u_d \quad (80)$$

where  $\lambda$  represents the feedback gain of the controller, which has to be tuned to reduce the error  $e$  between the desired displacement  $x_d$  and the current position  $x$ ,  $u_d$  represents the compensation component for disturbance and uncertainty in the system, which has to be determined by the estimator of the sliding mode controller.

$$e = x_d - x \Rightarrow \dot{e} = \dot{x}_d - \dot{x} = \dot{x}_d + \frac{x}{T} - \frac{u}{T} - (t) \quad (81)$$

The switching function  $S$  for the controller with switching action  $\Psi$  and state variable  $z$  is represented as in Equation (82)

$$S = z - e \quad (82)$$

$$\text{where } z = -\lambda e - \frac{1}{T}u_d + \psi \text{ with } Z(0) = e(0)$$

where,

$$\psi = -\eta \text{sign}(S), \text{ sign}(S) = \begin{cases} 1 & \text{if } S < 0 \\ 1 & \text{if } S > 0 \end{cases} \text{ such that } \eta > |\dot{e}(t)| \quad (83)$$

Considering a sliding system  $S = 0$  with Lyapunov candidate  $V = 0.5 S^2$ , the sliding condition is valid for  $\dot{V} < 0$  if  $S \neq 0$  where  $\dot{V} = S(\dot{z} - \dot{e}) = S[(-\eta \text{sign}(S) + \dot{\psi}(t))]$ . Since  $Z(0) = e(0)$ ,  $S = 0$  for  $t = 0$ . Thus,  $S = 0$  for  $t \geq 0$ , this indicates the existence of sliding mode at all times. With  $S = 0$ , the equivalent value of uncertainties and disturbances  $\Psi_{eq}$

corresponds to input with the average measured value through the first-order linear filter and switching action [208,209].

$$\Psi_{eq} = -\phi \text{ and } u_d = T\Psi_{eq} \text{ with } \tau\dot{\Psi}_{av} + \Psi_{av} = \Psi \quad (84)$$

To allow the disturbances and plant dynamics to pass through the filter, the time constant  $\tau$  is chosen to be as small as possible ( $\tau \approx 1/\lambda$ ). Thus, the error dynamics of the sliding mode control can be represented as Equation (85) [209]

$$\dot{e} + \lambda e = -\Psi_{eq} - \phi = 0 \quad (85)$$

### 8.3. Feedforward–Feedback Control of Piezoelectric Actuators

Though feedforward and feedback control approaches are advantageous, the experimental approach has established the model uncertainty associated with the simple feedforward control and the limited bandwidth with the pure feedback control. Therefore, the concept of feedforward–feedback control emerged, which follows an integrated approach that utilizes the advantages features of both feedforward and feedback control and is typically used for high-speed and high-precision operations of the piezoelectric actuators [212,213]. Figure 25 represents the block diagram of the feedforward–feedback control of the piezoelectric actuator.

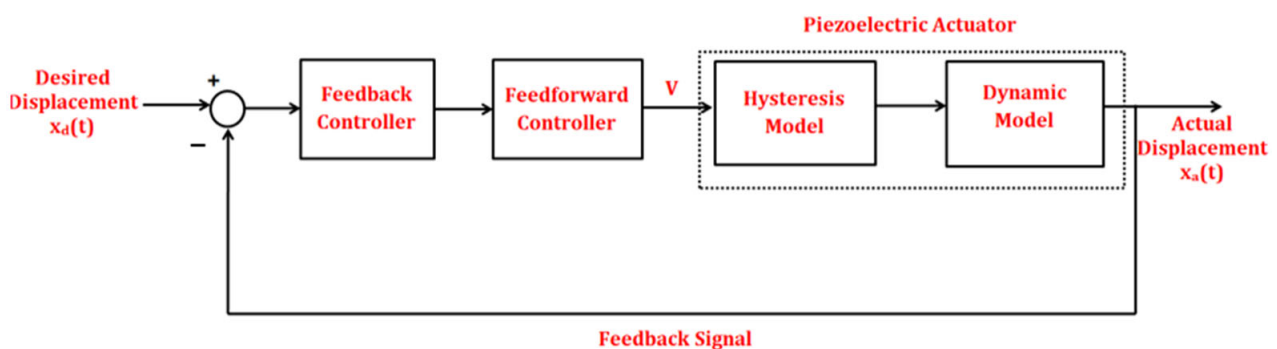


**Figure 25.** Block diagram of the feedforward–feedback control of the piezoelectric actuator.

The feedforward control usually adopts an inverse hysteresis compensator through the Preisach model, the Prandtl–Ishlinskii model, and the Bouc–Wen model, which compensates the inherent hysteresis nonlinearity of the system [214–216]. The feedback control looks after the model uncertainty associated with the piezoelectric actuator and eliminates the residual errors due to inaccuracy in modeling the hysteresis behavior. Commonly, the feedback control adopts PID-based controllers [217–219]; moreover, adaptive-based control [220],  $H_\infty$  control [221,222], and slide mode control [223] are effectively employed in feedforward–feedback control to have better performance.

### 8.4. Applications of Control Strategies in Piezoelectric Actuators

Over the past few years, several control methods have been proposed and physically implemented to eliminate the nonlinearity in the piezoelectric actuator under dynamic applications. The feedforward control has the advantage of ease of implementation among different control approaches due to the simple structure [171,172]. The feedforward control is based on the inverse hysteresis model, which describes the hysteresis behavior of the piezoelectric actuators. Thus, the Feedforward approach is effective in the elimination of hysteresis nonlinearity by providing appropriate compensation. However, positioning accuracy with feedforward control depends solely on the accuracy of the hysteresis model selected due to the open-loop characteristics [172,173]. Moreover, the Feedforward control approach cannot reject the effect of dynamic disturbances. However, the feedforward

approach can be effectively implemented in micro/nanopositioning due to the insignificant effect of load and negligible mass of the object to be positioned.

The feedback closed-loop control approach offers the advantage of real-time control of the piezoelectric actuator displacement with the capability of handling modeling uncertainties and nonlinearities. However, the hysteresis nonlinearities severely affect the system's stability with feedback control. Furthermore, feedback control is effective only in the low-frequency range with a limited travel range. The system complexity of closed-loop, coupled with the low gain margin, limits the application of the feedback controllers for high-frequency operations. The PID control approach is most widely used due to its simple structure and robust performance compared to other closed-loop feedback approaches. An optimized PID controller greatly enhances the tracking performance of the piezoelectric actuator under dynamic conditions [185–188]. However, the PID controllers require continuous monitoring due to the variation of controller parameters when external disturbances lead to system instability. A self-tuning fuzzy PID controller effectively manages the variation of controller parameters through a self-tuning algorithm in the presence of disturbances. The self-tuning fuzzy PID controller can adjust the controller parameter according to external disturbances. It adopts an online approach of adjusting the scaling factor of the input and output of the derivative and integral coefficients of the fuzzy PID controller, respectively [189–192].

The robustness of the PID controller has been enhanced through the implementation of fractional calculus. The performance of the fractional-order fuzzy PID (FOFPID) controller has proved to be better in terms of performance when compared with the conventional PID controller. The performance of the FOFPID controller depends on the order of the integral and derivative operators of the PID, fuzzy rules, the scaling factor of the input and the output, and controller parameters. The controller parameters need to be selected based on the dynamics of the piezoelectric actuators through a suitable optimization technique [193–196]. The disturbance observer-based fuzzy logic PID controller eliminates the external disturbances and uncertainties effectively to provide stable control of the piezoelectric actuator.

The hysteresis nonlinearity can be treated as a disturbance with the observer-based PID controller, eliminating the need to model the hysteresis behavior of the piezoelectric actuator. The controller parameters are optimized with appropriate tuning methods to reduce the nonlinearity existing in piezoelectric actuators [197–199]. Apart from the PID controller, many works on control of the piezoelectric actuator have reported the effectiveness of the  $H_\infty$  control approach.  $H_\infty$  control ensures robustness and excellent performance with a high rate of disturbances rejection and guaranteed stability of the piezoelectric actuator under dynamic operating conditions [205–207]. The sliding mode of control also ensures a robust control of the piezoelectric actuator and effectively eliminates undesirable dynamic nonlinearity. The significant advantage of sliding mode control is the insensitivity to plant parameter variation and external disturbances. The complexity of the feedback design is simplified with sliding mode control due to the decoupling of the overall motion of the piezoelectric actuator system into partial components of a lower dimension [209–211]. The combined approach of feedback and feedforward control significantly improves the performance when compared with feedforward and feedback control separately. Feedforward–feedback control effectively enhances the bandwidth, ensures improved precision motion, and eliminates noise, positioning errors, and disturbances [221,223]. However, the enhanced performance is achieved at the cost of increased complexity in the control architecture due to the feedforward and feedback control approach [55,224]. Table 5 highlights the application of different control methods in the position control of piezoelectric actuators.

Table 5. Application of different control strategies in the piezoelectric actuator technology.

Author	Year	Ref. No.	Control Method	Type of Actuator	Sensor Used in Control	Observation
W. T. Ang	2007	[164]	Feedforward	Piezo Stack	N/A	<ul style="list-style-type: none"> <li>Minimization of the error due to the dynamic interaction of the hysteresis and vibration for high-frequency tracking control of the piezo stack actuator</li> <li>Adopted the rate-dependent inverse PI hysteresis model</li> <li>Reduction in the maximum tracking RMS error and the maximum error by 81.7% and 74.4%, respectively in the frequency band of 1 Hz–19 Hz</li> </ul>
K. K. Leang	2009	[166]	Feedforward	Piezo Tube	N/A	<ul style="list-style-type: none"> <li>The inversion-based feedforward control to compensate hysteresis, vibration, and creep in the piezo tube actuator is considered for the Atomic Force Microscope</li> <li>Adopted the inverse Preisach hysteresis model</li> <li>A maximum difference of displacement is about 2% of the <math>\pm 30 \mu\text{m}</math> range</li> </ul>
G. Y. Gu	2012	[171]	Feedforward	Piezo Stack	N/A	<ul style="list-style-type: none"> <li>A Real-time Feedforward controller with inverse hysteresis compensation is considered</li> <li>Modified PI model with Identification of model parameters through the effective informed adaptive particle swarm optimization (EIA-PSO) algorithm</li> <li>Maximum tracking error is about 12% which is further reduced to 1% with the feedforward control with an overall reduction of 90%.</li> </ul>
D. Wang	2015	[173]	Feedforward	Piezo Tube	N/A	<ul style="list-style-type: none"> <li>Feedforward controller based on the direct inverse asymmetric PI hysteresis model (DISPI) is considered</li> <li>Estimation of model parameters through the least square fit algorithm</li> <li>Reduction in the mean RMS error by about 75% through the DI-API-based Feedforward control</li> </ul>
N. U. Rahman	2012	[187]	Feedback Classical PID	Piezo Cantilever	Piezo Strain Sensor	<ul style="list-style-type: none"> <li>The classical PID controller is considered for active vibration control of the piezoelectric beam</li> <li>Effective vibration suppression and doubling of damping factor when compared with the open loop response</li> <li>Sustained natural frequency of the beam, reduced value of modal vibration amplitude</li> </ul>
B. Ding	2016	[188]	Feedback Classical PID	Piezo Stack	Capacitive Sensor	<ul style="list-style-type: none"> <li>A self-tuning PID controller to track the trajectory of the piezoelectric actuator with hysteresis</li> <li>System dynamic model through the Bouc–Wen model</li> <li>Estimation of the model parameters and tuning of the controller through the particle swarm optimization method</li> <li>A good match between the desired and the experimental displacement of the actuator</li> </ul>

Table 5. Cont.

Author	Year	Ref. No.	Control Method	Type of Actuator	Sensor Used in Control	Observation
S. Bing	2008	[191]	Feedback Self-Tuning Fuzzy PID	Piezo Positioning Stage	Laser Vibrometer	<ul style="list-style-type: none"> <li>• Quick and precise control of tilt and piton movement in the precision fast positioning system (PFPM)</li> <li>• Enhancement of the frequency response up to 1.4 kHz to 1.45 kHz with the elimination of overshoot</li> <li>• Enhancement of the static and the dynamic response</li> </ul>
Dongjie Li	2017	[192]	Feedback Self-Tuning Fuzzy PID	Piezo Positioning Stage	-	<ul style="list-style-type: none"> <li>• Dynamic tracking control of multi-degree freedom piezo positioning stage</li> <li>• Dynamic model description through the Bouc–Wen Model</li> <li>• Minimization of the overshoot with the enhancement of transient response</li> <li>• Precise tracking of the actuator trajectory</li> </ul>
I. R. Birs	2017	[196]	Feedback Fractional Order Fuzzy PID	Piezo Cantilever	Piezo Strain Sensor	<ul style="list-style-type: none"> <li>• Vibration attenuation of the aircraft wing through the piezo patches</li> <li>• Controller tuning is carried out under the variable frequency depending on the magnitude and phase of the closed loop transfer function leading to attenuation of the resonant peak</li> <li>• Significant reduction in the vibration amplitude when compared with the passive case where the control algorithm remains off</li> </ul>
J. Yi	2009	[197]	Feedback Disturbance Observer PID	Piezo Cantilever	Fiber Optic Sensor	<ul style="list-style-type: none"> <li>• Disturbance observed PID controller for minimization of hysteresis error in the piezo cantilever</li> <li>• Elimination of phase lag in the tip displacement corresponding to the reference displacement with DOB PID controller</li> <li>• The convergence of the output displacement without any oscillations</li> <li>• The observed steady-state error is about 80 nm.</li> </ul>
N. Chuang	2010	[202]	Feedback H Infinity	Piezo Stack	Differential Probe	<ul style="list-style-type: none"> <li>• Minimization of hysteresis error in the piezo stack actuator through the H<math>\infty</math> controller</li> <li>• Effective elimination of the tracking error after the implementation of H<math>\infty</math> controller</li> <li>• Almost perfect match between the reference displacement and the output displacement from the actuator</li> </ul>
S. Xiao	2014	[203]	Feedback H Infinity	Piezo Stack	Capacitive Sensor	<ul style="list-style-type: none"> <li>• Tracking control and hysteresis compensation of the stack actuator</li> <li>• Modeling of rate-dependent hysteresis through the Bouc–Wen model</li> <li>• Reduction in the RMS error and the maximum error from 9.3656 <math>\mu\text{m}</math> and 11.8839 <math>\mu\text{m}</math> to 3.0701 <math>\mu\text{m}</math> and 5.8218 <math>\mu\text{m}</math> respectively at 100 Hz</li> </ul>

Table 5. Cont.

Author	Year	Ref. No.	Control Method	Type of Actuator	Sensor Used in Control	Observation
M. Brahim	2018	[206]	Feedback H Infinity	Rotary Piezo Motor	Torque Sensor	<ul style="list-style-type: none"> <li>• <math>H_{\infty}</math> controller proved to be effective in rejection of the sensor noise and the system oscillations when compared with the conventional PI controller</li> <li>• High precision motion without overshoot, and steady-state accuracy of <math>0.009^{\circ}</math> for an overall range of <math>90^{\circ}</math></li> </ul>
S. Huang	2009	[209]	Feedback Sliding Mode	Piezo Stack	LVDT	<ul style="list-style-type: none"> <li>• To achieve optimal tracking performance of the piezo stack actuator under the influence of uncertain hysteresis dynamics</li> <li>• Better tracking accuracy with the sinusoidal and the saw-toothed trajectory</li> <li>• Minimized tracking error of <math>0.5 \mu\text{m}</math> with the feedback sliding controller when compared with tracking error of <math>1.5 \mu\text{m}</math> achieved with the classical PID controller</li> </ul>
M. Wehr	2019	[210]	Feedforward Sliding Mode	Piezo Stack	N/A	<ul style="list-style-type: none"> <li>• SMC was designed with the state observer to compensate for the uncertainties in the piezoelectric stack actuator in a cold rolling mill for the adjustment of the roll gap</li> <li>• Achieved fast trajectory without any phase delay with elimination of dynamic disturbances</li> <li>• Mean tracking error of <math>5.38 \mu\text{m}</math> and <math>8.48 \mu\text{m}</math> at low force and high force receptively</li> </ul>
Z. Yu	2020	[211]	Feedback Sliding Mode	Piezo Positioning Stage	Laser Sensor	<ul style="list-style-type: none"> <li>• Compensation of the hysteresis dynamics in the piezo positioning stage</li> <li>• Description of the hysteresis through the Modified Prandtl–Ishlinskii (MPI) model</li> <li>• Parameter estimation through the particle swarm optimization</li> <li>• Reduction in the linearity error from 10% to 1% and the tracking error reduction by 90%</li> </ul>
H. Y. Chen	2018	[216]	Feedforward-Feedback	Piezo Stack	Load Cell	<ul style="list-style-type: none"> <li>• Hysteresis Compensation of the piezo stack actuator</li> <li>• Combination of Feedforward inverse hysteresis compensation with the Prandtl–Ishlinskii and Feedback control with the PID controller</li> <li>• Significant reduction in the hysteresis and tracking error</li> <li>• Root-mean-square error in the tracking performance is <math>0.0162 \mu\text{m}</math>, <math>0.0243 \mu\text{m}</math>, and <math>0.0292 \mu\text{m}</math> at 1 Hz, 3 Hz and 5 Hz respectively</li> </ul>
A. Saleem	2019	[218]	Feedforward-Feedback	Amplified Piezo Stack	Laser Sensor	<ul style="list-style-type: none"> <li>• Adaptive self-learning Feedforward–feedback controller for tracking the amplified piezo actuator</li> <li>• Description of the hysteretic behavior through the Bouc–Wen and ARMA models,</li> <li>• Parameter model estimation through the recursive least square</li> <li>• Maximum error tracking error is about <math>0.4 \mu\text{m}</math>, <math>0.5 \mu\text{m}</math>, and <math>0.5 \mu\text{m}</math> at 10 Hz, 30 Hz, and 50 Hz respectively</li> </ul>

Table 5. Cont.

Author	Year	Ref. No.	Control Method	Type of Actuator	Sensor Used in Control	Observation
I. Ahmad	2016	[222]	Feedforward-Feedback	Piezo Positioning Stage	N/A	<ul style="list-style-type: none"> <li>Minimization of error due to the dynamic interaction of hysteresis and vibration for high-frequency tracking control of the piezo stack,</li> <li>Adopted rate-dependent inverse PI hysteresis model</li> <li>Reduction in maximum the tracking RMS error and maximum error by 81.7% and 74.4%, respectively in the band of 1 Hz to 19 Hz</li> </ul>
C. Napole	2021	[225]	Feedforward With ANN	Piezo Stack	N/A	<ul style="list-style-type: none"> <li>Elimination of nonlinearity through artificial neural network (ANN) Feedforward close-loop compensator utilizing Quasi continuous sliding mode control (QCSMC)</li> <li>QCSM with ANN has superior performance compared to classical PID controllers.</li> <li>The difference in Integral of absolute error between QCSMC and PID is about 53.07%, 81.5% 33.6%, 46.5%, 79.7%, and 38.5% with Triangular, Sine, and Variable amplitude signals.</li> <li>The difference in root-mean-square error between QCSMC and PID is 46.5%, 79.7%, and 38.5% with Triangular, Sine, and Variable amplitude signals.</li> </ul>
S. Yu	2021	[226]	Feedback Sliding-Mode Control	Piezo Positioning Platform	-	<ul style="list-style-type: none"> <li>Bouc–Wen model and linear time-invariant system to model static and rate-dependent hysteresis coupled with extended state observer–based fractional order sliding-mode (ESO- FOSMC) control to eliminate higher order un-modelled dynamics and inverse compensation errors</li> <li>The positions error with extended state observer–based fractional order sliding-mode control is between 0.2992 <math>\mu\text{m}</math> to 0.9060 <math>\mu\text{m}</math> for a frequency range of 10 to 50 Hz.</li> </ul>
D. Li	2021	[227]	Feedback Fuzzy Controller	Piezo Stack	Laser Sensor	<ul style="list-style-type: none"> <li>A feedback controller based on fuzzy logic for the elimination of chatter in the milling tool</li> <li>Comb filtering pre-process the vibration displacements of the tool holder which eliminates spindle rotation frequency and its harmonic components</li> <li>The approach reduced the mean square value of the control voltage to 6.5% (2.3%) of that without comb filtering.</li> </ul>

Table 5. Cont.

Author	Year	Ref. No.	Control Method	Type of Actuator	Sensor Used in Control	Observation
S. Yu	2022	[228]	Feedforward Control With Composite Proportional–Integral Sliding Mode Control	Piezo Stack	Laser Sensor	<ul style="list-style-type: none"> <li>• High-precision motion control of the cell puncture mechanism driven by a piezoelectric stack through Hysteresis modeling and compensation</li> <li>• A feedforward (FF) control and proportional–integral sliding mode feedback (PIFB) control based on the Bouc–Wen inverse model to position the cell puncture mechanism</li> <li>• The maximum error and RMS error with the FF+PIFB control approach is about 0.0272 <math>\mu\text{m}</math>, 0.0235 <math>\mu\text{m}</math>, 0.0229 <math>\mu\text{m}</math> and 0.08 <math>\mu\text{m}</math>, 0.12 <math>\mu\text{m}</math>, 0.36 <math>\mu\text{m}</math> for sinusoidal signal, sinusoidal signal with variable frequency and amplitude and triangular signal respectively.</li> </ul>
B. Shi	2022	[229]	Feedforward /Feedback	Amplified Piezo Stack	Capacitive Sensor	<ul style="list-style-type: none"> <li>• The feedforward controller is built to compensate for the hysteresis characteristics with a rate-dependent P–I inverse hysteresis model with the relevant parameters and a feedback controller with an adaptive control algorithm to reduce the influence of external disturbance.</li> <li>• The settling time of the combined controller is 53 ms with a square wave, which is reduced by 75% when compared with the rate-dependent hysteresis model and proportional–integral–derivative controller.</li> <li>• The tracking error of 3.66% and 3.88% is achieved with the trajectory at 5 Hz and 20 Hz.</li> </ul>
Y. Xiong	2022	[230]	Feedforward Control	Piezo Positioning Platform	N/A	<ul style="list-style-type: none"> <li>• A recurrent neural network (RNN) is used in Feedforward control to control accuracy, reduce the training time, and online model updating</li> <li>• With RNN compensation, the maximum displacement error of the piezoelectric actuator is reduced to 0.465 <math>\mu\text{m}</math> at the operating frequency of 10 Hz.</li> </ul>
L. Cheng	2023	[231]	Feedback Sliding Mode	Piezo Stack	Strain Gauge Sensor	<ul style="list-style-type: none"> <li>• A finite-time sliding-mode controller (SMC) is proposed in combination with the disturbance observer (DOB) and a radial basis function (RBF) neural network (NN) (RBF-NN).</li> <li>• RBF-NN replaces the hysteresis model of the dynamic system, and a finite-time adaptive DOB estimates the disturbances of the system</li> <li>• With the proposed control method, the AAE of the actuator under sine and triangular trajectories is about 0.0063 <math>\mu\text{m}</math>, 0.0067 <math>\mu\text{m}</math>, 0.0257 <math>\mu\text{m}</math>, 0.0268 <math>\mu\text{m}</math> and 0.0132 <math>\mu\text{m}</math>, 0.0141 <math>\mu\text{m}</math>, 0.0142 <math>\mu\text{m}</math>, 0.0261 <math>\mu\text{m}</math> at 1 Hz, 50 Hz, 100 Hz, and 200 Hz respectively.</li> </ul>

Table 5. Cont.

Author	Year	Ref. No.	Control Method	Type of Actuator	Sensor Used in Control	Observation
C. Napole	2023	[232]	Feedforward /Feedback With Fuzzy Logic	Piezo Stack	Wheatstone Bridge	<ul style="list-style-type: none"> <li>• Feedback–feedforward algorithms, based on fuzzy logic in combination with neural networks, aimed at reducing the tracking error and improving the actuation signal of piezoelectric actuators</li> <li>• The fuzzy schemes displayed an improvement over the PID of around 60% at tracking operations</li> <li>• The rot mean square of the fuzzy logic control with neural network is about 0.016 <math>\mu\text{m}</math> to 0.0129 <math>\mu\text{m}</math> which was less than the conventional PID controller with 0.0202 <math>\mu\text{m}</math>.</li> </ul>

## 9. Concluding Remarks and Future Prospects

The piezoelectric actuators find extensive application in precision positioning and manipulation applications. Despite many advantageous features, the inherent system nonlinearity due to hysteresis creep and vibration degrades the performance of the piezoelectric actuators under dynamic conditions. This review aims to present different modeling and control approaches of piezoelectric actuators adopted to eliminate the inherent system nonlinearity of piezoelectric actuators. The survey included a descriptive narration of comprehensive dynamic modeling approaches and different methods of driving the piezoelectric actuators. The charge-based driving modes, such as capacitor insertion, time-controlled current amplification, capacitor-based sensing, and charge control with inverting configuration, effectively minimize hysteresis and creep. However, such approaches have the disadvantages of voltage drop and drift effects. Implementing digital charge control with suitable filters overcomes the problem of voltage drift. Despite the advantage of nonlinearity elimination in piezoelectric actuators through charge-based driving methods, the requirement of the unique controller design for specific actuators and the cost involved limits its widespread application.

A voltage-based driving method is a generalized approach for different piezoelectric actuators. However, the effectiveness of the voltage-based control method depends on the appropriate modeling of nonlinearities and control strategies adopted. Several models are proposed for modeling the hysteresis nonlinearity of the piezoelectric actuators. The rate-independent hysteresis models help model the hysteresis nonlinearity in low-frequency range applications. The rate-dependent models describe the hysteresis phenomenon in the higher range of the actuation frequency. The differential equation-based models are relatively easier to implement when compared with operator-based models. Further, the logarithmic approach defines the creep behavior of the piezoelectric actuator compared with the linear approach.

The positioning accuracy of the piezoelectric actuators depends on the control approach adopted under dynamic conditions. The feedforward control offers a simple solution for position control of the piezoelectric actuators with suitable compensation to overcome nonlinearity with a stable response. The high sensitivity to external disturbances and uncertainties limits the application of feedforward control. The feedback control approach can address external disturbances and system uncertainties and provide closed-loop, real-time control of the piezoelectric actuator. However, feedback control has the disadvantages of stability issues and low-frequency bandwidth. The cascaded feedforward–feedback controllers take the advantageous feature of both feedforward and feedback controllers and ensure stability and elimination of nonlinearity errors to a greater extent.

Based on the detailed survey of the piezoelectric actuators, the authors observed the following research suggestions.

- Development and enhancement of unique charge-based control method applicable to all types of piezoelectric actuators
- Development of realistic rate-dependent hysteresis models and inverse constructions to model the hysteresis behavior of the piezoelectric actuator at a very high-frequency range.
- Implementation of rate-dependent hysteresis models for multi-degree freedom actuators involving multiple piezoelectric actuators
- Development of an active vibration isolation approach to overcome the issues of dynamic vibration.
- Design, develop, and implement a novel control strategy to better control multi-degree freedom piezoelectric actuators and eliminate system nonlinearities to minimize errors.

**Author Contributions:** Conceptualization, M.K. and M.S.; methodology, M.K. and M.S.; formal analysis, M.K. and M.S.; investigation, M.K. and M.S.; resources, M.K. and M.S.; data curation, M.K. and M.S.; writing—M.K. and M.S.; review and editing, R.B. and N.N.; visualization, M.K. and M.S.; supervision, R.B. and N.N. All authors have read and agreed to the published version of the manuscript.

**Funding:** This research received no external funding.

**Conflicts of Interest:** The authors declare no conflict of interest.

## References

1. Jia, Z.-Y.; Ma, J.-W.; Song, D.-N.; Wang, F.-J.; Liu, W. A review of contouring-error reduction method in multi-axis CNC machining. *Int. J. Mach. Tools Manuf.* **2018**, *125*, 34–54. [[CrossRef](#)]
2. Wang, H.; Li, Y.; Wang, X.; Liu, Z.; Ahmed, M.F.; Zeng, C. Preparation and characterization of piezoelectric foams based on cyclic olefin copolymer. *Eng. Sci.* **2021**, *16*, 203–210. [[CrossRef](#)]
3. Su, Y.-F.; Han, G.; Kong, Z.; Nantung, T.; Lu, N. Embeddable piezoelectric sensors for strength gain monitoring of cementitious materials: The influence of Coating Materials. *Eng. Sci.* **2020**, *11*, 66–75. [[CrossRef](#)]
4. Muralidhara; Rao, R. Displacement characteristics of a piezo actuator-based prototype microactuator with a hydraulic displacement amplification system. *J. Mech. Sci. Technol.* **2015**, *29*, 4817–4822. [[CrossRef](#)]
5. Mohith, S.; Navin Karanth, P.; Kulkarni, S.M. Performance analysis of valveless micropump with disposable chamber actuated through Amplified Piezo Actuator (APA) for biomedical application. *Mechatronics* **2020**, *67*, 102347. [[CrossRef](#)]
6. Ling, M.; Cao, J.; Zeng, M.; Lin, J.; Inman, D.J. Enhanced mathematical modeling of the displacement amplification ratio for piezoelectric compliant mechanisms. *Smart Mater. Struct.* **2016**, *25*, 075022. [[CrossRef](#)]
7. Naik, N.; Suresh, P.; Yadav, S.; Nisha, M.P.; Arias-González, J.L.; Cotrina-Aliaga, J.C.; Bhat, R.; Jalageri, M.D.; Kaushik, Y.; Kunjibettu, A.B. A review on composite materials for energy harvesting in electric vehicles. *Energies* **2023**, *16*, 3348. [[CrossRef](#)]
8. Mohith, S.; Karanth, P.N.; Kulkarni, S.M. Experimental investigation on performance of disposable micropump with retrofit piezo stack actuator for biomedical application. *Microsyst. Technol.* **2019**, *25*, 4741–4752. [[CrossRef](#)]
9. El-Sayed, A.M.; Abo-Ismael, A.; El-Melegy, M.T.; Hamzaid, N.A.; Osman, N.A.A. Development of a Micro-Gripper Using Piezoelectric Bimorphs. *Sensors* **2013**, *13*, 5826–5840. [[CrossRef](#)]
10. Abondance, T.; Jayaram, K.; Jafferis, N.T.; Shum, J.; Wood, R.J. Piezoelectric Grippers for Mobile Micromanipulation. *IEEE Robot. Autom. Lett.* **2020**, *5*, 4407–4414. [[CrossRef](#)]
11. Jeon, J.; Han, C.; Han, Y.-M.; Choi, S.-B. A new type of a direct-drive valve system driven by a piezostack actuator and sliding spool. *Smart Mater. Struct.* **2014**, *23*, 075002. [[CrossRef](#)]
12. Sohn, J.W.; Choi, S.-B. Identification of Operating Parameters Most Strongly Influencing the Jetting Performance in a Piezoelectric Actuator-Driven Dispenser. *Appl. Sci.* **2018**, *8*, 243. [[CrossRef](#)]
13. Deng, G.; Cui, W.; Zhou, C.; Li, J. A piezoelectric jetting dispenser with a pin joint. *Optik* **2018**, *175*, 163–171. [[CrossRef](#)]
14. Cai, K.; Tian, Y.; Wang, F.; Zhang, D.; Shirinzadeh, B. Development of a piezo-driven 3-DOF stage with T-shape flexible hinge mechanism. *Robot. Comput. Manuf.* **2016**, *37*, 125–138. [[CrossRef](#)]
15. Eslami, B.; Solares, S.D. Experimental approach for selecting the excitation frequency for maximum compositional contrast in viscous environments for piezo-driven bimodal atomic force microscopy. *J. Appl. Phys.* **2016**, *119*, 084901. [[CrossRef](#)]
16. Muralidhara; Vasa, N.J.; Makaram, S. Investigations on a directly coupled piezoactuated tool feed system for micro-electro-discharge machine. *Int. J. Mach. Tools Manuf.* **2009**, *49*, 1197–1203. [[CrossRef](#)]
17. Tian, X.; Zhang, B.; Liu, Y.; Chen, S.; Yu, H. A novel U-shaped stepping linear piezoelectric actuator with two driving feet and low motion coupling: Design, modeling and experiments. *Mech. Syst. Signal Process.* **2019**, *124*, 679–695. [[CrossRef](#)]
18. Lu, Z.-Q.; Shao, D.; Fang, Z.-W.; Ding, H.; Chen, L.-Q. Integrated vibration isolation and energy harvesting via a bistable piezo-composite plate. *J. Vib. Control* **2020**, *26*, 779–789. [[CrossRef](#)]

19. Rodriguez-Fortun, J.M.; Orus, J.; Alfonso, J.; Gimeno, F.B.; Castellanos, J.A. Flatness-Based Active Vibration Control for Piezoelectric Actuators. *IEEE/ASME Trans. Mechatron.* **2013**, *18*, 221–229. [[CrossRef](#)]
20. Tavakolpour, A.R.; Mailah, M.; Mat Darus, I.Z.; Tokhi, O. Self-learning active vibration control of a flexible plate structure with piezoelectric actuator. *Simul. Model. Pract. Theory* **2010**, *18*, 516–532. [[CrossRef](#)]
21. Mohith, S.; Upadhyaya, A.R.; Navin, K.P.; Kulkarni, S.M.; Rao, M. Recent trends in piezoelectric actuators for precision motion and their applications: A review. *Smart Mater. Struct.* **2021**, *30*, 013002. [[CrossRef](#)]
22. Boukari, A.-F.; Carmona, J.-C.; Moraru, G.; Malburet, F.; Chaaba, A.; Douimi, M. Piezo-actuators modeling for smart applications. *Mechatronics* **2011**, *21*, 339–349. [[CrossRef](#)]
23. Xue, D.; Zhou, Y.; Bao, H.; Gao, J.; Zhou, C.; Ren, X. Large piezoelectric effect in Pb-free Ba(Ti, Sn)O<sub>3-x</sub>(Ba, Ca)TiO<sub>3</sub> ceramics. *Appl. Phys. Lett.* **2011**, *99*, 122901. [[CrossRef](#)]
24. Su, X.; Jia, Y.; Han, C.; Hu, Y.; Fu, Z.; Liu, K.; Yu, Y.; Yan, X.; Wang, Y. Flash sintering of lead zirconate titanate ceramics under an alternating current electrical field. *Ceram. Int.* **2019**, *45*, 5168–5173. [[CrossRef](#)]
25. Kholodkova, A.A.; Danchevskaya, M.N.; Ivakin, Y.D.; Muravieva, G.P.; Smirnov, A.D.; Tarasovskii, V.P.; Ponomarev, S.G.; Fionov, A.S.; Kolesov, V.V. Properties of barium titanate ceramics based on powder synthesized in supercritical water. *Ceram. Int.* **2018**, *44*, 13129–13138. [[CrossRef](#)]
26. Naik, R.; Mohit, S.; Chavan, S. Piezoelectric property investigation on PVDF/ZrO<sub>2</sub>/ZnO nanocomposite for energy harvesting application. *Eng. Res. Express* **2021**, *3*, 025003. [[CrossRef](#)]
27. Colorado, S.A.; Colorado, H.A. Manufacturing of zinc oxide structures by thermal oxidation processes as scalable methods towards inexpensive electric generators. *Ceram. Int.* **2017**, *43*, 15846–15855. [[CrossRef](#)]
28. Bakhtiari-Shahri, M.; Moeenfarid, H. Energy harvesting from unimorph piezoelectric circular plates under random acoustic and base acceleration excitations. *Mech. Syst. Signal Process.* **2019**, *130*, 502–523. [[CrossRef](#)]
29. Rios, S.A.; Fleming, A.J. A new electrical configuration for improving the range of piezoelectric bimorph benders. *Sens. Actuators A Phys.* **2015**, *224*, 106–110. [[CrossRef](#)]
30. Ozaki, T.; Hamaguchi, K. Performance of direct-driven flapping-wing actuator with piezoelectric single-crystal PIN-PMN-PT. *J. Micromech. Microeng.* **2018**, *28*, 025007. [[CrossRef](#)]
31. Almeida, A.; Andrews, G.; Jaiswal, D.; Hoshino, K. The Actuation Mechanism of 3D Printed Flexure-Based Robotic Microtweezers. *Micromachines* **2019**, *10*, 470. [[CrossRef](#)] [[PubMed](#)]
32. Habineza, D.; Rakotondrabe, M.; Le Gorrec, Y. Bouc–Wen Modeling and Feedforward Control of Multivariable Hysteresis in Piezoelectric Systems: Application to a 3-DoF Piezotube Scanner. *IEEE Trans. Control Syst. Technol.* **2015**, *23*, 1797–1806. [[CrossRef](#)]
33. Habineza, D.; Rakotondrabe, M.; Le Gorrec, Y. Simultaneous suppression of badly damped vibrations and cross-couplings in a 2-DoF piezoelectric actuator by using feedforward standard H<sub>∞</sub> approach. In *Next-Generation Robotics II; and Machine Intelligence and Bio-Inspired Computation: Theory and Applications IX*; SPIE: Baltimore, MD, USA, 2015; p. 94940L. [[CrossRef](#)]
34. Bu, Z.; Lin, S.; Huang, X.; Li, A.; Wu, D.; Zhao, Y.; Luo, Z.; Wang, L. A novel piezostack-driven jetting dispenser with corner-filletted flexure hinge and high-frequency performance. *J. Micromech. Microeng.* **2018**, *28*, 075001. [[CrossRef](#)]
35. Hwang, H.S.; Nasser, J.; Sodano, H.A. Piezoelectric Stack Actuator for Measurement of Interfacial Shear Strength at High Strain Rates. *Exp. Mech.* **2019**, *59*, 979–990. [[CrossRef](#)]
36. Santhya, M.; Upadhyaya, A.R.; Panambur, N.K.; Kulkarni, S.M. Performance analysis of a novel piezo actuated valveless micropump for biomedical application. *AIP Conf. Proc.* **2020**, *2236*, 070002. [[CrossRef](#)]
37. Dsouza, R.D.; Navin, K.P.; Theodoridis, T.; Sharma, P. Design, fabrication and testing of a 2 DOF compliant flexural microgripper. *Microsyst. Technol.* **2018**, *24*, 3867–3883. [[CrossRef](#)]
38. Dong, W.; Chen, F.; Yang, M.; Du, Z.-J.; Tang, J.; Zhang, D. Development of a highly efficient bridge-type mechanism based on negative stiffness. *Smart Mater. Struct.* **2017**, *26*, 095053. [[CrossRef](#)]
39. Chen, F.; Du, Z.-J.; Yang, M.; Gao, F.; Dong, W.; Zhang, D. Design and analysis of a three-dimensional bridge-type mechanism based on the stiffness distribution. *Precis. Eng.* **2018**, *51*, 48–58. [[CrossRef](#)]
40. Dong, W.; Chen, F.; Gao, F.; Yang, M.; Sun, L.; Du, Z.; Tang, J.; Zhang, D. Development and analysis of a bridge-lever-type displacement amplifier based on hybrid flexure hinges. *Precis. Eng.* **2018**, *54*, 171–181. [[CrossRef](#)]
41. Chen, F.; Gao, Y.; Dong, W.; Du, Z. Design and Control of a Passive Compliant Piezo-Actuated Micro-Gripper With Hybrid Flexure Hinges. *IEEE Trans. Ind. Electron.* **2020**, *68*, 11168–11177. [[CrossRef](#)]
42. Tian, X.; Liu, Y.; Chen, W.; Deng, J.; Liu, J. Development and experiment evaluation of an H-shape linear piezoelectric actuator operated in stepping mode. *Ceram. Int.* **2018**, *44*, S246–S249. [[CrossRef](#)]
43. Wang, Y.-J.; Yang, C.; Sue, C.-Y.; Wang, Y.-T. Analysis of a 0.1- $\mu$ m stepping bi-axis piezoelectric stage using a 2-DOF lumped model. *Microsyst. Technol.* **2020**, *26*, 425–436. [[CrossRef](#)]
44. Li, J.; Zhao, H.; Shao, M.; Zhou, X.; Huang, H.; Fan, Z. Design and experiment performances of an inchworm type rotary actuator. *Rev. Sci. Instrum.* **2014**, *85*, 085004. [[CrossRef](#)]
45. Shao, S.; Song, S.; Liu, K.; Xu, M. A piezo-driven rotary inchworm actuator featured with simple structure and high output torque. *Int. J. Appl. Electromagn. Mech.* **2019**, *59*, 317–325. [[CrossRef](#)]
46. Zhong, B.; Zhu, J.; Jin, Z.; He, H.; Sun, L.; Wang, Z. Improved inertial stick-slip movement performance via driving waveform optimization. *Precis. Eng.* **2019**, *55*, 260–267. [[CrossRef](#)]

47. Gao, Q.; He, M.; Lu, X.; Zhang, C.; Cheng, T. Simple and high-performance stick-slip piezoelectric actuator based on an asymmetrical flexure hinge driving mechanism. *J. Intell. Mater. Syst. Struct.* **2019**, *30*, 2125–2134. [[CrossRef](#)]
48. Grybas, I.; Bansevicius, R.; Jurenas, V.; Bubulis, A.; Janutenaite, J.; Kulvietis, G. Ultrasonic standing waves-driven high resolution rotary table. *Precis. Eng.* **2016**, *45*, 396–402. [[CrossRef](#)]
49. Wang, L.; Shu, C.; Zhang, Q.; Jin, J. A novel sandwich-type traveling wave piezoelectric tracked mobile system. *Ultrasonics* **2017**, *75*, 28–35. [[CrossRef](#)]
50. Liao, C.; Xu, M.; Xiao, R.; Han, W. Integrated design of piezo-actuated 2-DOF submillimeter-range super-resolution platform with self-sensing unit. *Mech. Syst. Signal Process.* **2020**, *139*, 106569. [[CrossRef](#)]
51. Chen, F.; Dong, W.; Yang, M.; Sun, L.; Du, Z. A PZT Actuated 6-DOF Positioning System for Space Optics Alignment. *IEEE/ASME Trans. Mechatron.* **2019**, *24*, 2827–2838. [[CrossRef](#)]
52. Li, J.; Huang, H.; Morita, T. Stepping piezoelectric actuators with large working stroke for nano-positioning systems: A review. *Sens. Actuators A Phys.* **2019**, *292*, 39–51. [[CrossRef](#)]
53. Wang, L.; Chen, W.; Liu, J.; Deng, J.; Liu, Y. A review of recent studies on non-resonant piezoelectric actuators. *Mech. Syst. Signal Process.* **2019**, *133*, 106254. [[CrossRef](#)]
54. Wang, S.; Rong, W.; Wang, L.; Xie, H.; Sun, L.; Mills, J.K. A survey of piezoelectric actuators with long working stroke in recent years: Classifications, principles, connections and distinctions. *Mech. Syst. Signal Process.* **2019**, *123*, 591–605. [[CrossRef](#)]
55. Gu, G.-Y.; Zhu, L.-M.; Su, C.-Y.; Ding, H.; Fatikow, S. Modeling and control of piezo-actuated nanopositioning stages: A survey. *IEEE Trans. Autom. Sci. Eng.* **2016**, *13*, 313–332. [[CrossRef](#)]
56. Rakotondrabe, M. Multivariable classical Prandtl–Ishlinskii hysteresis modeling and compensation and sensorless control of a nonlinear 2-dof piezoactuator. *Nonlinear Dyn.* **2017**, *89*, 481–499. [[CrossRef](#)]
57. Sabarianand, D.V.; Karthikeyan, P.; Muthuramalingam, T. A review on control strategies for compensation of hysteresis and creep on piezoelectric actuators based micro systems. *Mech. Syst. Signal Process.* **2020**, *140*, 106634. [[CrossRef](#)]
58. Gan, J.; Zhang, X. A review of nonlinear hysteresis modeling and control of piezoelectric actuators. *AIP Adv.* **2019**, *9*, 040702. [[CrossRef](#)]
59. Chen, J.; Peng, G.; Hu, H.; Ning, J. Dynamic Hysteresis Model and Control Methodology for Force Output Using Piezoelectric Actuator Driving. *IEEE Access* **2020**, *8*, 205136–205147. [[CrossRef](#)]
60. Chi, Z.; Xu, Q. Recent Advances in the Control of Piezoelectric Actuators. *Int. J. Adv. Robot. Syst.* **2014**, *11*, 182. [[CrossRef](#)]
61. Yang, Y. Piezoelectric Actuators Application and Hysteresis Modelling: A Brief Survey. *Open Access Libr. J.* **2023**, *10*, e10482. [[CrossRef](#)]
62. Hassani, V.; Tjahjowidodo, T.; Do, T.N. A survey on hysteresis modeling, identification and control. *Mech. Syst. Signal Process.* **2014**, *49*, 209–233. [[CrossRef](#)]
63. Goldfarb, M.; Celanovic, N. Modeling piezoelectric stack actuators for control of micromanipulation. *IEEE Control Syst.* **1997**, *17*, 69–79. [[CrossRef](#)]
64. Adriaens, H.J.M.T.S.; De Koning, W.L.; Banning, R. Modeling piezoelectric actuators. *IEEE/ASME Trans. Mechatron.* **2000**, *5*, 331–341. [[CrossRef](#)]
65. Gao, Y.; Zhang, D.; Yu, C.W. Dynamic modeling of a novel workpiece table for active surface grinding control. *Int. J. Mach. Tools Manuf.* **2001**, *41*, 609–624. [[CrossRef](#)]
66. Bazghaleh, M.; Grainger, S.; Mohammadzaheri, M. A review of charge methods for driving piezoelectric actuators. *J. Intell. Mater. Syst. Struct.* **2018**, *29*, 2096–2104. [[CrossRef](#)]
67. Moheimani, S.O.R. Invited Review Article: Accurate and fast nanopositioning with piezoelectric tube scanners: Emerging trends and future challenges. *Rev. Sci. Instrum.* **2008**, *79*, 071101. [[CrossRef](#)]
68. Minase, J.; Lu, T.-F.; Cazzolato, B.; Grainger, S. A review, supported by experimental results, of voltage, charge and capacitor insertion method for driving piezoelectric actuators. *Precis. Eng.* **2010**, *34*, 692–700. [[CrossRef](#)]
69. Ma, Y.T.; Huang, L.; Shao, W.W. New Open Loop Control Improves Linearity of Piezoelectric Actuators. *Adv. Mater. Res.* **2011**, *211–212*, 520–524. [[CrossRef](#)]
70. Ru, C.; Chen, L.; Shao, B.; Rong, W.; Sun, L. A new amplifier for improving piezoelectric actuator linearity based on current switching in precision positioning. *Meas. Sci. Technol.* **2008**, *19*, 015203. [[CrossRef](#)]
71. Špiller, M.; Hurák, Z. Hybrid charge control for stick–slip piezoelectric actuators. *Mechatronics* **2011**, *21*, 100–108. [[CrossRef](#)]
72. Moheimani, S.O.R.; Vautier, B.J.G. Resonant control of structural vibration using charge-driven piezoelectric actuators. *IEEE Trans. Control Syst. Technol.* **2005**, *13*, 1021–1035. [[CrossRef](#)]
73. Fleming, A.J.; Moheimani, S.O.R. A grounded-load charge amplifier for reducing hysteresis in piezoelectric tube scanners. *Rev. Sci. Instrum.* **2005**, *76*, 073707. [[CrossRef](#)]
74. Fleming, A.J. Quantitative scanning probe microscope topographies by charge linearization of the vertical actuator. *Rev. Sci. Instrum.* **2010**, *81*, 103701. [[CrossRef](#)]
75. Rios, S.A.; Fleming, A.J. Design of a Charge Drive for Reducing Hysteresis in a Piezoelectric Bimorph Actuator. *IEEE/ASME Trans. Mechatron.* **2016**, *21*, 51–54. [[CrossRef](#)]
76. Yi, K.A.; Veillette, R.J. A charge controller for linear operation of a piezoelectric stack actuator. *IEEE Trans. Control Syst. Technol.* **2005**, *13*, 517–526. [[CrossRef](#)]

77. Yang, C.; Li, C.; Zhao, J. A Nonlinear Charge Controller With Tunable Precision for Highly Linear Operation of Piezoelectric Stack Actuators. *IEEE Trans. Ind. Electron.* **2017**, *64*, 8618–8625. [[CrossRef](#)]
78. Yang, C.; Li, C.; Xia, F.; Zhu, Y.; Zhao, J.; Youcef-Toumi, K. Charge Controller With Decoupled and Self-Compensating Configurations for Linear Operation of Piezoelectric Actuators in a Wide Bandwidth. *IEEE Trans. Ind. Electron.* **2019**, *66*, 5392–5402. [[CrossRef](#)]
79. Jin, T.; Peng, Y.; Xing, Z.; Lei, L. A Charge Controller for Synchronous Linear Operation of Multiple Piezoelectric Actuators. *IEEE Access* **2019**, *7*, 90741–90749. [[CrossRef](#)]
80. Bazghaleh, M.; Grainger, S.; Mohammadzaheri, M.; Cazzolato, B.; Lu, T.-F. A digital charge amplifier for hysteresis elimination in piezoelectric actuators. *Smart Mater. Struct.* **2013**, *22*, 075016. [[CrossRef](#)]
81. Bazghaleh, M.; Grainger, S.; Cazzolato, B.; Lu, T.-F.; Oskouei, R. Implementation and analysis of an innovative digital charge amplifier for hysteresis reduction in piezoelectric stack actuators. *Rev. Sci. Instrum.* **2014**, *85*, 045005. [[CrossRef](#)]
82. Zhong, J.; Nishida, R.; Shinshi, T. A digital charge control strategy for reducing the hysteresis in piezoelectric actuators: Analysis, design, and implementation. *Precis. Eng.* **2021**, *67*, 370–382. [[CrossRef](#)]
83. Yang, C.; Xia, F.; Wang, Y.; Youcef-Toumi, K. Comprehensive study of charge-based motion control for piezoelectric nanopositioners: Modeling, instrumentation and controller design. *Mech. Syst. Signal Process.* **2022**, *166*, 108477. [[CrossRef](#)]
84. Gu, G.-Y.; Zhu, L.-M.; Su, C.-Y.; Ding, H. Motion Control of Piezoelectric Positioning Stages: Modeling, Controller Design, and Experimental Evaluation. *IEEE/ASME Trans. Mechatron.* **2013**, *18*, 1459–1471. [[CrossRef](#)]
85. Takács, J. A phenomenological mathematical model of hysteresis. *COMPEL Int. J. Comput. Math. Electr. Electron. Eng.* **2001**, *20*, 1002–1015. [[CrossRef](#)]
86. Mielke, A.; Theil, F. On rate-independent hysteresis models. *Nonlinear Differ. Equ. Appl.* **2004**, *11*, 151–189. [[CrossRef](#)]
87. Al Janaideh, M.; Rakheja, S.; Su, C.-Y. Experimental characterization and modeling of rate-dependent hysteresis of a piezoceramic actuator. *Mechatronics* **2009**, *19*, 656–670. [[CrossRef](#)]
88. Ma, F.; Zhang, H.; Bockstedte, A.; Foliente, G.C.; Paevere, P. Parameter Analysis of the Differential Model of Hysteresis. *J. Appl. Mech.* **2004**, *71*, 342–349. [[CrossRef](#)]
89. Jiang, C.; Deng, M.; Hayakawa, Y. Operator-based parallel compensation control for hysteresis using ELM-based stop-type PI model. In Proceedings of the 2012 IEEE International Conference on Mechatronics and Automation, Chengdu, China, 5–8 August 2012; pp. 2054–2058. [[CrossRef](#)]
90. Jiles, D.C.; Atherton, D.L. Theory of ferromagnetic hysteresis. *J. Magn. Magn. Mater.* **1986**, *61*, 48–60. [[CrossRef](#)]
91. Cao, S.; Wang, B.; Yan, R.; Huang, W.; Yang, Q. Optimization of Hysteresis Parameters for the Jiles-Atherton Model Using a Genetic Algorithm. *IEEE Trans. Appl. Supercond.* **2004**, *14*, 1157–1160. [[CrossRef](#)]
92. Smith, R.C.; Ounaies, Z. A Domain Wall Model for Hysteresis in Piezoelectric Materials. *J. Intell. Mater. Syst. Struct.* **2000**, *11*, 62–79. [[CrossRef](#)]
93. Massad, J.E.; Smith, R.C. A Domain Wall Model for Hysteresis in Ferroelastic Materials. *J. Intell. Mater. Syst. Struct.* **2003**, *14*, 455–471. [[CrossRef](#)]
94. Oh, J.H.; Bernstein, D.S. Semilinear Duhem model for rate-independent and rate-dependent hysteresis. *IEEE Trans. Autom. Control* **2005**, *50*, 631–645. [[CrossRef](#)]
95. Lin, C.-J.; Lin, P.-T. Tracking control of a biaxial piezo-actuated positioning stage using generalized Duhem model. *Comput. Math. Appl.* **2012**, *64*, 766–787. [[CrossRef](#)]
96. Xie, W.-F.; Fu, J.; Yao, H.; Su, C.-Y. Observer based control of piezoelectric actuators with classical Duhem modeled hysteresis. In Proceedings of the 2009 American Control Conference, St. Louis, MO, USA, 10–12 June 2009; pp. 4221–4226. [[CrossRef](#)]
97. D’souza, R.D.; Benny, B.; Sequeira, A.; Karanth, N. Hysteresis Modeling of Amplified Piezoelectric Stack Actuator for the Control of the Microgripper. *Am. Sci. Res. J. Eng. Technol. Sci. (ASRJETS)* **2016**, *15*, 265–281.
98. Xuehui, G.; Bo, S. Identification for Bouc-Wen hysteresis system with hopfield neural network. In Proceedings of the 2017 9th International Conference on Modelling, Identification and Control (ICMIC), Kunming, China, 10–12 July 2017; pp. 248–253. [[CrossRef](#)]
99. Mohith, S.; Rao, M.; Navin Karanth, P.; Kulkarni, S.M.; Upadhyaya, A.R. Development and assessment of large stroke piezo-hydraulic actuator for micro positioning applications. *Precis. Eng.* **2021**, *67*, 324–338. [[CrossRef](#)]
100. Ren, B.; San, P.P.; Ge, S.S.; Lee, T.H. Adaptive dynamic surface control for a class of strict-feedback nonlinear systems with unknown backlash-like hysteresis. In Proceedings of the 2009 American Control Conference, St. Louis, MO, USA, 10–12 June 2009; pp. 4482–4487. [[CrossRef](#)]
101. Zhou, J.; Wen, C.; Zhang, Y. Adaptive Backstepping Control of a Class of Uncertain Nonlinear Systems With Unknown Backlash-Like Hysteresis. *IEEE Trans. Autom. Control* **2004**, *49*, 1751–1757. [[CrossRef](#)]
102. Song, G.; Zhao, J.; Zhou, X.; de Abreu-Garcia, J. Tracking Control of a Piezoceramic Actuator With Hysteresis Compensation Using Inverse Preisach Model. *IEEE/ASME Trans. Mechatron.* **2005**, *10*, 198–209. [[CrossRef](#)]
103. Viswamurthy, S.; Ganguli, R. Modeling and compensation of piezoceramic actuator hysteresis for helicopter vibration control. *Sens. Actuators A Phys.* **2007**, *135*, 801–810. [[CrossRef](#)]
104. Iyer, R.V.; Tan, X. Control of hysteretic systems through inverse compensation: Algorithms, adaptation, and embedded implementation. *IEEE Control Syst.* **2009**, *29*, 83–99. [[CrossRef](#)]

105. Nguyen, P.-B.; Choi, S.-B.; Song, B.-K. A new approach to hysteresis modelling for a piezoelectric actuator using Preisach model and recursive method with an application to open-loop position tracking control. *Sens. Actuators A Phys.* **2018**, *270*, 136–152. [[CrossRef](#)]
106. Al Janaideh, M.; Rakheja, S.; Su, C.-Y. A generalized Prandtl–Ishlinskii model for characterizing the hysteresis and saturation nonlinearities of smart actuators. *Smart Mater. Struct.* **2009**, *18*, 045001. [[CrossRef](#)]
107. Chen, Y.; Qiu, J.; Palacios, J.; Smith, E.C. Tracking control of piezoelectric stack actuator using modified Prandtl–Ishlinskii model. *J. Intell. Mater. Syst. Struct.* **2013**, *24*, 753–760. [[CrossRef](#)]
108. Gu, G.-Y.; Zhu, L.-M.; Su, C.-Y. Modeling and Compensation of Asymmetric Hysteresis Nonlinearity for Piezoceramic Actuators With a Modified Prandtl–Ishlinskii Model. *IEEE Trans. Ind. Electron.* **2014**, *61*, 1583–1595. [[CrossRef](#)]
109. Al Janaideh, M.; Su, C.-Y.; Rakheja, S. Development of the rate-dependent Prandtl–Ishlinskii model for smart actuators. *Smart Mater. Struct.* **2008**, *17*, 035026. [[CrossRef](#)]
110. Banks, H.T.; Kurdila, A.J.; Webb, G. Identification of hysteretic control influence operators representing smart actuators part I: Formulation. *Math. Probl. Eng.* **1997**, *3*, 287–328. [[CrossRef](#)]
111. Li, Z.; Zhang, X. Model order reduction for the Krasnoselskii–Pokrovskii (KP) model. *Smart Mater. Struct.* **2019**, *28*, 095001. [[CrossRef](#)]
112. Vo-Minh, T.; Tjahjowidodo, T.; Ramon, H.; Van Brussel, H. A New Approach to Modeling Hysteresis in a Pneumatic Artificial Muscle Using The Maxwell-Slip Model. *IEEE/ASME Trans. Mechatron.* **2011**, *16*, 177–186. [[CrossRef](#)]
113. Miri, N.; Mohammadzaheri, M.; Chen, L. A comparative study of different physics-based approaches to modelling of piezoelectric actuators. In Proceedings of the 2013 IEEE/ASME International Conference on Advanced Intelligent Mechatronics, Wollongong, NSW, Australia, 9–12 July 2013; pp. 1211–1216. [[CrossRef](#)]
114. Liu, Y.; Du, D.; Qi, N.; Zhao, J. A Distributed Parameter Maxwell-Slip Model for the Hysteresis in Piezoelectric Actuators. *IEEE Trans. Ind. Electron.* **2019**, *66*, 7150–7158. [[CrossRef](#)]
115. Yeh, T.-J.; Lu, S.-W.; Wu, T.-Y. Modeling and Identification of Hysteresis in Piezoelectric Actuators. *J. Dyn. Syst. Meas. Control* **2006**, *128*, 189–196. [[CrossRef](#)]
116. Hegewald, T.; Kaltenbacher, B.; Kaltenbacher, M.; Lerch, R. Efficient Modeling of Ferroelectric Behavior for the Analysis of Piezoceramic Actuators. *J. Intell. Mater. Syst. Struct.* **2008**, *19*, 1117–1129. [[CrossRef](#)]
117. Deng, L.; Tan, Y. Diagonal recurrent neural network with modified backlash operators for modeling of rate-dependent hysteresis in piezoelectric actuators. *Sens. Actuators A Phys.* **2008**, *148*, 259–270. [[CrossRef](#)]
118. Zhou, M.; Wang, J. Research on Hysteresis of Piezoceramic Actuator Based on the Duhem Model. *Sci. World J.* **2013**, *2013*, 814919. [[CrossRef](#)] [[PubMed](#)]
119. Liu, Y.; Shan, J.; Gabbert, U.; Qi, N. Hysteresis and creep modeling and compensation for a piezoelectric actuator using a fractional-order Maxwell resistive capacitor approach. *Smart Mater. Struct.* **2013**, *22*, 115020. [[CrossRef](#)]
120. Zsurzsan, T.-G.; Andersen, M.A.; Zhang, Z.; Andersen, N.A. Preisach model of hysteresis for the Piezoelectric Actuator Drive. In Proceedings of the IECON 2015—41st Annual Conference of the IEEE Industrial Electronics Society, Yokohama, Japan, 9–12 November 2015; pp. 002788–002793. [[CrossRef](#)]
121. Gan, J.; Zhang, X.; Wu, H. A generalized Prandtl–Ishlinskii model for characterizing the rate-independent and rate-dependent hysteresis of piezoelectric actuators. *Rev. Sci. Instrum.* **2016**, *87*, 035002. [[CrossRef](#)]
122. Wang, G.; Chen, G. Identification of piezoelectric hysteresis by a novel Duhem model based neural network. *Sens. Actuators A Phys.* **2017**, *264*, 282–288. [[CrossRef](#)]
123. Qin, Y.; Zhao, X.; Zhou, L. Modeling and Identification of the Rate-Dependent Hysteresis of Piezoelectric Actuator Using a Modified Prandtl–Ishlinskii Model. *Micromachines* **2017**, *8*, 114. [[CrossRef](#)]
124. Gan, J.; Zhang, X. An enhanced Bouc–Wen model for characterizing rate-dependent hysteresis of piezoelectric actuators. *Rev. Sci. Instrum.* **2018**, *89*, 115002. [[CrossRef](#)]
125. Luo, Y.; Qu, Y.; Zhang, Y.; Xu, M.; Xie, S.; Zhang, X. Hysteretic modeling and simulation of a bilateral piezoelectric stack actuator based on Preisach model. *Int. J. Appl. Electromagn. Mech.* **2019**, *59*, 271–280. [[CrossRef](#)]
126. Li, Z.; Shan, J.; Gabbert, U. Inverse Compensation of Hysteresis Using Krasnoselskii–Pokrovskii Model. *IEEE/ASME Trans. Mechatron.* **2018**, *23*, 966–971. [[CrossRef](#)]
127. Gan, J.; Mei, Z.; Chen, X.; Zhou, Y.; Ge, M.-F. A Modified Duhem Model for Rate-Dependent Hysteresis Behaviors. *Micromachines* **2019**, *10*, 680. [[CrossRef](#)]
128. Gan, J.; Zhang, X. Nonlinear Hysteresis Modeling of Piezoelectric Actuators Using a Generalized Bouc–Wen Model. *Micromachines* **2019**, *10*, 183. [[CrossRef](#)] [[PubMed](#)]
129. Chen, Y.; Huang, Q.; Wang, H.; Qiu, J. Hysteresis modeling and tracking control for piezoelectric stack actuators using neural-Preisach model. *Int. J. Appl. Electromagn. Mech.* **2019**, *61*, 445–459. [[CrossRef](#)]
130. Li, Y.; Feng, Y.; Feng, J.; Liu, Y. Parameter Identification Based on PSO Algorithm for Piezoelectric Actuating System with Rate-dependent Prandtl–Ishlinskii Hysteresis Modeling Method. In Proceedings of the 2019 IEEE 4th International Conference on Advanced Robotics and Mechatronics (ICARM), Toyonaka, Japan, 3–5 July 2019; pp. 36–41. [[CrossRef](#)]
131. Pan, W.; Xu, R.; Zhou, M. Modeling of Hysteresis for Piezo-driven Stages using a Rate-dependent Krasnosel’skii–Pokrovskii Model. In Proceedings of the 2019 Chinese Control Conference (CCC), Guangzhou, China, 27–30 July 2019; pp. 1604–1609. [[CrossRef](#)]

132. Liu, D.; Fang, Y.; Wang, H. Intelligent Rate-Dependent Hysteresis Control Compensator Design With Bouc-Wen Model Based on RMSO for Piezoelectric Actuator. *IEEE Access* **2020**, *8*, 63993–64001. [[CrossRef](#)]
133. Liu, L.; Yun, H.; Li, Q.; Ma, X.; Chen, S.-L.; Shen, J. Fractional Order Based Modeling and Identification of Coupled Creep and Hysteresis Effects in Piezoelectric Actuators. *IEEE/ASME Trans. Mechatron.* **2020**, *25*, 1036–1044. [[CrossRef](#)]
134. Dong, R.; Tan, Y. A modified Prandtl–Ishlinskii modeling method for hysteresis. *Phys. B Condens. Matter* **2009**, *404*, 1336–1342. [[CrossRef](#)]
135. Jiang, H.; Ji, H.; Qiu, J.; Chen, Y. A modified prandtl-ishlinskii model for modeling asymmetric hysteresis of piezoelectric actuators. *IEEE Trans. Ultrason. Ferroelectr. Freq. Control* **2010**, *57*, 1200–1210. [[CrossRef](#)]
136. Wang, X.; Pommier-Budinger, V.; Gourinat, Y.; Reysset, A. A modified Preisach model for hysteresis in piezoelectric actuators. In Proceedings of the 2013 IEEE 11th International Workshop of Electronics, Control, Measurement, Signals and their application to Mechatronics, Toulouse, France, 24–26 June 2013; pp. 1–6. [[CrossRef](#)]
137. Song, X.; Duggen, L.; Lassen, B.; Mangeot, C. Modeling and identification of hysteresis with modified Preisach model in piezoelectric actuator. In Proceedings of the 2017 IEEE International Conference on Advanced Intelligent Mechatronics (AIM), Munich, Germany, 3–7 July 2017; pp. 1538–1543. [[CrossRef](#)]
138. Lin, F.-J.; Shieh, H.-J.; Huang, P.-K. Adaptive Wavelet Neural Network Control With Hysteresis Estimation for Piezo-Positioning Mechanism. *IEEE Trans. Neural Netw.* **2006**, *17*, 432–444. [[CrossRef](#)]
139. Zhao, X.; Tan, Y. Neural network based identification of Preisach-type hysteresis in piezoelectric actuator using hysteretic operator. *Sens. Actuators A Phys.* **2006**, *126*, 306–311. [[CrossRef](#)]
140. Li, P.; Yan, F.; Ge, C.; Zhang, M. Ultra-precise tracking control of piezoelectric actuators via a fuzzy hysteresis model. *Rev. Sci. Instrum.* **2012**, *83*, 085114. [[CrossRef](#)]
141. Li, P.; Yan, F.; Ge, C.; Wang, X.; Xu, L.; Guo, J.; Li, P. A simple fuzzy system for modelling of both rate-independent and rate-dependent hysteresis in piezoelectric actuators. *Mech. Syst. Signal Process.* **2013**, *36*, 182–192. [[CrossRef](#)]
142. Xu, Q.; Wong, P.-K. Hysteresis modeling and compensation of a piezostage using least squares support vector machines. *Mechatronics* **2011**, *21*, 1239–1251. [[CrossRef](#)]
143. Wong, P.-K.; Xu, Q.; Vong, C.-M.; Wong, H.-C. Rate-Dependent Hysteresis Modeling and Control of a Piezostage Using Online Support Vector Machine and Relevance Vector Machine. *IEEE Trans. Ind. Electron.* **2012**, *59*, 1988–2001. [[CrossRef](#)]
144. Zhou, C.; Feng, C.; Aye, Y.N.; Ang, W.T. A Digitized Representation of the Modified Prandtl–Ishlinskii Hysteresis Model for Modeling and Compensating Piezoelectric Actuator Hysteresis. *Micromachines* **2021**, *12*, 942. [[CrossRef](#)] [[PubMed](#)]
145. Shan, X.; Song, H.; Cao, H.; Zhang, L.; Zhao, X.; Fan, J. A Dynamic Hysteresis Model and Nonlinear Control System for a Structure-Integrated Piezoelectric Sensor-Actuator. *Sensors* **2021**, *21*, 269. [[CrossRef](#)] [[PubMed](#)]
146. Ahmed, K.; Yan, P.; Li, S. Duhem Model-Based Hysteresis Identification in Piezo-Actuated Nano-Stage Using Modified Particle Swarm Optimization. *Micromachines* **2021**, *12*, 315. [[CrossRef](#)] [[PubMed](#)]
147. Zhou, C.; Yuan, M.; Feng, C.; Ang, W.T. A Modified Prandtl–Ishlinskii Hysteresis Model for Modeling and Compensating Asymmetric Hysteresis of Piezo-Actuated Flexure-Based Systems. *Sensors* **2022**, *22*, 8763. [[CrossRef](#)]
148. Wang, W.; Zhang, J.; Xu, M.; Chen, G. Hysteresis Characteristics and MPI Compensation of Two-Dimensional Piezoelectric Positioning Stage. *Micromachines* **2022**, *13*, 321. [[CrossRef](#)]
149. Baziyad, A.G.; Ahmad, I.; Bin Salamah, Y. Precision Motion Control of a Piezoelectric Actuator via a Modified Preisach Hysteresis Model and Two-Degree-of-Freedom H-Infinity Robust Control. *Micromachines* **2023**, *14*, 1208. [[CrossRef](#)]
150. Lu, J.; Wang, J.; Bo, Y.; Zhang, X. Hysteresis Modeling and Compensation for a Fast Piezo-Driven Scanner in the UAV Image Stabilization System. *Drones* **2023**, *7*, 392. [[CrossRef](#)]
151. Rakotondrabe, M.; Clévy, C.; Lutz, P. Complete Open Loop Control of Hysteretic, Creeped, and Oscillating Piezoelectric Cantilevers. *IEEE Trans. Autom. Sci. Eng.* **2010**, *7*, 440–450. [[CrossRef](#)]
152. Islam, M.S.; Beamish, J. Piezoelectric creep in LiNbO<sub>3</sub>, PMN-PT and PZT-5A at low temperatures. *J. Appl. Phys.* **2019**, *126*, 204101. [[CrossRef](#)]
153. Jung, H.; Gweon, D.-G. Creep characteristics of piezoelectric actuators. *Rev. Sci. Instrum.* **2000**, *71*, 1896–1900. [[CrossRef](#)]
154. Georgiou, H.M.S.; Ben Mrad, R. Dynamic electromechanical drift model for PZT. *Mechatronics* **2008**, *18*, 81–89. [[CrossRef](#)]
155. Rakotondrabe, M. Modeling and compensation of multivariable creep in multi-DOF piezoelectric actuators. In Proceedings of the 2012 IEEE International Conference on Robotics and Automation, Saint Paul, MN, USA, 14–18 May 2012; pp. 4577–4581. [[CrossRef](#)]
156. He, X.; Wang, D.; Wang, L.; Melnik, R. Modelling of creep hysteresis in ferroelectrics. *Philos. Mag.* **2018**, *98*, 1256–1271. [[CrossRef](#)]
157. Croft, D.; Shed, G.; Devasia, S. Creep, Hysteresis, and Vibration Compensation for Piezoactuators: Atomic Force Microscopy Application. *J. Dyn. Syst. Meas. Control* **2001**, *123*, 35–43. [[CrossRef](#)]
158. Wang, X.; Budinger, V.; Gourinat, Y. A Specific Methodology of Creep Compensation for Piezoelectric Actuators by Open-Loop Control. *Appl. Mech. Mater.* **2013**, *281*, 141–145. [[CrossRef](#)]
159. Liu, Y.; Shan, J.; Qi, N. Creep modeling and identification for piezoelectric actuators based on fractional-order system. *Mechatronics* **2013**, *23*, 840–847. [[CrossRef](#)]
160. Changhai, R.; Lining, S. Hysteresis and creep compensation for piezoelectric actuator in open-loop operation. *Sens. Actuators A Phys.* **2005**, *122*, 124–130. [[CrossRef](#)]

161. Devasia, S.; Eleftheriou, E.; Moheimani, S.O.R. A Survey of Control Issues in Nanopositioning. *IEEE Trans. Control Syst. Technol.* **2007**, *15*, 802–823. [[CrossRef](#)]
162. Ghariieb, W. Creep compensation in piezoelectric actuators for nanopositioning technology. *Int. J. Nanomanuf.* **2009**, *4*, 267–273. [[CrossRef](#)]
163. Liu, Y.F.; Li, J.; Hu, X.H.; Zhang, Z.M.; Cheng, L.; Lin, Y.; Zhang, W.J. Modeling and control of piezoelectric inertia–friction actuators: Review and future research directions. *Mech. Sci.* **2015**, *6*, 95–107. [[CrossRef](#)]
164. Ang, W.T.; Khosla, P.K.; Riviere, C.N. Feedforward Controller With Inverse Rate-Dependent Model for Piezoelectric Actuators in Trajectory-Tracking Applications. *IEEE/ASME Trans. Mechatron.* **2007**, *12*, 134–142. [[CrossRef](#)]
165. Lin, C.J.; Chen, S.Y. Evolutionary algorithm based feedforward control for contouring of a biaxial piezo-actuated stage. *Mechatronics* **2009**, *19*, 829–839. [[CrossRef](#)]
166. Leang, K.K.; Zou, Q.; Devasia, S. Feedforward control of piezoactuators in atomic force microscope systems: Inversion-based compensation for dynamics and hysteresis. *IEEE Control Syst.* **2009**, *29*, 70–82. [[CrossRef](#)]
167. Xiao, S.; Li, Y. Modeling and High Dynamic Compensating the Rate-Dependent Hysteresis of Piezoelectric Actuators via a Novel Modified Inverse Preisach Model. *IEEE Trans. Control Syst. Technol.* **2013**, *21*, 1549–1557. [[CrossRef](#)]
168. Rakotondrabe, M. Bouc–Wen Modeling and Inverse Multiplicative Structure to Compensate Hysteresis Nonlinearity in Piezoelectric Actuators. *IEEE Trans. Autom. Sci. Eng.* **2011**, *8*, 428–431. [[CrossRef](#)]
169. Feng, Y.; Rabbath, C.A.; Su, C.-Y. Inverse Duhem Model Based Robust Adaptive Control for Flap Positioning System with SMA actuators. *IFAC Proc. Vol.* **2011**, *44*, 8126–8131. [[CrossRef](#)]
170. Gu, G.-Y.; Zhu, L.-M. Motion control of piezoceramic actuators with creep, hysteresis and vibration compensation. *Sens. Actuators A Phys.* **2013**, *197*, 76–87. [[CrossRef](#)]
171. Gu, G.-Y.; Yang, M.-J.; Zhu, L.-M. Real-time inverse hysteresis compensation of piezoelectric actuators with a modified Prandtl–Ishlinskii model. *Rev. Sci. Instrum.* **2012**, *83*, 065106. [[CrossRef](#)]
172. Rahman, M.A.; Al Mamun, A.; Yao, K. Rate dependent direct inverse hysteresis compensation of piezoelectric micro-actuator used in dual-stage hard disk drive head positioning system. *Rev. Sci. Instrum.* **2015**, *86*, 085002. [[CrossRef](#)]
173. Wang, D.; Yu, P.; Wang, F.; Chan, H.-Y.; Zhou, L.; Dong, Z.; Liu, L.; Li, W.J. Improving Atomic Force Microscopy Imaging by a Direct Inverse Asymmetric PI Hysteresis Model. *Sensors* **2015**, *15*, 3409–3425. [[CrossRef](#)]
174. Yu, G.-R.; You, C.-S.; Hong, R.-J. Self-Tuning Fuzzy Control of a Piezoelectric Actuator System. In Proceedings of the 2006 IEEE International Conference on Systems, Man and Cybernetics, Taipei, Taiwan, 8–11 October 2006; pp. 1108–1113. [[CrossRef](#)]
175. Lin, C.-J.; Yang, S.-R. Precise positioning of piezo-actuated stages using hysteresis-observer based control. *Mechatronics* **2006**, *16*, 417–426. [[CrossRef](#)]
176. Sun, F.; Qi, S.; Bao, J.; Xu, F.; Zhao, W. Design and PID Control of Piezoelectric Micro-motion Stage. In Proceedings of the 2018 IEEE International Conference on Intelligence and Safety for Robotics (ISR), Shenyang, China, 24–27 August 2018; pp. 110–115. [[CrossRef](#)]
177. Bruno, N.; Zhu, Y.; Liu, C.; Gao, Q.; Li, Y. Development of a piezoelectric high speed on/off valve and its application to pneumatic closed-loop position control system. *J. Mech. Sci. Technol.* **2019**, *33*, 2747–2759. [[CrossRef](#)]
178. Alexandrov, A.G.; Palenov, M.V. Adaptive PID controllers: State of the art and development prospects. *Autom. Remote Control* **2014**, *75*, 188–199. [[CrossRef](#)]
179. Sharkawy, A.B. Genetic fuzzy self-tuning PID controllers for antilock braking systems. *Eng. Appl. Artif. Intell.* **2010**, *23*, 1041–1052. [[CrossRef](#)]
180. Huba, M. Comparing 2DOF PI and predictive disturbance observer based filtered PI control. *J. Process Control* **2013**, *23*, 1379–1400. [[CrossRef](#)]
181. Zheng, Q.; Goforth, F.J. A disturbance rejection based control approach for hysteretic systems. In Proceedings of the 49th IEEE Conference on Decision and Control (CDC), Atlanta, GA, USA, 15–17 December 2010; pp. 3748–3753. [[CrossRef](#)]
182. Liang, Y.; Xu, S.; Hong, K.; Wang, G.; Zeng, T. Neural network modeling and single-neuron proportional–integral–derivative control for hysteresis in piezoelectric actuators. *Meas. Control.* **2019**, *52*, 1362–1370. [[CrossRef](#)]
183. Chuang, N.; Petersen, I.R. Robust  $H_\infty$  control of hysteresis in a piezoelectric stack actuator. *IFAC Proc. Vol.* **2008**, *41*, 1996–2001. [[CrossRef](#)]
184. Soleymanzadeh, D.; Ghafarirad, H.; Zareinejad, M. Sensorless adaptive sliding mode position control for piezoelectric actuators with charge leakage. *J. Intell. Mater. Syst. Struct.* **2020**, *31*, 40–52. [[CrossRef](#)]
185. Medhat, A.; Youssef, M. Optimized PID tracking controller for piezoelectric hysteretic actuator model. *World J. Model. Simul.* **2013**, *9*, 223–234.
186. Wu, H.; Su, W.; Liu, Z. PID controllers: Design and tuning methods. In Proceedings of the 2014 9th IEEE Conference on Industrial Electronics and Applications, Hangzhou, China, 9–11 June 2014; pp. 808–813. [[CrossRef](#)]
187. Rahman, N.U.; Alam, M.N. Active vibration control of a piezoelectric beam using PID controller: Experimental study. *Lat. Am. J. Solids Struct.* **2012**, *9*, 657–673. [[CrossRef](#)]
188. Ding, B.; Li, Y.; Xiao, X.; Tang, Y. Optimized PID tracking control for piezoelectric actuators based on the Bouc–Wen model. In Proceedings of the 2016 IEEE International Conference on Robotics and Biomimetics (ROBIO), Qingdao, China, 3–7 December 2016; pp. 1576–1581. [[CrossRef](#)]

189. Wahid, N.; Hassan, N. Self-Tuning Fuzzy PID Controller Design for Aircraft Pitch Control. In Proceedings of the 2012 Third International Conference on Intelligent Systems Modelling and Simulation, Kota Kinabalu, Malaysia, 8–10 February 2012; pp. 19–24. [\[CrossRef\]](#)
190. Zhou, L.; Chen, G. Intelligent Vibration Control for High-Speed Spinning Beam Based on Fuzzy Self-Tuning PID Controller. *Shock Vib.* **2015**, *2015*, 617038. [\[CrossRef\]](#)
191. Bing, S.; Weibin, R.; Bin, G.; Changhai, R.; Lining, S. Modeling and control of a novel piezoelectric actuated precision fast positioning system. *Smart Mater. Struct.* **2008**, *17*, 025032. [\[CrossRef\]](#)
192. Li, D.; Fu, Y.; Yang, L. Coupling dynamic modeling and simulation of three-degree-of-freedom micromanipulator based on piezoelectric ceramic of fuzzy PID. *Mod. Phys. Lett. B* **2017**, *31*, 1750140. [\[CrossRef\]](#)
193. Rebai, A.; Guesmi, K.; Gozim, D.; Hemici, B. Design of an optimized fractional order fuzzy PID controller for a piezoelectric actuator. In Proceedings of the 2014 15th International Conference on Sciences and Techniques of Automatic Control and Computer Engineering (STA), Hammamet, Tunisia, 21–23 December 2014; pp. 456–461. [\[CrossRef\]](#)
194. Haji, V.H.; Monje, C.A. Fractional order fuzzy-PID control of a combined cycle power plant using Particle Swarm Optimization algorithm with an improved dynamic parameters selection. *Appl. Soft Comput.* **2017**, *58*, 256–264. [\[CrossRef\]](#)
195. Zamani, A.-A.; Tavakoli, S.; Etedali, S.; Sadeghi, J. Online tuning of fractional order fuzzy PID controller in smart seismic isolated structures. *Bull. Earthq. Eng.* **2018**, *16*, 3153–3170. [\[CrossRef\]](#)
196. Birs, I.R.; Folea, S.; Muresan, C.I. An optimal fractional order controller for vibration attenuation. In Proceedings of the 2017 25th Mediterranean Conference on Control and Automation (MED), Valletta, Malta, 3–6 July 2017; pp. 828–832. [\[CrossRef\]](#)
197. Yi, J.; Chang, S.; Shen, Y. Disturbance-Observer-Based Hysteresis Compensation for Piezoelectric Actuators. *IEEE/ASME Trans. Mechatron.* **2009**, *14*, 456–464. [\[CrossRef\]](#)
198. Ishigami, Y.; Takahashi, S.; Kawajiri, T.; Ishimaru, I. Disturbance Feedback System with PID Control and Disturbance Observer for Spectroscopic Measurement Device. *IFAC Proc. Vol.* **2011**, *44*, 2448–2451. [\[CrossRef\]](#)
199. Basha, S.M.; Swarup, A. Disturbance observer based fuzzy PID and robust PID autopilot design for bank-to-turn missile. In Proceedings of the 2017 8th International Conference on Computing, Communication and Networking Technologies (ICCCNT), Delhi, India, 3–5 July 2017; pp. 1–7. [\[CrossRef\]](#)
200. Helfrich, B.E.; Lee, C.; Bristow, D.A.; Xiao, X.H.; Dong, J.; Alleyne, A.G.; Salapaka, S.M.; Ferreira, P.M. Combined  $H_\infty$ -feedback and iterative learning control design with application to nanopositioning systems. In Proceedings of the 2008 American Control Conference, Seattle, WA, USA, 11–13 June 2008; pp. 3893–3900. [\[CrossRef\]](#)
201. Lee, G.; You, K.; Kang, T.; Yoon, K.J.; Lee, J.O.; Park, J.K. Modeling and Design of H-Infinity Controller for Piezoelectric Actuator LIPCA. *J. Bionic Eng.* **2010**, *7*, 168–174. [\[CrossRef\]](#)
202. Chuang, N.; Petersen, I.R. Robust  $H_\infty$  Control of Hysteresis in a Piezoelectric Stack Actuator. *J. Dyn. Syst. Meas. Control* **2013**, *135*, 064501. [\[CrossRef\]](#)
203. Xiao, S.; Li, Y. Dynamic compensation and  $H_\infty$  control for piezoelectric actuators based on the inverse Bouc–Wen model. *Robot. Comput. Manuf.* **2014**, *30*, 47–54. [\[CrossRef\]](#)
204. Jiaqiang, E.; Qian, C.; Liu, H.; Liu, G. Design of the  $H_\infty$  robust control for the piezoelectric actuator based on chaos optimization algorithm. *Aerosp. Sci. Technol.* **2015**, *47*, 238–246. [\[CrossRef\]](#)
205. Brahim, M.; Bahri, I.; Bernard, Y. Modeling and robust closed loop position controllers of Piezoelectric Actuator Drive (PAD). In Proceedings of the 2017 14th International Multi-Conference on Systems, Signals & Devices (SSD), Marrakech, Morocco, 28–31 March 2017; pp. 560–565. [\[CrossRef\]](#)
206. Brahim, M.; Bernard, Y.; Bahri, I. Modelling, design, and real time implementation of robust H-infinity position control of piezoelectric actuator drive. *Int. J. Mechatron. Autom.* **2018**, *6*, 151. [\[CrossRef\]](#)
207. Lan, X.; Liang, D.; Mao, C.; Li, A.; Wang, J. Design of Two-degree-of-freedom  $H_\infty$  Controller for Three-dimensional Piezo-positioning System. In Proceedings of the 2019 IEEE 3rd Information Technology, Networking, Electronic and Automation Control Conference (ITNEC), Chengdu, China, 15–17 March 2019; pp. 1078–1082. [\[CrossRef\]](#)
208. Shen, J.-C.; Jywe, W.-Y.; Chiang, H.-K.; Shu, Y.-L. Precision tracking control of a piezoelectric-actuated system. *Precis. Eng.* **2008**, *32*, 71–78. [\[CrossRef\]](#)
209. Huang, S.; Tan, K.K.; Lee, T.H. Adaptive Sliding-Mode Control of Piezoelectric Actuators. *IEEE Trans. Ind. Electron.* **2009**, *56*, 3514–3522. [\[CrossRef\]](#)
210. Wehr, M.; Stockert, S.; Ionescu, C.; Abel, D.; Hirt, G. Sliding Mode Control of Piezoelectric Stack Actuators for Roll Gap Adjustment in a Cold Rolling Mill. In Proceedings of the 2019 IEEE/ASME International Conference on Advanced Intelligent Mechatronics (AIM), Hong Kong, China, 8–12 July 2019; pp. 1207–1214. [\[CrossRef\]](#)
211. Yu, Z.; Wu, Y.; Fang, Z.; Sun, H. Modeling and compensation of hysteresis in piezoelectric actuators. *Heliyon* **2020**, *6*, e03999. [\[CrossRef\]](#) [\[PubMed\]](#)
212. Rakotondrabe, M.; Agnus, J.; Lutz, P. Feedforward and IMC-feedback control of a nonlinear 2-DOF piezoactuator dedicated to automated micropositioning tasks. In Proceedings of the 2011 IEEE International Conference on Automation Science and Engineering, Trieste, Italy, 24–27 August 2011; pp. 393–398. [\[CrossRef\]](#)
213. Liu, Y.; Shan, J.; Gabbert, U. Feedback/feedforward control of hysteresis-compensated piezoelectric actuators for high-speed scanning applications. *Smart Mater. Struct.* **2015**, *24*, 015012. [\[CrossRef\]](#)

214. Ko, P.-J.; Wang, Y.-P.; Tien, S.-C. Inverse-feedforward and robust-feedback control for high-speed operation on piezo-stages. *Int. J. Control* **2013**, *86*, 197–209. [[CrossRef](#)]
215. Zhou, M.; Zhang, Q.; Wang, J. Feedforward-Feedback Hybrid Control for Magnetic Shape Memory Alloy Actuators Based on the Krasnosel'skii-Pokrovskii Model. *PLoS ONE* **2014**, *9*, e97086. [[CrossRef](#)]
216. Chen, H.-Y.; Liang, J.-W. Hysteresis compensation of a piezoelectric-stack-actuator-driven (PSA-driven) system using inversion-based models and feedback control. *J. Intell. Fuzzy Syst.* **2018**, *35*, 3243–3253. [[CrossRef](#)]
217. Li, Z.; Huang, N.; Zhong, Y.; Ma, G.; Liu, G.; Zhu, D. Feedback Feed-Forward Control of Piezoelectric Positioning Stages and Experimental Evaluation. In Proceedings of the 2018 Chinese Automation Congress (CAC), Xi'an, China, 30 November–2 December 2018; pp. 3758–3762. [[CrossRef](#)]
218. Saleem, A.; Al Hattali, M.; Shafiq, M.; Bahadur, I. Tracking Control of Piezoelectric Actuators using Feedforward/Feedback Learning-based Controller. In Proceedings of the 2019 6th International Conference on Control, Decision and Information Technologies (CoDIT), Paris, France, 23–26 April 2019; pp. 1981–1985. [[CrossRef](#)]
219. Chi, Z.; Jia, M.; Xu, Q. Fuzzy PID Feedback Control of Piezoelectric Actuator with Feedforward Compensation. *Math. Probl. Eng.* **2014**, *2014*, 107184. [[CrossRef](#)]
220. Sousa, F.M.M.; Amarante, V.M.B.; Fonseca, R.R. Adaptive Fuzzy Feedforward-Feedback Controller Applied to Level Control in an Experimental Prototype. *IFAC-PapersOnLine* **2019**, *52*, 219–224. [[CrossRef](#)]
221. Beijen, M.A.; Heertjes, M.F.; Butler, H.; Steinbuch, M.  $H_\infty$  feedback and feedforward controller design for active vibration isolators. *IFAC-PapersOnLine* **2017**, *50*, 13384–13389. [[CrossRef](#)]
222. Ahamd, I.; Abdurraqueeb, A.M.  $H_\infty$  control design with feed-forward compensator for hysteresis compensation in piezoelectric actuators. *Automatika* **2017**, *57*, 691–702. [[CrossRef](#)]
223. Velasco, J.; Barambones, O.; Calvo, I.; Zubia, J.; de Ocariz, I.S.; Chouza, A. Sliding Mode Control with Dynamical Correction for Time-Delay Piezoelectric Actuator Systems. *Materials* **2020**, *13*, 132. [[CrossRef](#)] [[PubMed](#)]
224. Leang, K.K.; Devasia, S. Feedback-Linearized Inverse Feedforward for Creep, Hysteresis, and Vibration Compensation in AFM Piezoactuators. *IEEE Trans. Control Syst. Technol.* **2007**, *15*, 927–935. [[CrossRef](#)]
225. Napole, C.; Barambones, O.; Derbeli, M.; Calvo, I. Advanced Trajectory Control for Piezoelectric Actuators Based on Robust Control Combined with Artificial Neural Networks. *Appl. Sci.* **2021**, *11*, 7390. [[CrossRef](#)]
226. Yu, S.; Feng, Y.; Yang, X. Extended state observer-based fractional order sliding-mode control of piezoelectric actuators. *Proc. Inst. Mech. Eng. Part I J. Syst. Control Eng.* **2021**, *235*, 39–51. [[CrossRef](#)]
227. Li, D.; Cao, H.; Chen, X. Fuzzy control of milling chatter with piezoelectric actuators embedded to the tool holder. *Mech. Syst. Signal Process.* **2021**, *148*, 107190. [[CrossRef](#)]
228. Yu, S.; Xie, M.; Wu, H.; Ma, J.; Li, Y.; Gu, H. Composite proportional-integral sliding mode control with feedforward control for cell puncture mechanism with piezoelectric actuation. *ISA Trans.* **2022**, *124*, 427–435. [[CrossRef](#)]
229. Shi, B.; Shi, R.; Wang, F. Design of an adaptive feedforward/feedback combined control for piezoelectric actuated micro positioning stage. *Precis. Eng.* **2022**, *78*, 199–205. [[CrossRef](#)]
230. Xiong, Y.; Jia, W.; Zhang, L.; Zhao, Y.; Zheng, L. Feedforward Control of Piezoelectric Ceramic Actuators Based on PEA-RNN. *Sensors* **2022**, *22*, 5387. [[CrossRef](#)]
231. Cheng, L.; Chen, W.; Tian, L.; Xie, Y. A Finite-Time Sliding-Mode Controller Based on the Disturbance Observer and Neural Network for Hysteretic Systems with Application in Piezoelectric Actuators. *Sensors* **2023**, *23*, 6246. [[CrossRef](#)] [[PubMed](#)]
232. Napole, C.; Barambones, O.; Derbeli, M.; Calvo, I. Design and experimental validation of a piezoelectric actuator tracking control based on fuzzy logic and neural compensation. *Fuzzy Sets Syst.* **2023**, *464*, 108449. [[CrossRef](#)]

**Disclaimer/Publisher's Note:** The statements, opinions and data contained in all publications are solely those of the individual author(s) and contributor(s) and not of MDPI and/or the editor(s). MDPI and/or the editor(s) disclaim responsibility for any injury to people or property resulting from any ideas, methods, instructions or products referred to in the content.